NOAA OAR Special Report

PMEL Tsunami Forecast Series: Vol. 68
A Tsunami Forecast Model for Virginia Beach, Virginia

(Draft)

Liujuan Tang
Christopher Moore

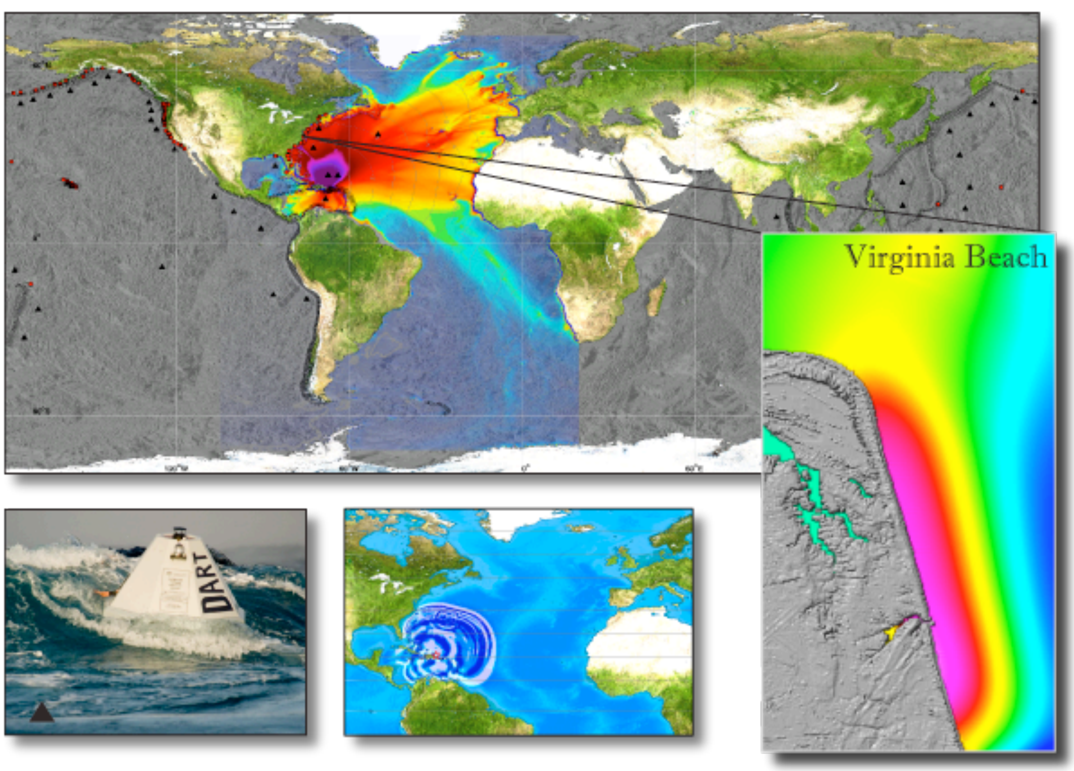

April 2013

NOAA Center for Tsunami Research (NCTR)
Pacific Marine Environmental Laboratory

Contents

Abstract 3

1 Introduction 4

2 Forecast Method 5

2.1 Construction of a Propagation Scenario Based on Deep-Ocean Tsunameter Measurements and Pre-Computed Tsunami Source Functions 5

2.2 Coastal Predictions by Using High-Resolution Forecast Models in Real-Time. 7

3 Model Development 8

3.1 Forecast area 8

3.2 Bathymetry and Topography 9

3.3 Model Setup 10

4 Results and Discussion 11

4.1 Sensitivity of modeled amplitude to friction coefficients 11

4.2 Model verification and stability testing 12

5 Summary and Conclusions 13

Acknowledgements 14

References 15

Tables 19

Appendix A. 22

A1. Reference model *.in file for Virginia Beach, Virginia—updated for 2013 22

A2. Forecast model *.in file for Virginia Beach, Virginia—updated for 2013 24

Figures 25

Appendix B Propagation Database: Atlantic Ocean Unit Sources 63

Appendix C SIFT Testing Report 74

List of Tables

Table 1 Tsunami source functions in the Pacific, Atlantic and Indian Oceans................ 19
Table 2 MOST setups for the Virginia Beach reference and forecast models................. 20
Table 3 Sources of the 9 simulated magnitude-9.3 tsunamis and the maximum computed wave crests at the Virginia Beach warning point... 21

PMEL Tsunami Forecast Series: Vol. 68

A Tsunami Forecast Model for Virginia Beach, Virginia

Liujuan Tang and Christopher Moore

Abstract

This report documents the development and testing of a tsunami forecast model for Virginia Beach, Virginia as part of NOAA's operational tsunami forecast system. Based on the Method of Splitting Tsunamis (MOST) model, the forecast model performs calculations on bathymetry grids with a horizontal resolution of 2 arc-seconds. At this resolution it is capable of simulating four hours of tsunami wave dynamics in under ten minutes of computational time. A reference inundation model of higher resolution (1/3 arc-seconds) was also developed in parallel, to provide a reference for the forecast model. Both models were tested with nine simulated magnitude-9.3 tsunamis from different source regions and one micro tsunami. Good agreement was observed between the model computations, and the numerical consistency between the model results for the maximum amplitudes and currents indicate reliability, robustness, and stability of the forecast model.

The study shows that mega tsunamis from subduction zone earthquakes near the Puerto Rico Trench can cause severe inundation at Virginia Beach. The results also highlight that large waves can arrive 12-30 hours after the first wave arrival for far-field, small to medium sized tsunamis (maximum wave amplitudes near or smaller than 1 meter). This typical long arrival time requires longer warning duration for such events. Wavelet analyses show broad and relatively long resonant periods from 0.5 hours to several hours, also suggesting the necessity for long warning durations.

The simulated magnitude-9.3 tsunamis show an impressive local variability of tsunami amplitudes at Virginia Beach, and indicate the complexity of forecasting tsunami amplitudes at a coastal location. It is essential to use high-resolution models to provide the accuracy useful for coastal tsunami forecasts and practical guidance.

1 Introduction

The National Oceanic and Atmospheric Administration (NOAA) Center for Tsunami Research, located at NOAA's Pacific Marine Environmental Laboratory (PMEL), has developed a tsunami forecasting system for operational use by NOAA's two Tsunami Warning Centers located in Hawaii and Alaska (Titov *et al.*, 2005; Titov, 2009). The forecast system combines real-time deep-ocean tsunami measurements from tsunameters (González *et al*., 2005; Meinig *et al*., 2005, Bernard *et al*., 2006, Bernard and Titov, 2007) and the Method of Splitting Tsunami (MOST) model, a suite of finite difference numerical codes based on the nonlinear shallow water wave equations (Titov and Synolakis, 1998; Titov and González, 1997; Synolakis *et al*., 2008; *Titov et al*., 2011) to produce real-time forecasts of tsunami arrival time, heights, periods and inundation. To achieve accurate and detailed forecasts of tsunami impact for specific sites, high-resolution tsunami forecast models are under development for United States coastal communities at risk (Tang *et al.*, 2008a; 2009; 2010; Arcas and Uslu, 2010; Righi and Arcas, 2010; Uslu *et al*. 2010; Wei and Arcas, 2010). The resolution of these models has to be high enough to resolve the dynamics of a tsunami inside a particular harbor, including influences of major harbor structures such as breakwaters and seawalls. These models have been integrated as crucial components into the tsunami forecast system.

As of March 2013 the forecast system real-time measurements come from a network of 58 tsunameter stations deployed at optimal locations in the Pacific, Atlantic, Indian Oceans, Caribbean Sea, the Gulf of Mexico and South China Sea (*Spillane et al*., 2008). While the buoy array is owned and maintained by nine different nations (U.S.A., Australia, Chile, China, Japan, India, Indonesia, Thailand and Russian), the data from the entire array are made publically available in real-time via the Global Telecommunications System (GTS). The data from the tsunameters is used to provide guidance by comparing them to pre-computed open ocean model results. These pre-computed propagation models currently cover all three ocean basins (Pacific, Atlantic, and Indian), and are comprised of 1,725 different tsunami scenarios with initial deformations covering the major tsunamigenic subduction zones throughout the world (Figure 1 and Table 1). High-resolution forecast inundation models are now set up for 75 U.S. coastal communities (e.g. Fig. 1). The fully implemented system will use real-time data from the tsunameter network to provide high-resolution tsunami forecasts for at least 75 communities in the U.S. by 2013, with additional models envisioned later for smaller communities. Since its first testing in the 17 November 2003 Rat Island tsunami, the forecast system has produced experimental real-time forecasts for more than 20 tsunamis in the Pacific and Indian oceans (Titov *et al*., 2005; Wei *et al*., 2008; Titov, 2009; Titov and Tang, 2011; Tang *et al*., 2012; http://nctr.pmel.noaa.gov/database_devel.html). The forecast method has also been tested with data from nine additional events that produced deep-ocean tsunameter data including several near-field tsunamis (http://nctr.pmel.noaa.gov/database_devel.html; Titov *et a*l., 2005; Tang *et al*., 2008b; Wei *et al*., 2012).

This report describes the development and testing of the Virginia Beach forecast model. The objective in developing this model is to provide NOAA's Tsunami Warning Centers the ability to assess danger posed to Virginia Beach following tsunami generation in the Atlantic Ocean Basin with a goal to provide accurate and timely forecasts to enable the community to respond appropriately. Dr. Aurelio Mercado developed the first version of a Virginia Beach forecast model in 2007. It was updated in 2008 and had been working in the tsunami forecast system. As new bathymetric/topographic and tsunami data came in and the model development technique progressed further, the model had been updated and re-tested in March 2013. A secondary objective of the report is to explore the potential tsunami impact from earthquakes at major subduction zones in the Atlantic Ocean to the city by using the developed forecast model. Wavelet analysis was applied to investigate the local responses to tsunami waves.

The report is organized as follows. Section 2 briefly introduces NOAA's tsunami forecast method. Section 3 describes the model development. Section 4 presents the results and discussion, which includes model sensitivity study to friction coefficient, model verification, and testing for simulated tsunamis. A summary and conclusion are provided in section 5.

2 Forecast Method

NOAA's real-time tsunami forecasting scheme is a process that comprises two steps: (1) construction of a propagation scenario via inversion of deep ocean tsunameter measurements with pre-computed tsunami source functions; and (2) coastal predictions by running high-resolution forecast models in real time (Titov *et al*. 1999; 2005; Titov 2009; Tang *et al*., 2009, Tang *et al*., 2012). The tsunameter-constrained tsunami source, the corresponding offshore scenario from the tsunami source function database, and high-resolution forecast models cover the entire evolution of earthquake-generated tsunamis, generation, propagation and coastal inundation, providing a complete tsunami forecast capability.

2.1 Construction of a Propagation Scenario Based on Deep-Ocean Tsunameter Measurements and Pre-Computed Tsunami Source Functions

Several real-time data sources, including seismic data, coastal tide gage and deep-ocean data have been used for tsunami warning and forecasting (Satake *et al*., 2008; Whitmore, 2003; Titov, 2009). NOAA's strategy for the real-time forecasting is to use deep-ocean measurements at tsunameter stations, also known as DART™ (Deep-ocean Assessment and Reporting of Tsunami) buoys, as the primary data source due to several key features: (1) tsunameters provide a direct measure of tsunami waves, unlike seismic data, which are an indirect measure of tsunamis, (2) deep ocean tsunami measurements are in general the earliest tsunami information available, since tsunamis propagate much faster in deep ocean than in shallow coastal area where coastal tide gages are located, (3) compared to coastal tide gages, tsunameter data with a high signal to noise ratio can be obtained without interference from harbor and local shelf effects, and (4) wave dynamics of tsunami propagation in deep water is assumed to be linear (Kânoğlu and Synolakis, 2006; Liu, 2009). This linear process allows application of efficient inversion schemes.

Time series of tsunami observations in deep water (depths << wave length) can be decomposed into a linear combination of a set of tsunami source functions in the time domain by a linear Least Squares method (Percival *et al.*, 2011). The coefficients obtained through this inversion process are called *tsunami source coefficients*. During real-time tsunami forecasting, seismic waves propagate much faster than tsunami waves so the initial seismic magnitude can be estimated before the tsunameter data are available. Since time is of the essence, this initial tsunami forecast is based on the seismic magnitude only. An updated forecast will be made via the inversion method when tsunameter is available.

Titov *et al*. (1999; 2001) conducted sensitivity studies on far-field deep-water tsunamis with different parameters of an elastic deformation model described in Gusiakov (1978) and Okada (1985). The results showed source magnitude and location essentially define far-field tsunami signals for a wide range of subduction zone earthquakes. Other parameters have a secondary influence and can be pre-defined during the forecast. Based on these results, tsunami source function databases for the Pacific, Atlantic, and Indian Oceans have been built using these pre-defined source parameters: length = 100 km, width = 50 km, slip = 1 m, rake = 90 or -90 and rigidity = 4.5×10^{10} N/m^2. The other parameters (strike, dip, and depth) are location-specific and are chosen with knowledge of the subduction zone where they are located. Details of the propagation database are described in Gica *et al*. (2008). Each tsunami source function models a tsunami generated by a typical magnitude-7.5 earthquake with predefined source parameters mentioned above. Figure 1 shows the locations of tsunami source functions. Figure 2 shows the maximum amplitudes at Virginia Beach offshore from the tsunami source functions in Atlantic Ocean.

The tsunami source functions in the database are computed with a time step of 10 seconds and a spatial resolution of 4-arc-minute (approximately 7.4 km along the north-south direction). The output (offshore wave height and depth-average velocities of the entire domain) are then compressed and saved every 1 minute in time and 16-arc-minute in space (Tolkova, 2007). As inundation is calculated by the high resolution forecast models, the propagation scenarios do not include inundation, and a reflection boundary condition is enforced at 20 m water depth (Gica *et al*., 2008), and friction is assumed to be negligible.

When tsunami waves propagate into shallow water, the steady-state assumption requires no net energy losses or gains. The decrease in transport speed must be compensated by an increase in energy density in order to maintain a constant energy flux. The low spatial resolution and simplified boundary conditions of the propagation model result in inaccuracies in near-shore dynamics. As a consequence, the numerical dissipation (due to the low spatial resolution) will cause energy decay in the propagation modeling (Tang *et al*., 2012). Based on the consideration of energy conservation, we have developed high-resolution, site-specific inundation forecast models built on the MOST model to more accurately simulate the near shore wave dynamics.

That percentage of energy released from an earthquake that is transferred into the water column during tsunami generation is difficult to accurately model using seismic methods. However, the goal of tsunameter inversion is not to quantify the energy at the initial stage of tsunami generation. Instead, we try to quantify the amount of wave energy that propagates outside the source area in the form of surface long gravity waves, which can be well measured by the tsunameter stations. Since it is this propagating energy that results in the impacts at the coast, we estimate the tsunami source (the propagation scenario) by directly measuring the deep ocean tsunami data. Regardless of the details of earthquake processes for tsunami generation at the initial stage, the inversion can ensure the propagation scenario gives the best approximation to the tsunami measurements, and therefore, the best estimation of the total energy transferred to the tsunami waves. The database can provide offshore forecasts of tsunami amplitudes and all other wave parameters immediately once the inversion is complete. The tsunami source, constrained by real-time tsunami measurements, provides an accurate offshore tsunami scenario without additional time-consuming deep-water model runs.

2.2 Coastal Predictions by Using High-Resolution Forecast Models in Real-Time.

High-resolution forecast models are designed for the final stage of the evolution of tsunami waves: coastal runup and inundation. Once the tsunameter-constrained tsunami source is obtained (as a linear combination of tsunami source functions), the pre-computed time series of offshore wave height and depth-averaged velocity from the model propagation scenario are applied as the dynamic boundary conditions for the forecast models. This saves the simulation time of basin-wide tsunami propagation. Tsunami inundation and nearshore currents are highly nonlinear processes, therefore a linear combination would not provide an accurate solution. A high-resolution model is also required to resolve shorter tsunami wavelengths nearshore with accurate bathymetric/topographic data. The forecast models are constructed with the Method of Splitting Tsunami (MOST) model, a finite difference tsunami inundation model based on the nonlinear shallow-water wave equations (Titov and Synolakis, 1998; Titov and González, 1997; Synolakis *et al*., 2008; *Titov et al*., 2011). Each forecast model contains three telescoping computational grids with increasing resolution, covering regional, intermediate and near shore areas. Run-up and inundation are computed at the coastline. The highest resolution grid includes the population center and coastal water level stations for forecast verification. The grids are derived from the best available bathymetric/topographic data at the time of development, and will be updated as new survey data become available.

The forecast models are optimized for speed and accuracy. By reducing the computational areas and grid resolutions, each model is optimized to provide 4-hour event forecasting results in a maximum of 10 minutes of computational time using asingle processor, while still providing enough accuracy for forecasting. To ensure forecast accuracy at every step of the process, the model output is validated with historical tsunami records when available and compared to numerical results from the original full-resolution, and full-extent "reference" inundation model. In order to provide warning guidance over a long duration during a tsunami event, each forecast model has been developed to provide simulation output for up to 24 hours (or 30 hours for the Atlantic sites) from the time of tsunami generation.

3 Model Development

3.1 Forecast area

Virginia Beach is a coastal city in the mid-Atlantic region in the southeastern corner of Virginia, within the geologic region called the Atlantic Coastal Plain (Tayler *et al*., 2007). The city is bordered by the Atlantic Ocean to the east and the Chesapeake Bay to the north (Fig. 4). The Atlantic Coastal Plain features a thick basement layer of igneous and metamorphic rock overlain with a thick wedge of sediment that increases in thickness and dips towards the eastern shoreline (Tayler *et al*., 2007). This sedimentary wedge consists primarily of eroded clays, sands, and gravel from the Appalachian mountains, covered with a thin layer of marine sands deposited in a series of sea level changes. Chesapeake Bay also contains an impact crater estimated to be 35 million years old, stretching 90 km in diameter (USGS Fact Sheet 049-98). As the plains were uplifted, numerous peninsulas were incised by stream cutting, with the larger rivers forming tidal rivers.

Virginia Beach's enormous popularity is derived from 28 miles of beach front which, according to the Guinness Book of Records, is the largest pleasure beach in the world. The present-day beach extent is shown in Figure 5. Since the late 1920s, the city has experienced tremendous growth both as a resort and as a center of industry for the East Coast. Virginia Beach is the largest city in Virginia. Figure 6 shows the population density for the city, with many high-density tracts right along the coveted beach front area.

The nearest Nation Ocean Service tide gage is the Chesapeake Bay Bridge Tunnel station (e.g. Allen et al., 2008), which is about 18 km northwest of the warning point for Virginia Beach. According to the station, the mean rage of tide is 0.777m. The mean high water is used as the reference level for the forecast model to provide a worst case for inundation forecast.

Although no tsunami run-up data were found for Virginia Beach from NGDC's database, due to its low lying coastal area, high coastal population density and the potential tsunami hazard from Caribbean Sea subduction zone earthquakes, Virginia Beach is in need of a forecast model to aid site-specific evacuation decisions.

3.2 Bathymetry and Topography

In January of 2007, NOAA's National Geophysical Data Center (NGDC) developed a 1/3″ digital elevation model (DEM) covering the Virginia Beach, Virginia region (Taylor et al., 2007). At the latitude of Virginia Beach, Virginia (36°51′ N, 76°00′ W) 1/3 arc-second of latitude is equivalent to 10.27 meters; 1/3 ″of longitude is equivalent to 8.26 meters. The details of this "base" DEM development can be found in Taylor *et al*. (2007), and an overview is provided here:

The DEM was generated from diverse digital datasets in the region (sources shown in Fig. 7) and were designed to represent modern morphology. The digital data were obtained from several U.S. federal, state and local agencies:

(1) Bathymetry data include

- NOAA's National Ocean Service (NOS) hydrographic survey data
- Recent NOS shallow-water multibeam survey data
- USACE surveys of dredged shipping channels and the Intracoastal Waterway
- NGDC-digitized Atlantic Intracoastal Waterway
- ENC-extracted sounding data

(2) Topography dataset include:

- City of Virginia Beach 2004 LiDAR data with ~2m spacing
- USGS 1999 NED 1/3 to 1 arc-second data.

All dataset were shifted to the World Geodetic System 1984 (WGS84) horizontal datum and transferred to the MHW vertical datum.

A grid generation algorithm was used to generate 36 arc-second and 60 arc-second grids for the high-resolution reference model, covering the East coast of Virginia. The data consisted largely of the above-referenced 1/3 arc-second Virginia Beach DEM, but outside it's extent, data were also used from the following sources:

- Virginia Beach VA 1/3″
- Morehead City, NC 1/3 ″
- Ocean City, MD 1/3 ″
- Cape Hatteras 1/3 ″
- Savannah GA 1/3 ″
- Atlantic City NJ 1/3 ″
- Nantucket MA 1/3 ″
- Montauk NY 1/3 ″

- Daytona Beach FL 1/3 ″
- Myrtle Beach SC 1/3 ″
- East Coast 9 ″
- Atlantic Test 1 ′ (ETOPO1 from NGDC)

The bathymetry and topography at Virginia Beach used in the development of this forecast model was based on the 1/3″ DEM provided by the National Geophysical Data Center. The author considers it to be a good representation of the local topography/bathymetry. As new digital elevation models become available, the forecast model will be updated and report updates will be posted at:

http://nctr.pmel.noaa.gov/forecast_reports/

3.3 Model Setup

By sub-sampling the DEMs described in section 3.2, two sets of computational grids were derived for Virginia Beach, a reference inundation model and the optimized forecast model.

The reference grids consist of four levels of telescoping grids with increasing resolution (Fig. 8). The A-grid covers the coast of Virginia in 36 arc-second. The B-grid covers Virginia Beach City, Chesapeake Bay and Pamlico Sound in 12 arc-second resolution, and run-up and inundation simulations are computed at the coastline in C grid with full 1/3 arc-second resolution.

To improve the computational speed for operational use, the forecast model needs to reduce the number of grid nodes, while still accurately capturing model dynamics. The Virginia Beach forecast model has three levels of telescoping grids (Fig. 9). Due to the shallow, wide continental shelf offshore, a 60 arc-second resolution was necessary for the forecast A-grid, to propagate the wave from the propagation database (16 arc-second) to the forecast site. An 18 arc-second resolution was used for the forecast B-grid, and run-up and inundation simulations are computed at the coastline in C-grid at 2 arc-second resolution. Figure 8c shows the Virginia Beach warning point at 284.0286°E , 6.8530°N in 6.0 m of water depth.

Grid details at each level and input parameters are summarized in Table 3. As will be discussed in Section 4.1, a small friction coefficient is chosen due to the shallow continental shelf of U.S. East Coast. Reflection boundary conditions imposed at different water depth of 0.5-10m were tested. We have noticed that even with 0.5 m, waves could not propagate into some shallow areas in A- and B- grids. Due to the small friction coefficient, a slightly deep offshore water depth of 5 m is chosen here to make the models stable for all tested scenarios. Therefore, reflection boundary conditions were imposed at 5 meter water depth for the A- and B- grids

All model runs were tested on a DELL PowerEdge R510 computer equipped with two Xeon E5670 processors at 2.93 Ghz, each with 12 MBytes of cache and 32GB memory. The processors are hex core and support hyperthreading, resulting in the computer performing as a 24 processor machine. Additionally, the testing computer supports 10 Gigabit Ethernet for fast network connections. This computer configuration is similar or the same as the configurations of the computers installed at the Tsunami Warning Centers so the compute times should only vary slightly. For a 4-hour event simulation, it takes eight processors 2 hours for the reference model while it takes only ~8 minutes on a single processor for the forecast model.

4 Results and Discussion

4.1 Sensitivity of modeled amplitude to friction coefficients

Accurate simulation of tsunami induced current, run-up and inundation requires high-resolution bathymetry and topography data in the run-up area and good tsunami source and model parameters. Titov *et al*. (2005) have shown that, under these conditions, the MOST run-up and inundation agree quite well with the stereo aerial photo data and field survey data on Okushiri Island by the 12 July 1993 Hokkaido-Nansei-Oki Mw 7.8 earthquake. Wei *et al*. (2012) have also shown excellent agreement between the modeled near-field run-up and inundation and the survey data for the March 11, 2011 Japan tsunami.

At present, one major difficulty is the lack of high quality inundation/run-up and current measurements to verify the accuracy of topography and to calibrate the friction coefficient. Modeling work in similar near-shore geometry has suggested that lowering the friction coefficient for areas with beach slope shallower than 1:50 can have a marked affect on inundation. In this section, we focus on the sensitivity of modeled amplitude at Virginia Beach to the friction coefficient.

Figure 11 shows different Manning roughness coefficients (n) can affect the tsunami amplitude and inundations significantly at Virginia Beach for a Puerto Rico magnitude-9.3 tsunami. The testes are done using a set of testing grids with resolutions of 120, 18 and 3 arc-second for the A- B and C grids respectively. The Manning roughness coefficient (n) ranges from 0-0.04. The roughness coefficient can affect results not only within C-grid, but also the amplitudes in the B-grid, and those over the shallow continental shelf (depth less than 100-200m) in the A-grid.

The above results indicate friction does influence the results, and it is very difficult to provide the friction coefficient that is reasonable, since there are actually many factors involved -- not only the roughness itself, but the approximation inherent in the shear stress of the flow, turbulent parameterization, and numerical dissipation approximation. The Manning formula used in the MOST model is an engineering empirical “roughness” estimation only. Using any specific number is not really validated in any way for tsunamis and the choice of a specific coefficient for a specific site is fairly arbitrary. The goal is to account for friction that we know exists, and to improve the stability of the runs for a particular site. The best way to validate the friction is with observation data, but such data is rarely available for east coast sites, especially for inundation. For our application, we want to be conservative in choosing the coefficient.

So for Virginia Beach, with beach slopes sometimes approaching 1:75, we use the smallest possible friction value that produces consistent stable computations: n=0.01. It should be noted for MOST version 4, n can be set to different values for different grids. For example we can set n=0 for the A- and B-grids, while a relatively larger n can be chosen for C-grid to stabilize the model for large run-up/run-down. Model locations with steeper beach profiles and deeper shelf depths may be best run with n set to the more common west-coast value of n=0.025-0.03.

4.2 Model verification and stability testing

Figure 2 shows the maximum amplitude offshore at Virginia Beach from the propagation database. The Puerto Rico trench can easily be identified as the most hazardous tsunami-generating area for Virginia Beach, with large offshore amplitudes and fast arrivals. A set of nine simulated magnitude-9.3 tsunamis was selected here for further examination (Table 3). Each simulated earthquake involves 20 tsunami source functions (10 pairs) and a uniform 25-m coefficient. Both the Virginia Beach reference and forecast models were tested with the nine scenarios.

Figure 12 show the amplitude (η) time series at the Virginia Beach warning point for the simulated magnitude-9.3 tsunamis. Table 3 summarize the η_{max} and uncertainty due to different model setup. The uncertainty are computed as:

$$uncertainty = \frac{\left|\eta_{\max 2} - \eta_{\max 1}\right|}{\eta_{\max 1}} \times 100$$

where η_{max1} and η_{max2} are the maximum water surface elevation computed by the reference and forecast models respectively.

Based on the nine scenarios, the uncertainty in η_{max} at the Virginia Beach warning point computed by the forecast model is within 22%. The largest error of 1.07 m in η_{max} among the tested tsunamis occurs in the 5th, Puerto Rico scenario, where η_1 =4.94 m and η_{max2} =6.01m cm, 22% overestimated (Fig. 12.5). The arrival time of the maximum amplitudes can be 10-30 hours after the first wave. The forecast model was tested by running the model up to 30 hours after the earthquake to ensure capturing the maximum in the run.

Figure 13 shows the model is also stable for a micro tsunami (about 0.22mm in amplitude) generated by a magnitude-6.8 earthquake in the distant South Sandwich Islands subduction zone. Accurate forecasting of small tsunamis gives forecasters the confidence to issue an all-clear for small events.

Wavelet analyses were performed for the scenarios to explore peak resonant periods, T_P, at the Virginia Beach warning point. Figures 14 show the amplitude spectrograms. The site shows relatively long and broad resonant periods from 0.5 to 4.5 hours (Fig. 15b).

Figure 16 shows both the reference and forecast models produced similar maximum water elevation, maximum current and inundation limit in the study area. Large maximum currents can be seen in both the reference and forecast models for many of the scenarios, especially over the shallow areas.

Tsunami waves in the study area vary significantly for the 9 magnitude-9.3 scenarios. The 5th Puerto Rico scenario produces waves with amplitudes over 6 meters at the Virginia Beach warning point. The inundation and run-up for these aphysical synthetic test sources can be significant, but model shows stable characteristics even for these large amplitude overland flows. The 4th Dominica scenario generated wave amplitudes of over 2 meters at Virginia Beach. These results show the complexity and high nonlinearity of tsunami waves nearshore, which again demonstrate the value of high-resolution forecast model for providing accurate site-specific forecast details.

5 Summary and Conclusions

A tsunami forecast model was developed for Virginia Beach, Virginia. The computational grids for the Virginia Beach forecast model were derived from the best available bathymetric and topographic data sources. The forecast model is optimally constructed at 2 arc-second resolution, to enable a 4 hour inundation simulation within ~8 minutes of computational time using a single processor. A reference inundation model of higher resolution of 1/3 arc-second was also developed in parallel, to provide a modeling reference for the forecast model. Both models were tested for a set of nine simulated magnitude-9.3 tsunamis. One point at the Virginia Beach, 284.0286°E , 6.8530°N in 6.0 meters of water depth, was chosen as the warning point for the site.

The modeled amplitude, inundation and current are sensitive to the friction coefficient. Due to the lack of data for calibration and to be on the conservative side, we use the smallest possible friction value, n=0.01, that produces consistent stable computations for both models.

Based on the nine tested scenarios, the uncertainty in η_{max} due to grid setup at the Virginia Beach warning point computed by the forecast model is within 22%. The modeled inundation limits and currents agree reasonably well between the forecast and reference models. Wavelet analyses show broad and relatively long resonant periods from 0.5 to several hours for the site.

Mega-tsunamis from the Puerto Rico subduction zone can cause appreciable inundation at the site. The results also highlight the fact that, due to the broad continental shelf on the east coast, the maximum wave can arrive 12-30 hours after the first wave, requiring longer warning duration for such events. The simulated magnitude-9.3 tsunamis show an impressive local variability of tsunami amplitudes at Virginia Beach, and indicate the complexity of forecasting tsunami amplitudes at this coastal location. It is essential to use high-resolution models in order to provide enough accuracy to be useful for coastal tsunami forecasts and practical guidance.

Acknowledgements

The authors thank Jean C. Newman for comments, discussion, assistance and preparing the cover image; Vasily V. Titov and Yong Wei for discussion; Lindsey Wright for SIFT testing; David. R. Borg-Breen and Nancy N. Soreide for IT support; Sandra Bigley for comments and editing; and National Geographic Data Center for Virginia Beach DEM.

Funding for this publication and all work leading to development of a tsunami forecast model for Virginia Beach was provided by the National Oceanic and Atmospheric Administration. This publication was partially funded by the Joint Institute for the Study of the Atmosphere and Ocean (JISAO) under NOAA Cooperative Agreement No. NA10OAR4320148 and NA08OAR4320899, JISAO Contribution No. 2094. This is PMEL Contribution No. 3407.

References

Allen, A.L., N.A. Donoho, S.A. Duncan, S.K. Gill, C.R. McGrath, R. S. Meyer, M. R. Samant (2008), NOAA's National Ocean Service Supports Tsunami Detection and Warning through Operation of Coastal Tide Stations, In: Solutions to Coastal Disasters 2008 /Tsunamis/: Proceedings of Sessions of the Conference, April 13-16, 2008 Turtle Bay, Oahu, Hawaii. American Society of Civil Engineers.

Arcas, D., and B. Uslu (2010): A Tsunami Forecast Model for Crescent City, California. NOAA OAR Special Report, PMEL Tsunami Forecast Series: Vol. *2*, 112 pp, Gov. Print. Off., Seattle, Wash.

Bernard, E.N., H.O. Mofjeld, V.V. Titov, C.E. Synolakis, and F.I. González (2006): Tsunami: Scientific frontiers, mitigation, forecasting, and policy implications. Proc. Roy. Soc. Lon. A, 364(1845), doi: 10.1098/rsta.2006.1809, 1989–2007.

Bernard, E., and V.V. Titov (2007): Improving tsunami forecast skill using deep ocean observations, Mar. Technol. Soc. J., 40(3), 23–26.

Gica E., Spillane, M.C., Titov, V.V., Chamberlin, C.D. and Newman, J.C. (2008): Development of the forecast propagation database for NOAA's Short-Term Inundation Forecast for Tsunamis (SIFT). NOAA Tech. Memo. OAR PMEL-139, 89pp.

Gusiakov, V.K. (1978): Static displacement on the surface of an elastic space. Ill-posed problems of mathematical physics and interpretation of geophysical data, Novosibirsk, VC SOAN SSSR, 23–51 (in Russian).

Gonzalez, F.I., E.N. Bernard, C. Meinig, M. Eble, H.O. Mofjeld, and S. Stalin (2005): The NTHMP tsunameter network. *Nat. Hazards*, 35(1), Special Issue, U.S. National Tsunami Hazard Mitigation Program, 25-39.

Liu, P. L.-F. (2009): Tsunami modeling—Propagation, in The Sea, vol. 15, edited by E. Bernard and A. Robinson, chap. 9, pp. 295– 319, Harvard Univ. Press, Cambridge, Mass.

Meinig, C., S.E. Stalin, A.I. Nakamura, F. González, and H.G. Milburn (2005): Technology Developments in Real-Time Tsunami Measuring, Monitoring and Forecasting. In Oceans 2005 MTS/IEEE, 19–23 September 2005, Virginia, D.C.

National Geophysical Data Center, Global Tsunami Database (2000 BC to present): http://www.ngdc.noaa.gov/seg/hazard/tsu_db.shtml

Okada, Y., 1985, Surface deformation due to shear and tensile faults in a half-space.*Bull. Seismol. Soc. Am*., 75, 1135-1154.

Percival, D.B., D.W. Denbo, M.C. Eble, E. Gica, H.O. Mofjeld, M.C. Spillane, L. Tang, and V.V. Titov (2011): Extraction of tsunami source coefficients via inversion of DART® buoy data. *Nat. Hazards*, 58(1), doi: 10.1007/s11069-010-9688-1, 567–590.

Satake, K., Y. Hasegawa, Y. Nishimae and Y. Igarashi (2008), Recent Tsunamis That Affected the Japanese Coasts and Evaluation of JMA's Tsunami Warnings. OS42B-03, AGU Fall Meeting, San Francisco.

Spillane, M.C., E. Gica, V.V. Titov, and H.O. Mofjeld (2008): Tsunameter network design for the U.S. DART® arrays in the Pacific and Atlantic Oceans, Tech. Memo, OAR PMEL-143, 165pp., Gov. Print. Off., Seattle, Wash.

Synolakis, C.E., E.N. Bernard, V.V. Titov, U. Kânoğlu, and F.I. González (2008): Validation and verification of tsunami numerical models. Pure Appl. Geophys., 165(11–12), 2197–2228.

Tang, L., C. Chamberlin, E. Tolkova, M. Spillane, V.V. Titov, E.N. Bernard, and H.O. Mofjeld (2006): Assessment of potential tsunami impact for Pearl Harbor, Hawaii. NOAA Tech. Memo. OAR PMEL-131.

Tang, L., C. Chamberlin and V.V. Titov, (2008a): Developing tsunami forecast inundation models for Hawaii: procedures and testing, *NOAA Tech. Memo., OAR PMEL -141*, 46 pp.

Tang, L., V.V. Titov, Y. Wei, H.O. Mofjeld, M. Spillane, D. Arcas, E.N. Bernard, C. Chamberlin, E. Gica, and J. Newman (2008b): Tsunami forecast analysis for the May 2006 Tonga tsunami. J. Geophys. Res., 113, C12015, doi: 10.1029/2008JC004922.

Tang, L., V. V. Titov, and C. D. Chamberlin (2009): Development, Testing, and Applications of Site-specific Tsunami Inundation Models for Real-time Forecasting. *J. Geophys. Res*., 114, C12025, doi:10.1029/2009JC005476..

Tang, L., V.V. Titov and C.D. Chamberlin (2010): A Tsunami Forecast Model for Hilo, Hawaii. NOAA OAR Special Report, PMEL Tsunami Forecast Series: Vol. 1, 44 *pp.*

Tang, L., V. V. Titov, E. Bernard, Y. Wei, C. Chamberlin, J. C. Newman, H. Mofjeld, D. Arcas, M. Eble, C. Moore, B. Uslu, C. Pells, M. C. Spillane, L. M. Wright, and E. Gica (2012): Direct energy estimation of the 2011 Japan tsunami using deep-ocean pressure measurements. *J. Geophys. Res., 117*, C08008, doi:10.1029/2011JC007635.

Taylor, L.A., B.W. Eakins, K.S. Carignan, R.R. Warnken, T. Sazonova, D.C. Schoolcraft, and G.F. Sharman (2007): Digital Elevation Model for Virginia Beach, Virginia: Procedures, Data Sources and Analysis, NOAA, National Geophysical Data Center, Boulder, Colorado

Titov, V. V., C. W. Moore, D. J. M. Greenslade, C. Pattiaratchi, R. Badal, C. E. Synolakis, and U. Kânoğlu (2011): A new tool for inundation modeling: Community Modeling Interface for Tsunamis (ComMIT). Pure Appl. Geophys., 168, 2121–2131, doi:10.1007/s00024-011-0292-4.

Titov, V. V., and L. Tang (2011): Estimating tsunami magnitude in real time usingttsunameter data, paper presented at XXV IUGG General Assembly, Melbourne, Victoria, Australia, 28 Jun to 7 Jul.

Titov, V.V. (2009): Tsunami forecasting. Chapter 12 in The Sea, Volume 15: Tsunamis, Harvard University Press, Cambridge, MA and London, England, 371–400.

Titov, V.V., F.I. González, E.N. Bernard, M.C. Eble, H.O. Mofjeld, J.C. Newman, and A.J. Venturato (2005): Real-time tsunami forecasting: Challenges and solutions. *Natural Hazards*, 35(1), Special Issue, U.S. National Tsunami Hazard Mitigation Program, 41–58.

Titov, V. V., Mofjeld, H. O., Gonza´ lez, F. I., and Newman, J. C.: 2001, Offshore forecasting of Virginian tsunamis in Hawaii. In: G. T. Hebenstreit (ed.), Tsunami Research at the End of a Critical Decade. Birmingham, England, Kluwer Acad. Pub., Netherlands, pp. 75–90.

Titov, V.V., H.O. Mofjeld, F.I. Gonzalez and J.C. Newman (1999): Offshore forecasting of Virginia-Aleutian subduction zone tsunamis in Hawaii. NOAA Technical Memorandum. ERL PMEL-114, January 1999, 22 pp.

Titov, V.V. and C.S. Synolakis (1998): Numerical modeling of tidal wave runup. *Journal of Waterway, Port, Coastal and Ocean Engineering*, ASCE, 124(4), 157-171.

Titov, V.V. and F.I. Gonzalez (1997): Implementation and testing of the Method of Splitting Tsunami (MOST) model. NOAA Technical Memorandum. NOAA Pacific Marine Environmental Laboratory, ERL PMEL-112, Nov. 1997, 11 pp.

Tolkova, E. (2007): Compression of MOST Propagation Database. NOAA Tech. Memo. OAR PMEL-134, NTIS: PB2007-108218, 9 pp., Gov. Print. Off., Seattle, Wash.

USGS Fact Sheet 049-98, The Chesapeake Bay Bolide Impact: A New View of Coastal Plain Evolution, http://pubs.usgs.gov/fs/fs49-98/index.html.

Wei, Y., E. Bernard, L. Tang, R. Weiss, V. Titov, C. Moore, M. Spillane, M. Hopkins, and U. Kânoğlu (2008): Real-time experimental forecast of the Peruvian tsunami of August 2007 for U.S. coastlines. Geophys. Res. Lett., 35, L04609, doi: 10.1029/2007GL032250.

Wei, Y., and D. Arcas (2010): A tsunami forecast model for Kodiak, Alaska. NOAA OAR Spec. Rep./PMEL Tsunami Forecast Ser. 4, 96 pp., Gov. Print. Off., Seattle, Wash.

Wei, Y., C. Chamberlin, V.V. Titov, L. Tang, and E.N. Bernard (2012): Modeling of 2011 Japan Tsunami - lessons for near-field forecast. Pure Appl. Geophys., doi: 10.1007/s00024-012-0519-z.

Whitmore, P.M. (2003): Tsunami amplitude prediction during events: A test based on previous tsunamis. In *Science of Tsunami Hazards*, 21, 135–143

Tables

Table 1 Tsunami source functions in the Pacific, Atlantic and Indian Oceans.

Source Zone			Tsunami source functions		Run time
No.	**Abbr.**	**Name**	**Line/zone**	**Numbers**	**(hour)**
1	ACSZ	Aleutian-Alaska-Canada-Cascadia	BAZYXW	184	24
2	CSSZ	Central-South American	BAZYX	382	30
3	EPSZ	East Philippines	BA	44	30
4	KISZ	Kamchatka-Kuril-Japan Trench-Izu Bonin-Marianas-Yap	BAZYXW	229	24
5	MOSZ	Manus Ocean Convergence Boundary	BA	34	24
6	NVSZ	New Britain-Solomons-Vanuatu	BA	74	24
7	NGSZ	North New Guinea	BA	30	30
8	NTSZ	New Zealand-Kermadec-Tonga	BA	81	24
9	NZSZ	South New Zealand	BA	14	30
10	RNSZ	New Ryukus-Kyushu-Nankai	BA	44	24
11	KBSZ	Kamchatskii-Bering Source Zone	BAZ	13	24
			Subtotal:	**1129**	
12	ATSZ	Atlantic	BA	214	36
13	SSSZ	South Sandwich	BAZ	33	36
			Subtotal:	**247**	
14	IOSZ	Adaman-Nicobar-Sumatra-Java	BAZY	307	24
15	MKSZ	Makran	BA	20	24
16	WPSZ	West Philippines	BA	22	24
			Subtotal:	**349**	
			Total:	**1725**	

Table 2 MOST setups for the Virginia Beach reference and forecast models.

Grid	Region	Reference Model			Forecast model		
		Coverage Lon. (^{o}E) Lat. (^{o}N)	**Cell Size (")**	**Time Step (sec)**	**Coverage Lon. (^{o}E) Lat. (^{o}N)**	**Cell Size (")**	**Time Step (sec)**
A	Virginia	281.9241-289.6941 32.5007-41.3507	36 (778x886)	3.5	281.9224-289.7057 32.6774-41.344	60 (468x521)	5.2
B	Virginia	282.8707-285.6541 34.764-39.6474	12 (836x1466)	1.5	283.5391-284.7141 36.1024-37.9324	18 (236x367)	5.2
C	Virginia Beach	283.9953-284.0796 36.8143-36.9476	1/3 (911x1441)	0.4	283.9686-284.0791 59.5064-59.6647	2 (200x354)	2.6
Minimum offshore depth (m)		5			5		
Water depth for dry land (m)		0.1			0.1		
Friction coefficient (n^2)		0.0001			0.0001		
Computational time for a 4-hr simulation		~ 2 hours using 8 processors			7.86 min using 1 processor		

Table 3 Sources of the 9 simulated magnitude-9.3 tsunamis and the maximum computed wave crests at the Virginia Beach warning point.

No.	Subd. Zone	Source	alpha	Ref. model etamax (m)	Ref. model tmax (hour)	Forecast Model etamax (m)	Forecast Model tmax (hour)	Error (m)	Error (%)	Location
1	atsz	AB 1- 10	25	0.45	15.774	0.45	31.487	-0.00	0	Panama
2	atsz	AB 12- 21	25	0.53	16.641	0.49	16.680	-0.05	-9	Colombia
3	atsz	AB 22- 31	25	0.96	17.801	0.86	17.805	-0.09	-10	Venezuela
4	atsz	AB 38- 47	25	2.52	4.753	2.47	5.277	-0.05	-2	Dominica
5	atsz	AB 48- 57	25	4.94	4.473	6.01	4.429	1.07	22	Puerto Rico
6	atsz	AB 58- 67	25	1.06	4.663	1.09	4.704	0.03	3	Cayman
7	atsz	AB 68- 77	25	0.23	26.085	0.23	26.002	0.01	0	Gulf of Honduras
8	atsz	AB 82- 91	25	1.33	5.060	1.38	5.095	0.04	3	U.S. Virgin Is.
9	sssz	AB 1- 10	25	0.63	28.460	0.58	28.471	-0.05	-7	South Sandwich Is.

Appendix A.

Since the initial development of the forecast model for Virginia Beach, Virginia, the parameters for the input file for running the forecast and reference models have been changed to reflect changes to the MOST model code. The following appendix lists the new input files for Virginia Beach.

A1. Reference model *.in file for Virginia Beach, Virginia—updated for 2013

```
# -----------   MOST Run 1  -------------
# 0. Preparations
echo '#--------------------------------------------------#'
echo '#                Preprocess MOST input         #'
echo '#--------------------------------------------------#'
set main_dir="/home/tg23/data/tang/sims/virginiabeach/"
set np="8"
setenv OMP_NUM_THREADS $np
set path_w="$main_dir/virgv4_S03_at_ab22T31rb2_c1_05m_fp01_19h/"

set path_e="most4"
set path_src="/grid/tg23/data/tang/src_nc/src_sim_test/virg/S03_at_ab22T31_virg_"

if ( -d $path_w )  then
echo $path_w 'exist'
  cd $path_w
else
  echo Creating directory $path_w
  mkdir $path_w
  cd  $path_w
endif
ln -sf /home/tg23/data/tang/bathy/virginiabeach/virg_rb2//*.nc .
# -----------------------------------------------------------
# 1. Generate INPUT for MOST
# ~~~~~~~~~~~~~~~~~~~~~~~
# ~~~~~~~~~~~A~~~~~~~~~~~
cat > most3_facts_nc.inA<< EOF
0.005     Minimum amplitude of input offshore wave (m):
5        Input minimum depth for offshore (m)
0.1      Input "dry land" depth for inundation (m)
0.0001     Input friction coefficient (n**2)
2         Number of grids
2          Interpolation domain for outer boundary
2          inner boundary
RA_VirginiaBeach_36ss_20130211.nc
RB_VirginiaBeach_12s_20130211.nc
1           Runup flag
```

```
3.5      Input time step (sec)
19543    Input amount of steps
0             COntunue after input stops
9    Input number of steps between snapshots
1     saving inner boundaries every n-th timestep
1       ...Saving grid every n-th node, n=
0       1=initial deformation
EOF
cp most3_facts_nc.inA most3_facts_nc.in
#$path_e A  $path_src most3_facts_nc.in
# ~~~~~~~~~~~~~~~~~~~~~~~
# ~~~~~~~~~~~B~~~~~~~~~~~~
cat > most3_facts_nc.inB<< EOF
0.005    Minimum amplitude of input offshore wave (m):
5       Input minimum depth for offshore (m)
0.1      Input "dry land" depth for inundation (m)
0.0001    Input friction coefficient (n**2)
2        Number of grids
2         Interpolation domain for outer boundary
2         inner boundary
RB_VirginiaBeach_12s_20130211.nc
RC_Virginia_Beach_1_3s_c2_NGDC.nc
1           Runup flag
1.5      Input time step (sec)
45600    Input amount of steps
0             COntunue after input stops
20    Input number of steps between snapshots
1     saving inner boundaries every n-th timestep
1       ...Saving grid every n-th node, n=
0       1=initial deformation
EOF
cp most3_facts_nc.inB most3_facts_nc.in
$path_e B A most3_facts_nc.in
# ~~~~~~~~~~~~~~~~~~~~~~~
# ~~~~~~~~~~~C~~~~~~~~~~~~
cat > most3_facts_nc.inC<< EOF
0.005    Minimum amplitude of input offshore wave (m):
-300       Input minimum depth for offshore (m)
0.1      Input "dry land" depth for inundation (m)
0.0001    Input friction coefficient (n**2)
1        Number of grids
2         Interpolation domain for outer boundary
2         inner boundary
RC_Virginia_Beach_1_3s_c2_NGDC.nc
2           Runup flag
0.38      Input time step (sec)
180000    Input amount of steps
0             COntunue after input stops
79    Input number of steps between snapshots
1     saving inner boundaries every n-th timestep
1       ...Saving grid every n-th node, n=
0       1=initial deformation
EOF
cp most3_facts_nc.inC most3_facts_nc.in
$path_e C B most3_facts_nc.in
```

A2. Forecast model *.in file for Virginia Beach, Virginia—updated for 2013

```
0.0001          Minimum amplitude of input offshore wave (m):
5               Input minimum depth for offshore (m)
0.1             Input "dry land" depth for inundation (m)
0.0001          Input friction coefficient (n**2)
1               runup flag for grids A and B (1=yes,0=no)
300.0    blowup limit
2.6             Input time step (sec)
16615           Input amount of steps
2               Compute "A" arrays every n-th time step, n=
2               Compute "B" arrays every n-th time step, n=
10              Input number of steps between snapshots
0               ...Starting from
1               ...Saving grid every n-th node, n=
FA_Virg_Beach_60s_20130211.ssl
FB_Virg_Beach_18s_20130211.ssl
FC_Virg_Beach_2s_c7_NGDC.ssl
/grid/tg23/data/tang/src_nc/src_sim_test/virg/
./
1 1 1 1         NetCDF output for A, B, C, SIFT
1               Timeseries locations:
3 109 223       Virginia Beach  284.0286E   36.8530N, 6 m depth
```

Figures

Figure 1 (a) Overview of the tsunami Forecast System. System components include tsunameter (DART) network (yellow triangles), pre-computed tsunami source function (unfilled black rectangles) and high-resolution forecast models (red squares). Filled color shows the computed offshore maximum sea surface elevation in m for a simulated magnitude-9.3 Caribbean tsunami (#5). Contours indicate the travel time in hours. 28

Figure 2 Maximum sea surface elevation ($\eta_{\max}$) offshore Virginia Beach from 214 magnitude-7.5 earthquakes. Data were taken from NCTR's pre-computed propagation database for Atlantic Ocean. Heights and colors of the bars represent $\eta_{\max}$ and the first arrival at the offshore point (74.1333°W, 36.9461°N; water depth = 2269 m) respectively. 1-9, locations for nine simulated magnitude-9.3 tsunamis........ 29

Figure 3 Historical tsunamis in Atlantic Ocean and Caribbean Sea (National Geographic Data Center's database). 30

Figure 4 NOAA charts, (a) 13003 and (b) 12208, show Virginia Beach Soundings in fathoms at Mean Lower Low Water. Contour and summit elevation values are in feet above Mean Sea Level........ 32

Figure 4 Aerial photos of Virginia Beach........ 34

Figure 6 Population density at Virginia Beach (2000 Census). 35

Figure 7 Bathymetric and topographic data source overview for the high-resolution Virginia Beach DEM. Image courtesy of Tayler *et al.* (2007). 36

Figure 8 Grid setup for the Virginia Beach reference model. Resolutions are (a) 36", (b) 12" and(c) 1/3" . Red boxes are boundaries of the telescoped grids for the reference model. 39

Figure 9 Grid setup for the Virginia Beach forecast model. Grid resolutions are (a) 60 ", (b) 18", and (c) 2". Red boxes, boundaries of the telescoping grids. Red dot, Virginia Beach warning point (284.0286°E, 36.8530°N; water depth= 6m). 42

Figure 10 Sensitivity of η to friction coefficients. Results were computed by a set of testing grids (Fig. 11) for a magnitude 9.3 Caribbean tsunami. 43

Figure 11 Sensitivity of η_{max} to friction coefficients. Results were computed by a set of testing grids for a magnitude-9.3 Caribbean tsunami........ 44

Figure 12 Modeled η time series by the Virginia Beach reference and forecast models for simulated magnitude-9.3 tsunamis........ 46

Figure 13 Modeled η time series computed by the Virginia Beach forecast model for a simulated micro tsunami. The tsunami was generated from a Magnitude 6.8 earthquake from South Sandwich Islands Subduction (0.1 × B11)........ 47

Figure 14 (a) Modeled η time series at Virginia Beach warning point for the nine simulated magnitude-9.3 tsunamis. (b) Wavelet–derived amplitude spectrogram for the reference model. (c and d) Real part of the spectrograms computed by the reference and forecast models. 52

Figure 15 (a) Forecast uncertainty in the η_{max} at the Virginia Beach warning point. (b) Uncertainty v.s. peak period. η_{max1} and T_{p1}, maximum water elevation and peak period at the warning point from the reference model. η_{max2} and T_{p2}, maximum water surface elevation and peak period at the warning point computed by the forecast model. 53

Figure 16 Maximum water elevation and current computed by the Virginia Beach reference and forecast models for the simulated magnitude-9.3 tsunamis. 62

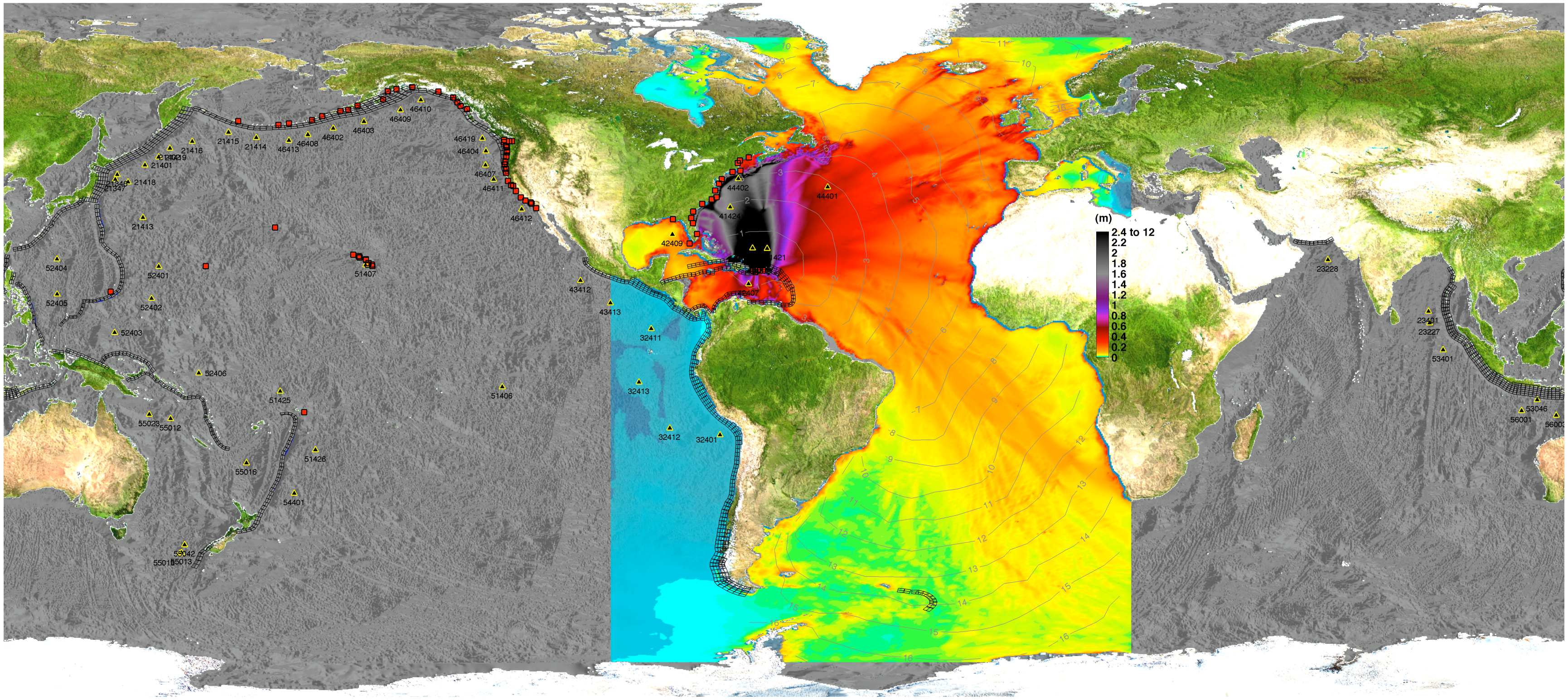

Figure 1 (a) Overview of the tsunami Forecast System. System components include tsunameter (DART) network (yellow triangles), pre-computed tsunami source function (unfilled black rectangles) and high-resolution forecast models (red squares). Filled color shows the computed offshore maximum sea surface elevation in m for a simulated magnitude-9.3 Caribbean tsunami (#5). Contours indicate the travel time in hours.

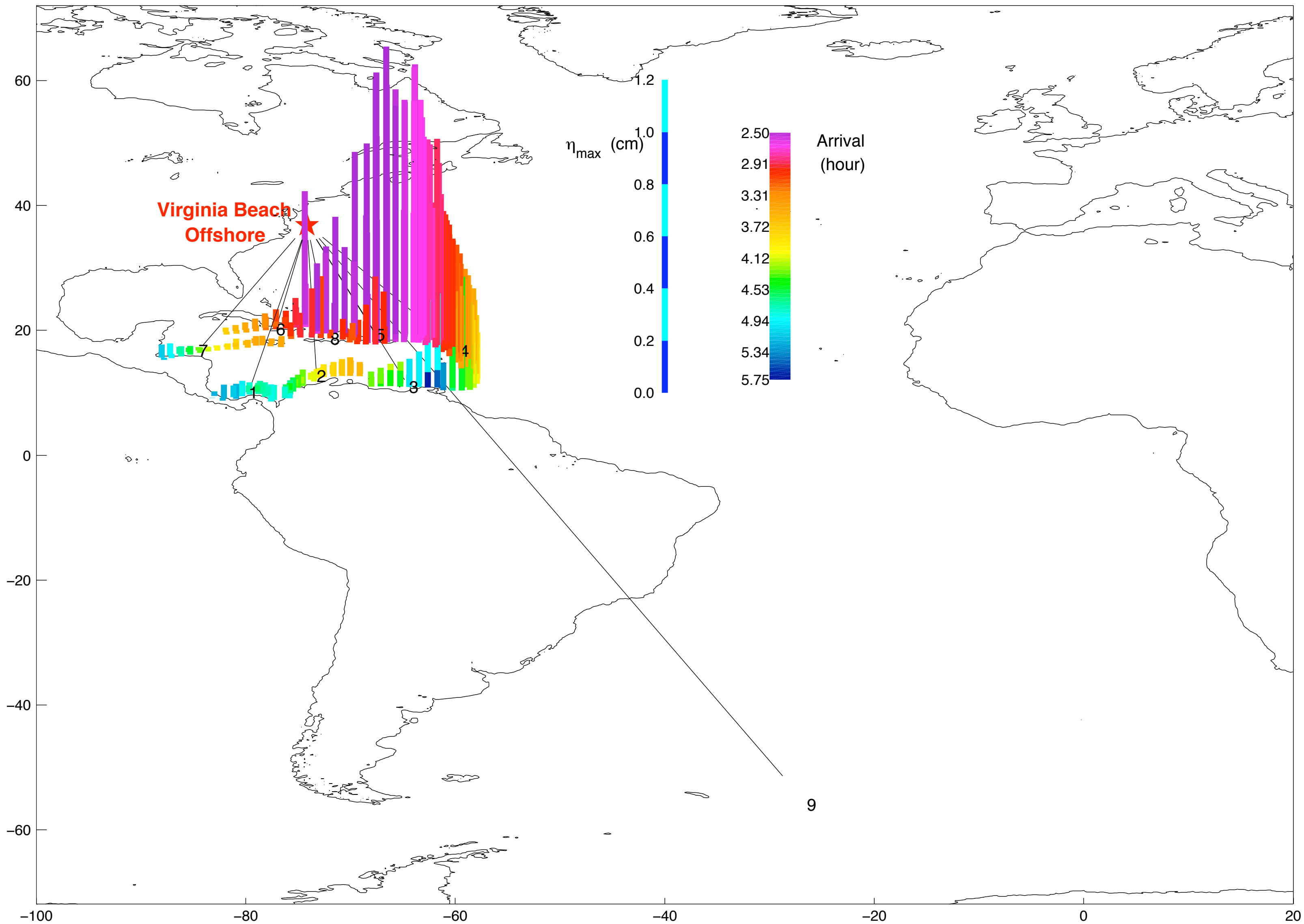

Figure 2 Maximum sea surface elevation (η_{max}) offshore Virginia Beach from 214 magnitude-7.5 earthquakes. Data were taken from NCTR's pre-computed propagation database for Atlantic Ocean. Heights and colors of the bars represent η_{max} and the first arrival at the offshore point (74.1333°W, 36.9461°N; water depth = 2269 m) respectively. 1-9, locations for nine simulated magnitude-9.3 tsunamis.

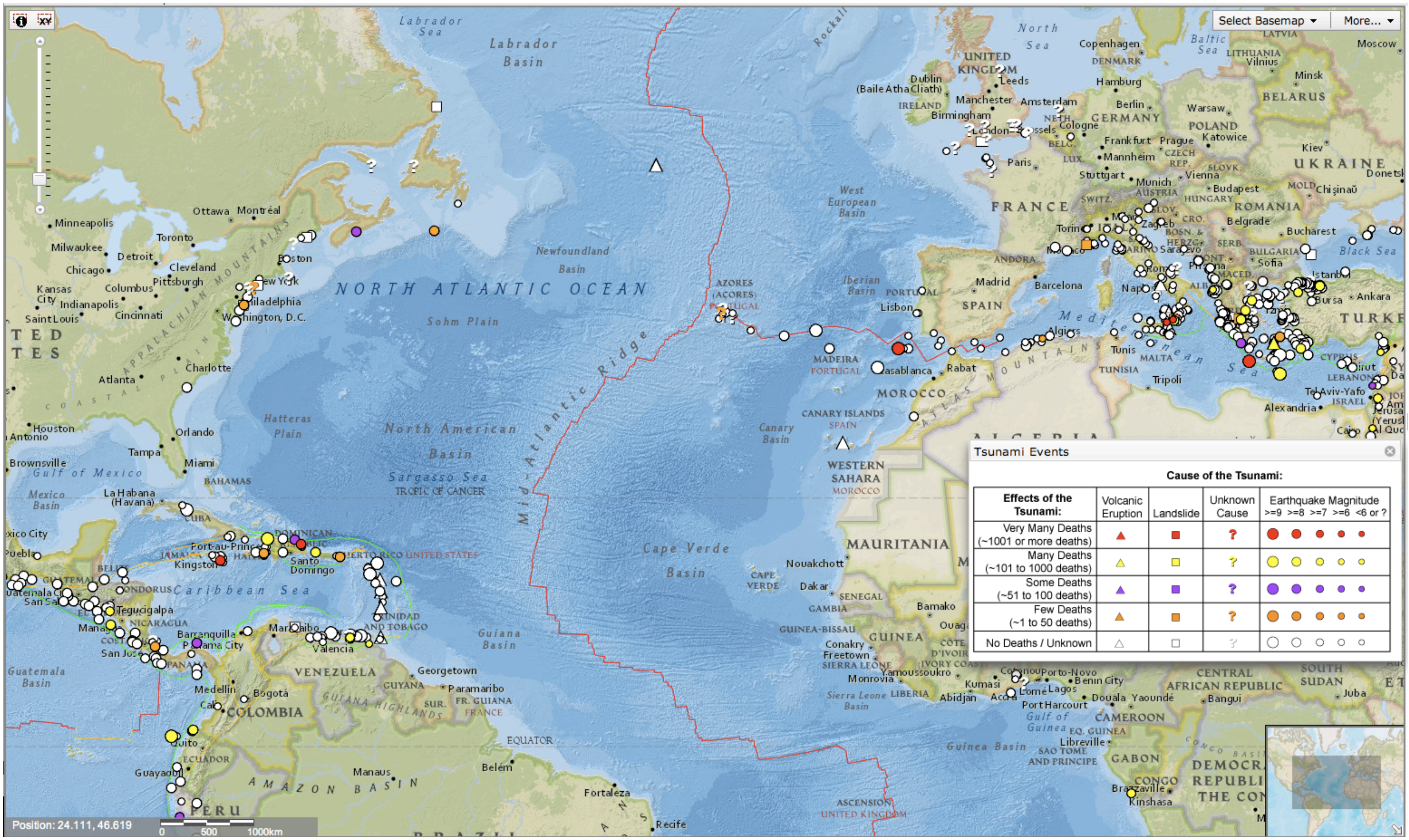

Figure 3 Historical tsunamis in Atlantic Ocean and Caribbean Sea (National Geographic Data Center's database).

(a)

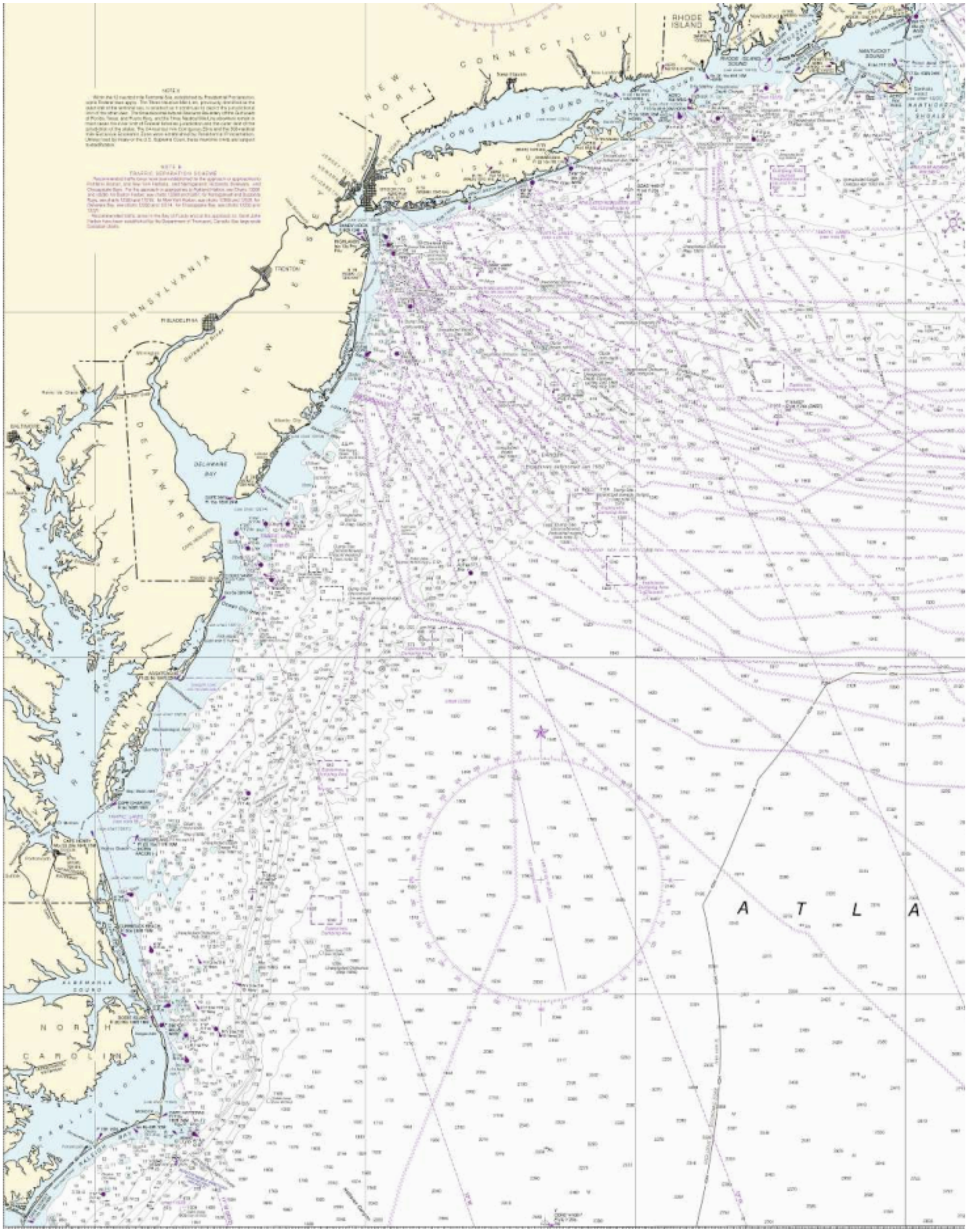
CONNECTICUT
RHODE ISLAND
NEW YORK
LONG ISLAND SOUND
LONG ISLAND
PENNSYLVANIA
TRENTON
PHILADELPHIA
NEW JERSEY
DELAWARE
DELAWARE BAY
BALTIMORE
ALBEMARLE SOUND
NORTH CAROLINA
PAMLICO SOUND
A T L A

(b)

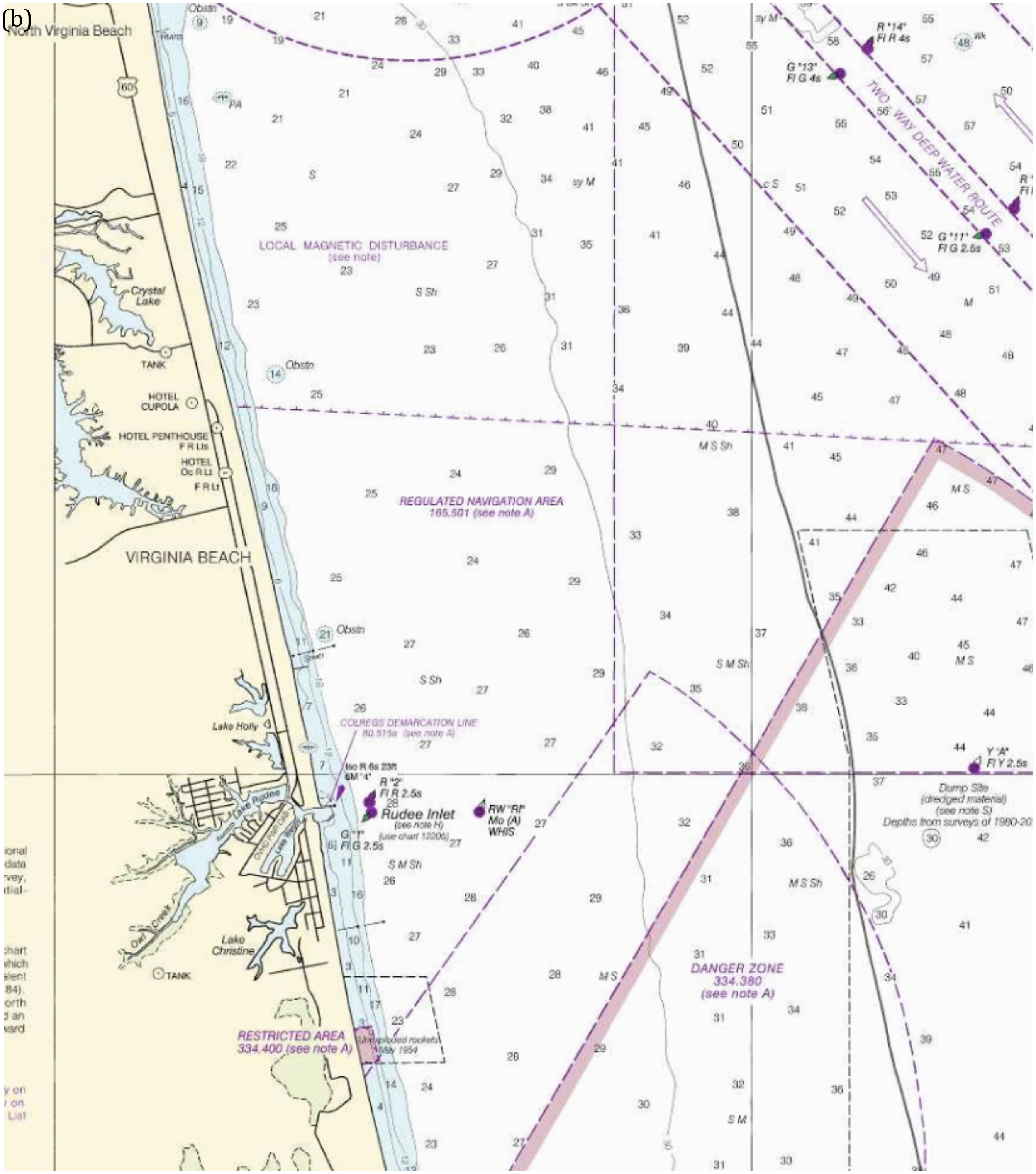

Figure 4 NOAA charts, (a) 13003 and (b) 12208, show Virginia Beach Soundings in fathoms at Mean Lower Low Water. Contour and summit elevation values are in feet above Mean Sea Level.

(a)

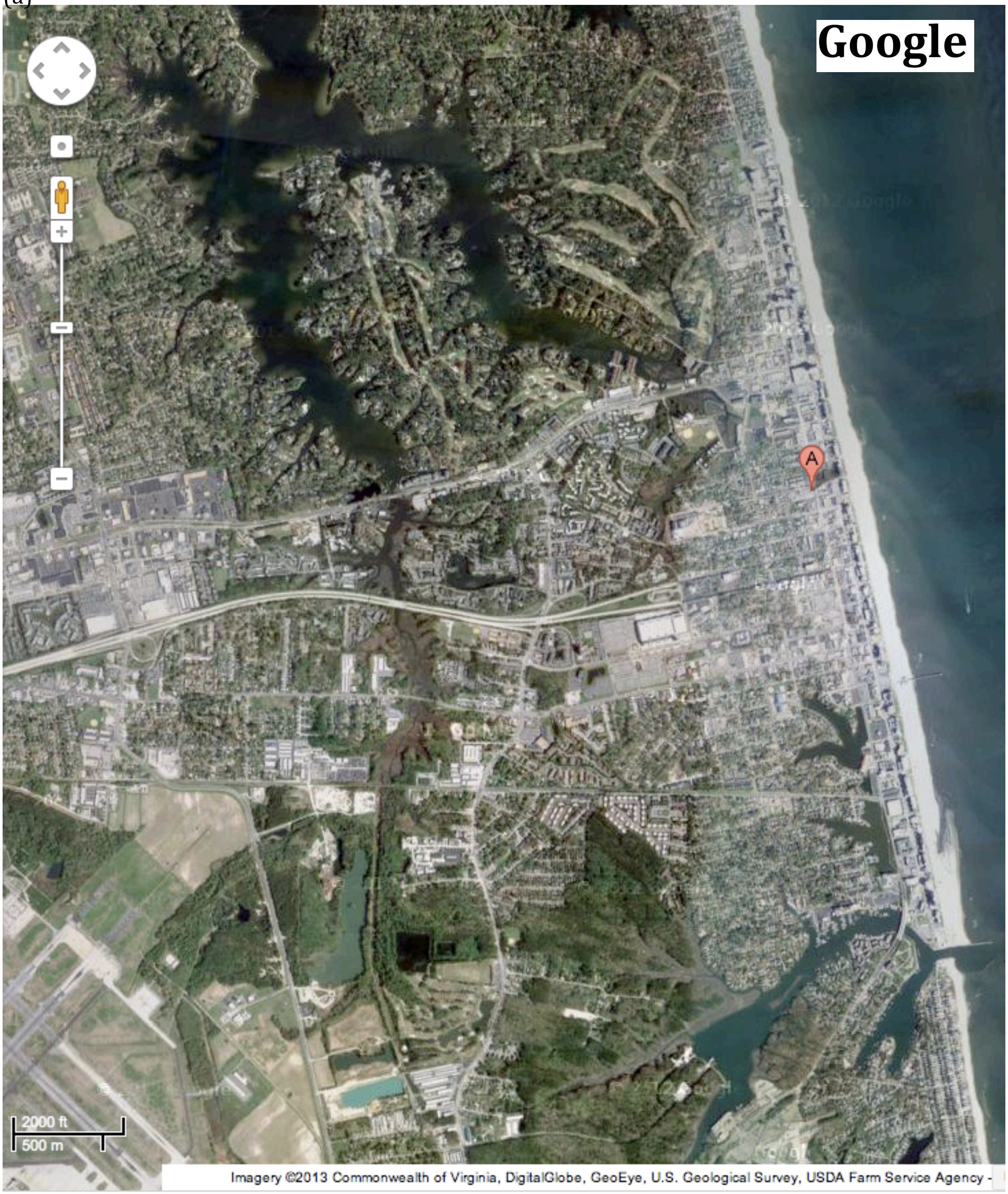
Google
A
2000 ft
500 m
Imagery ©2013 Commonwealth of Virginia, DigitalGlobe, GeoEye, U.S. Geological Survey, USDA Farm Service Agency -

(b)

Figure 5 Aerial photos of Virginia Beach.

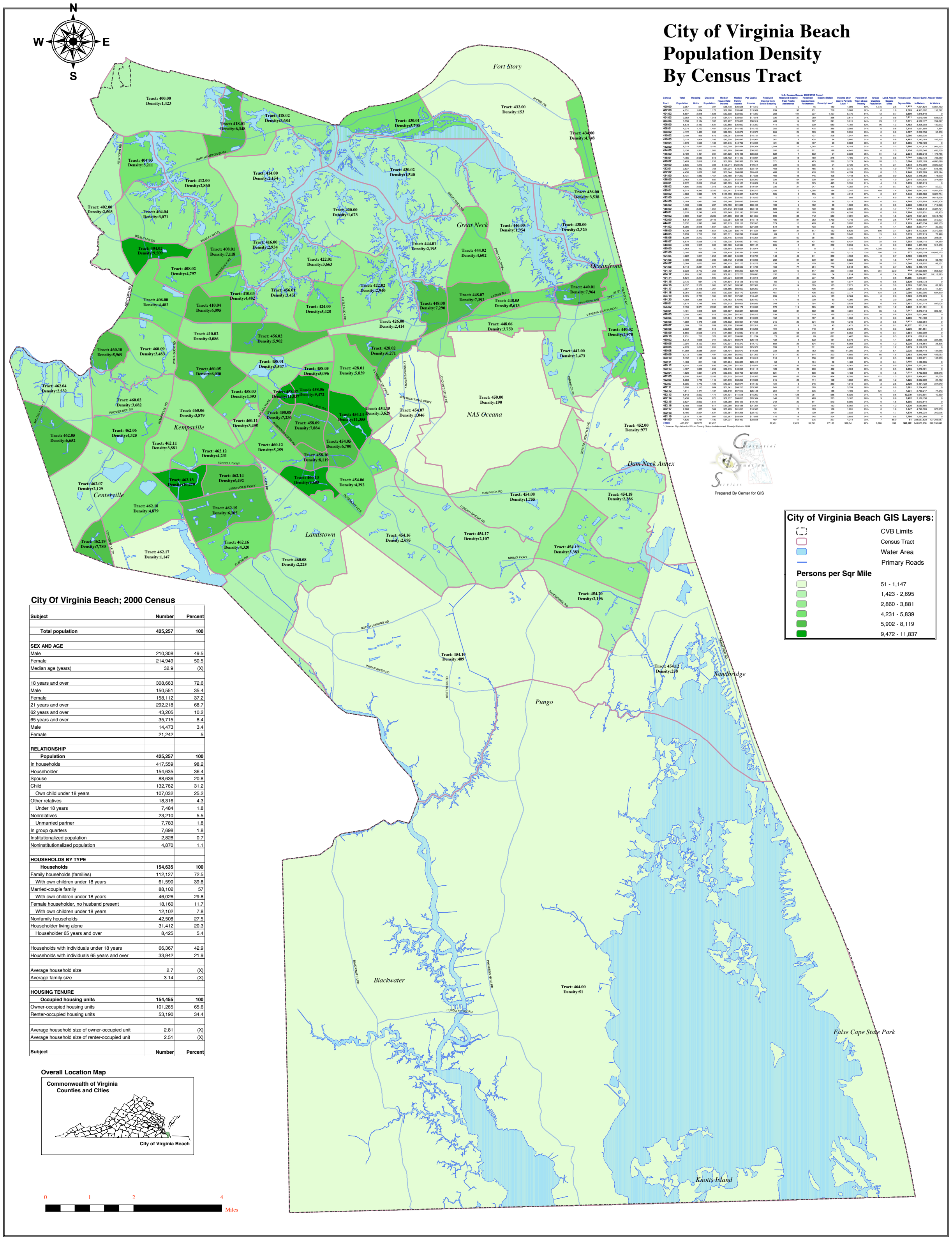

Subject	Number	Percent
Total population	**425,257**	**100**
SEX AND AGE		
Male	210,308	49.5
Female	214,949	50.5
Median age (years)	32.9	(X)
18 years and over	308,663	72.6
Male	150,551	35.4
Female	158,112	37.2
21 years and over	292,218	68.7
62 years and over	43,205	10.2
65 years and over	35,715	8.4
Male	14,473	3.4
Female	21,242	5
RELATIONSHIP		
Population	**425,257**	**100**
In households	417,559	98.2
Householder	154,635	36.4
Spouse	88,636	20.8
Child	132,762	31.2
Own child under 18 years	107,032	25.2
Other relatives	18,316	4.3
Under 18 years	7,484	1.8
Nonrelatives	23,210	5.5
Unmarried partner	7,783	1.8
In group quarters	7,698	1.8
Institutionalized population	2,828	0.7
Noninstitutionalized population	4,870	1.1
HOUSEHOLDS BY TYPE		
Households	**154,635**	**100**
Family households (families)	112,127	72.5
With own children under 18 years	61,590	39.8
Married-couple family	88,102	57
With own children under 18 years	46,026	29.8
Female householder, no husband present	18,160	11.7
With own children under 18 years	12,102	7.8
Nonfamily households	42,508	27.5
Householder living alone	31,412	20.3
Householder 65 years and over	8,425	5.4
Households with individuals under 18 years	66,367	42.9
Households with individuals 65 years and over	33,942	21.9
Average household size	2.7	(X)
Average family size	3.14	(X)
HOUSING TENURE		
Occupied housing units	**154,455**	**100**
Owner-occupied housing units	101,265	65.6
Renter-occupied housing units	53,190	34.4
Average household size of owner-occupied unit	2.81	(X)
Average household size of renter-occupied unit	2.51	(X)
Subject	**Number**	**Percent**

Figure 6 Population density at Virginia Beach (2000 Census).

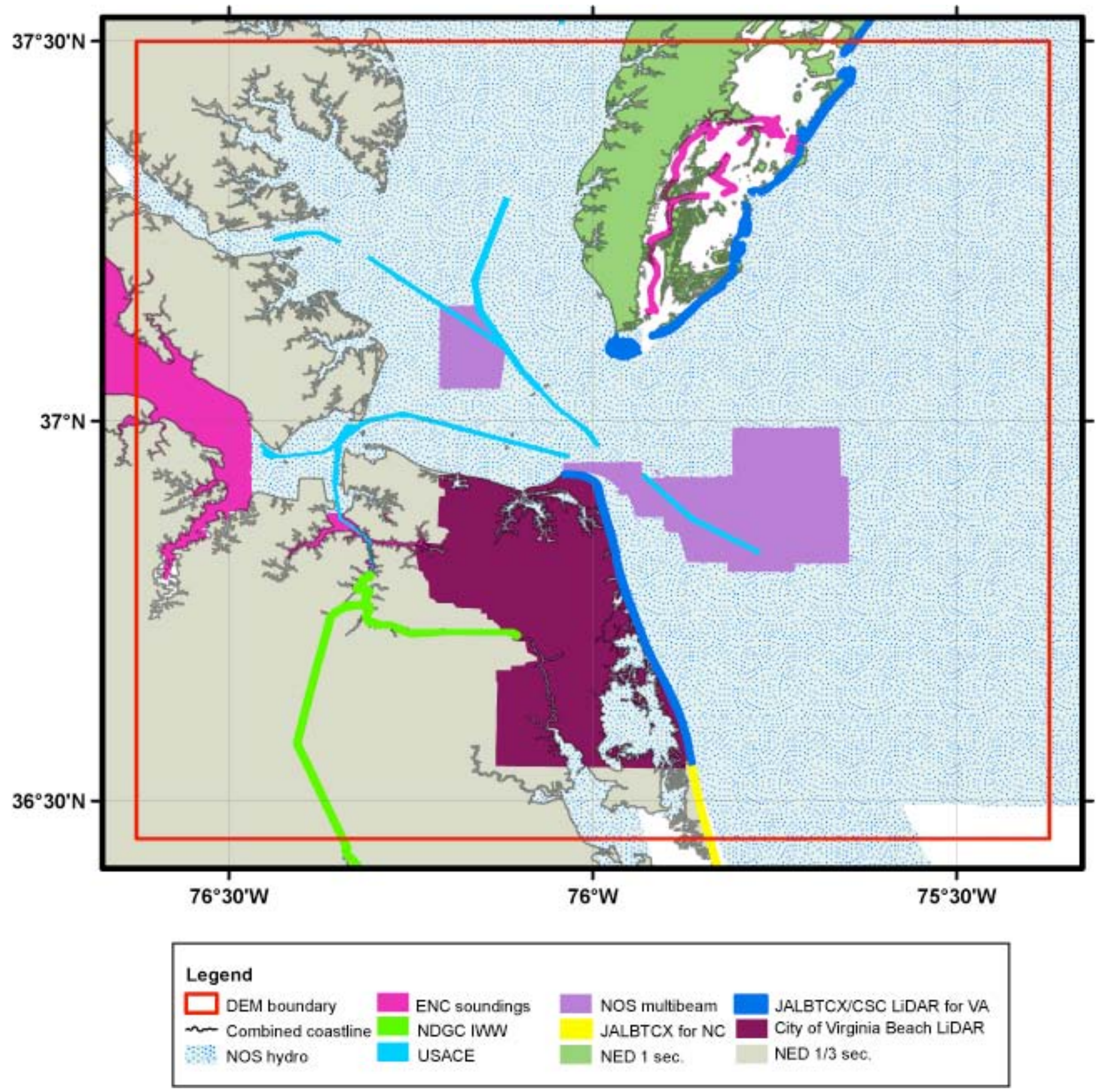

Figure 7 Bathymetric and topographic data source overview for the high-resolution Virginia Beach DEM. Image courtesy of Tayler *et al*. (2007).

(a)

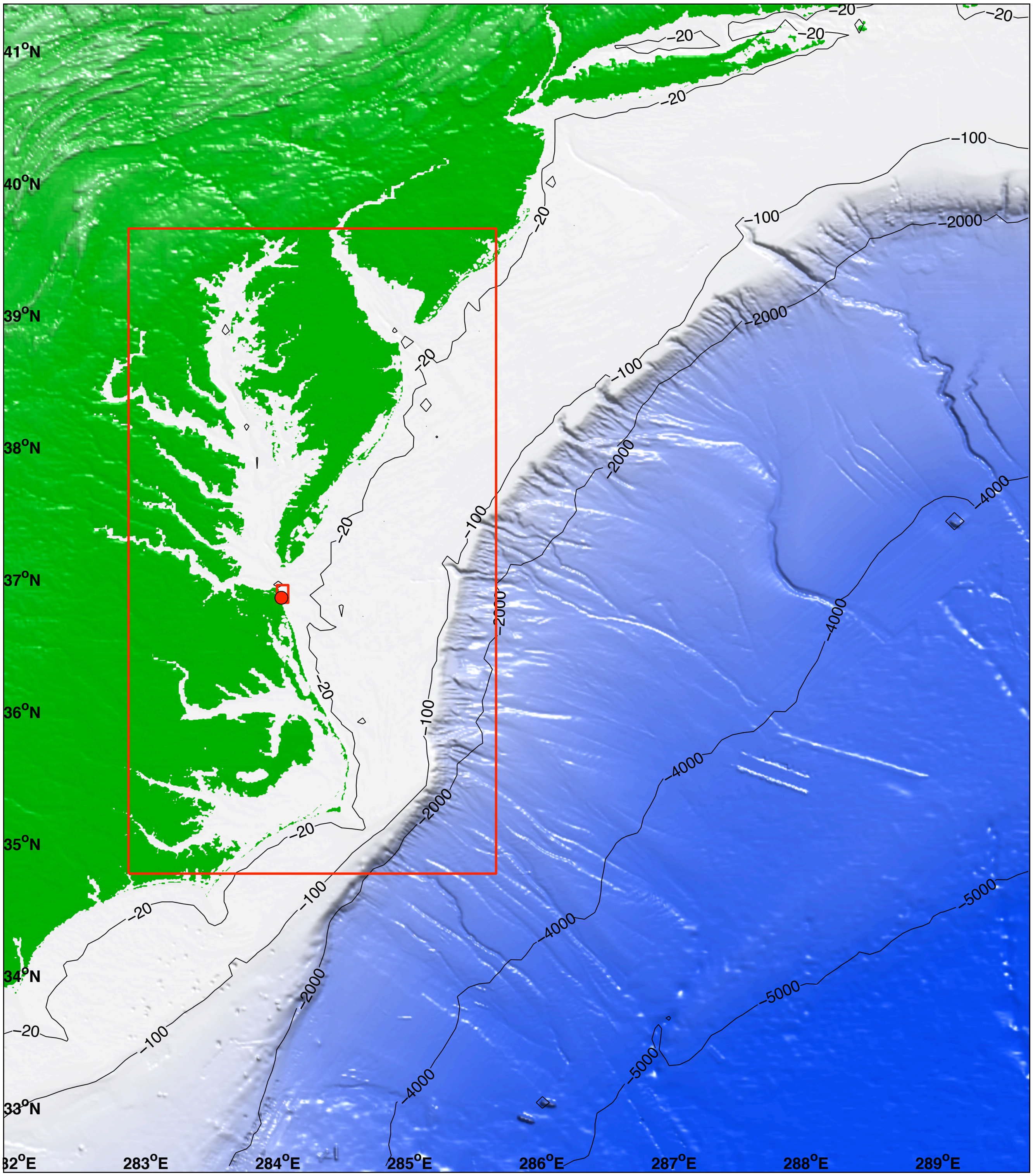
41°N
40°N
39°N
38°N
37°N
36°N
35°N
34°N
33°N
282°E
283°E
284°E
285°E
286°E
287°E
288°E
289°E
−20
−100
−2000
−4000
−5000

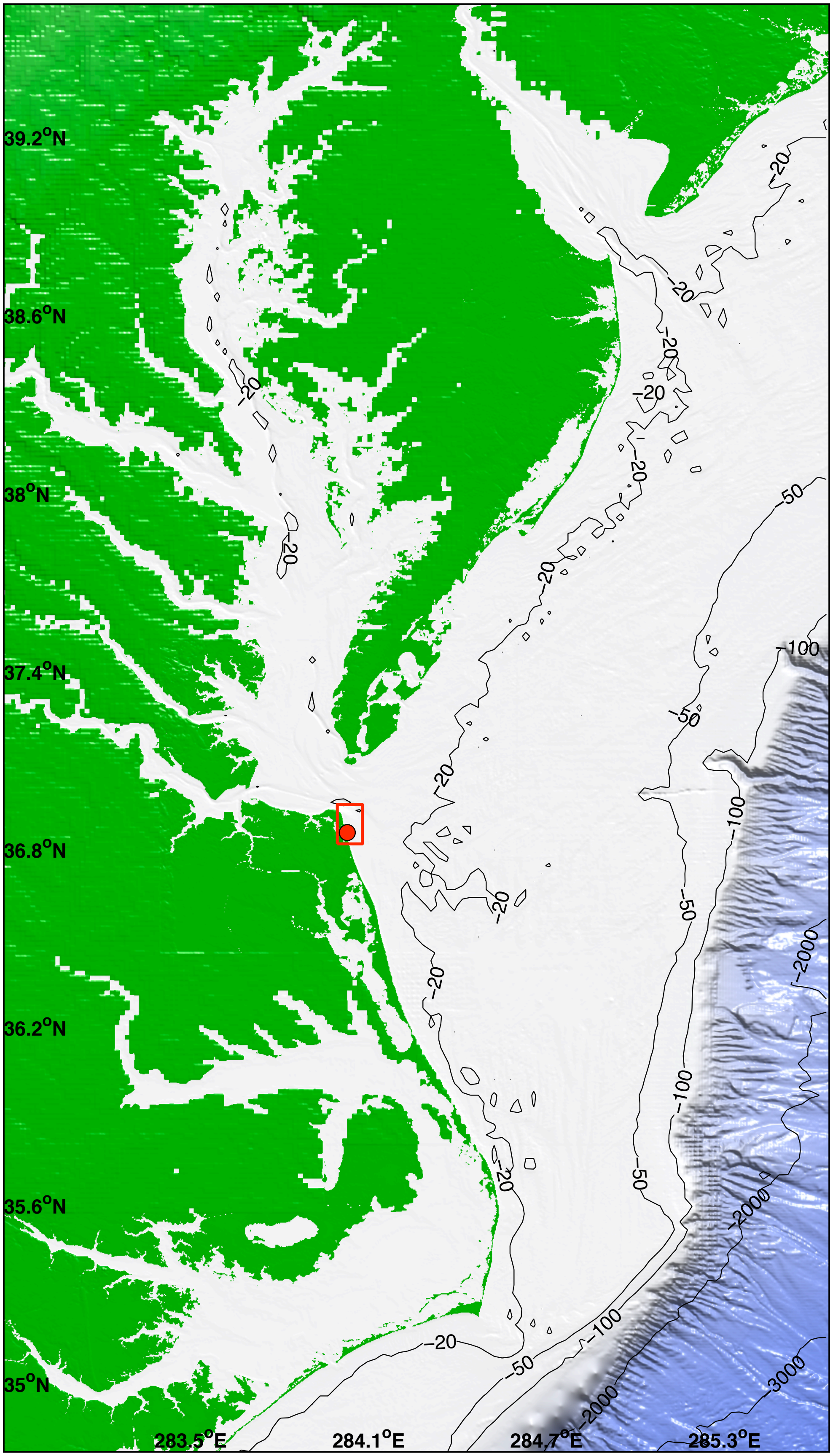
39.2°N
38.6°N
38°N
37.4°N
36.8°N
36.2°N
35.6°N
35°N
283.5°E
284.1°E
284.7°E
285.3°E
-20
-50
-100
-2000
-3000

(b)

(c) 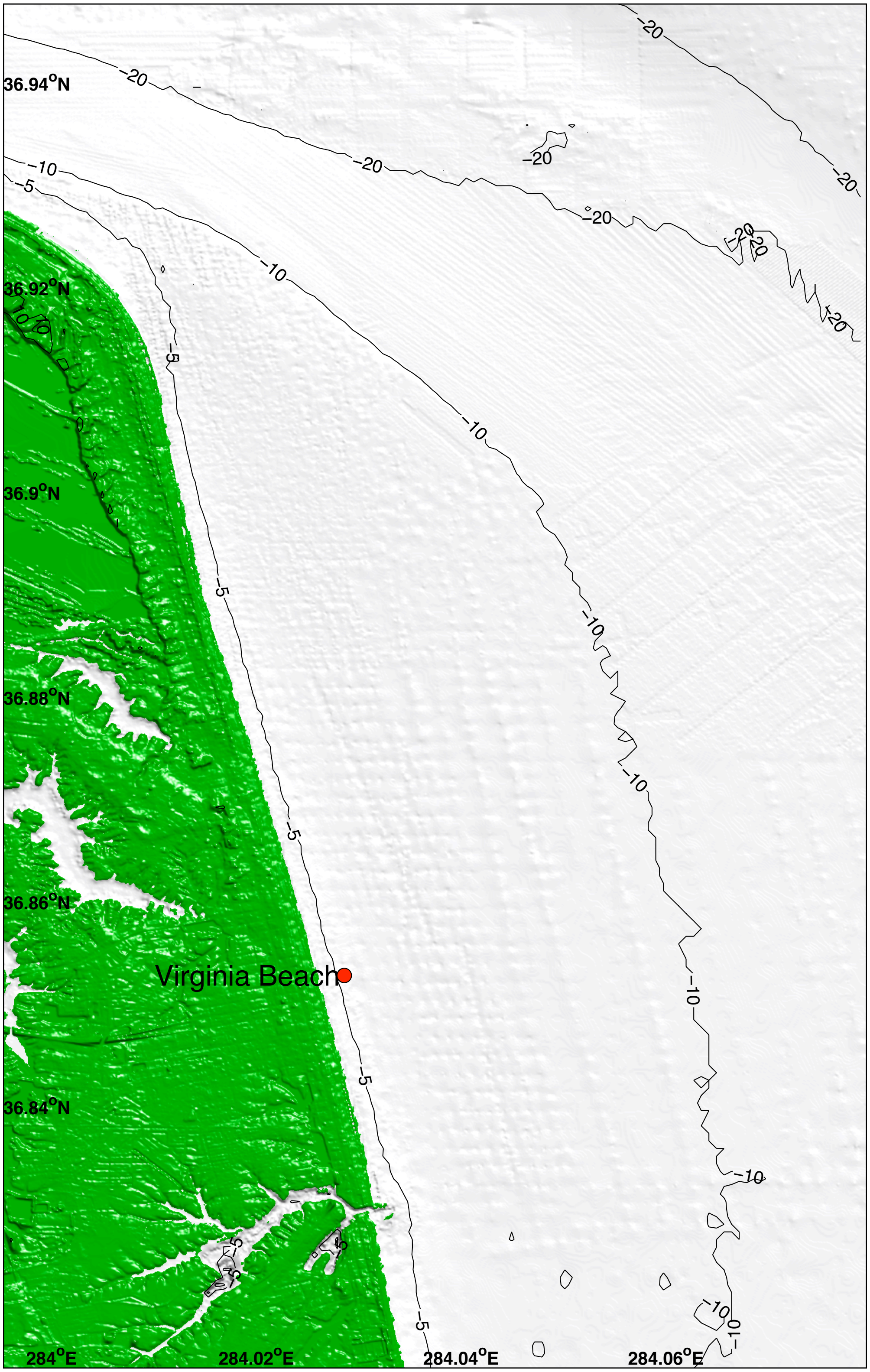

Figure 8 Grid setup for the Virginia Beach reference model. Resolutions are (a) 36”, (b) 12” and(c) 1/3” . Red boxes are boundaries of the telescoped grids for the reference model.

(a)

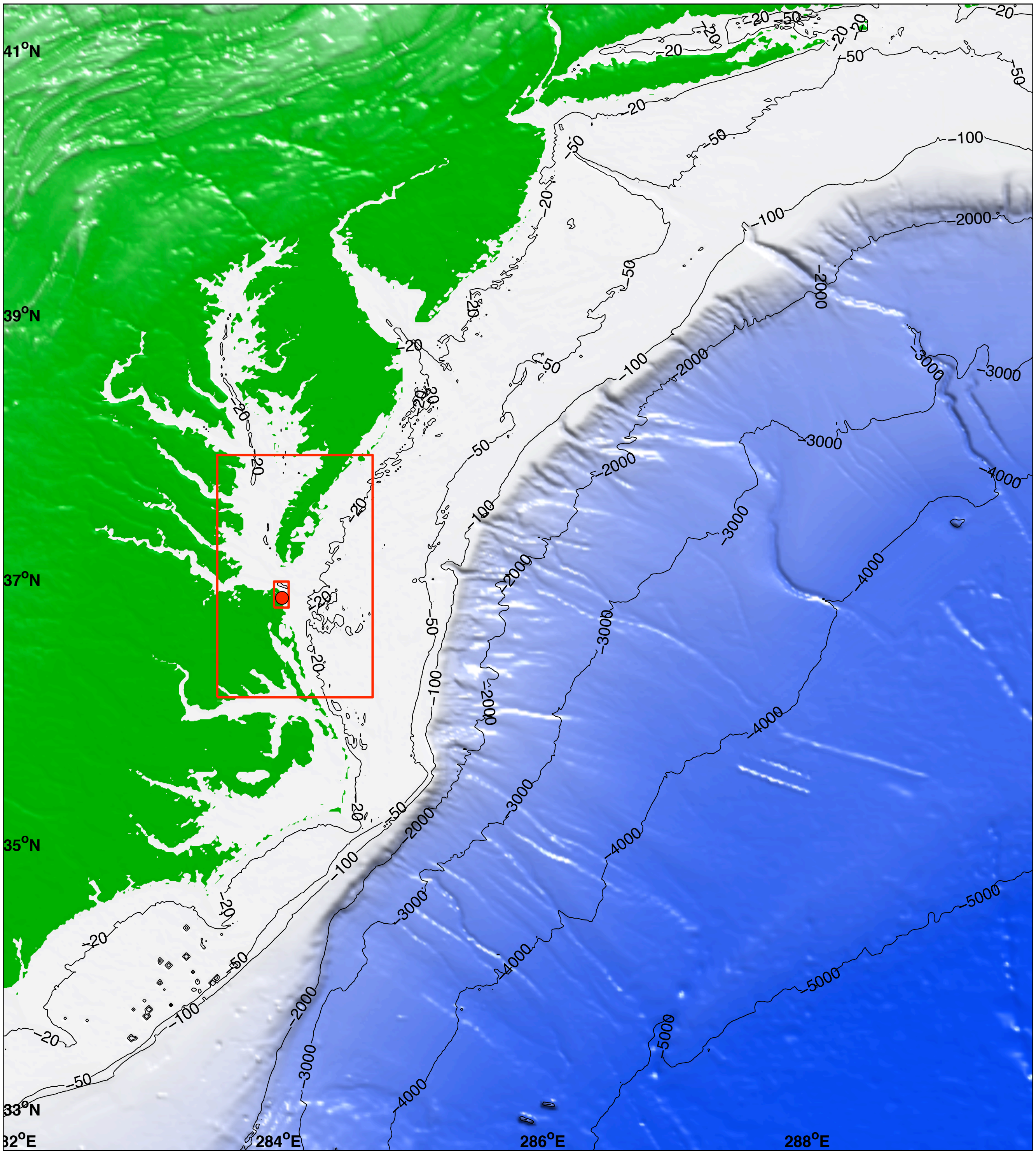

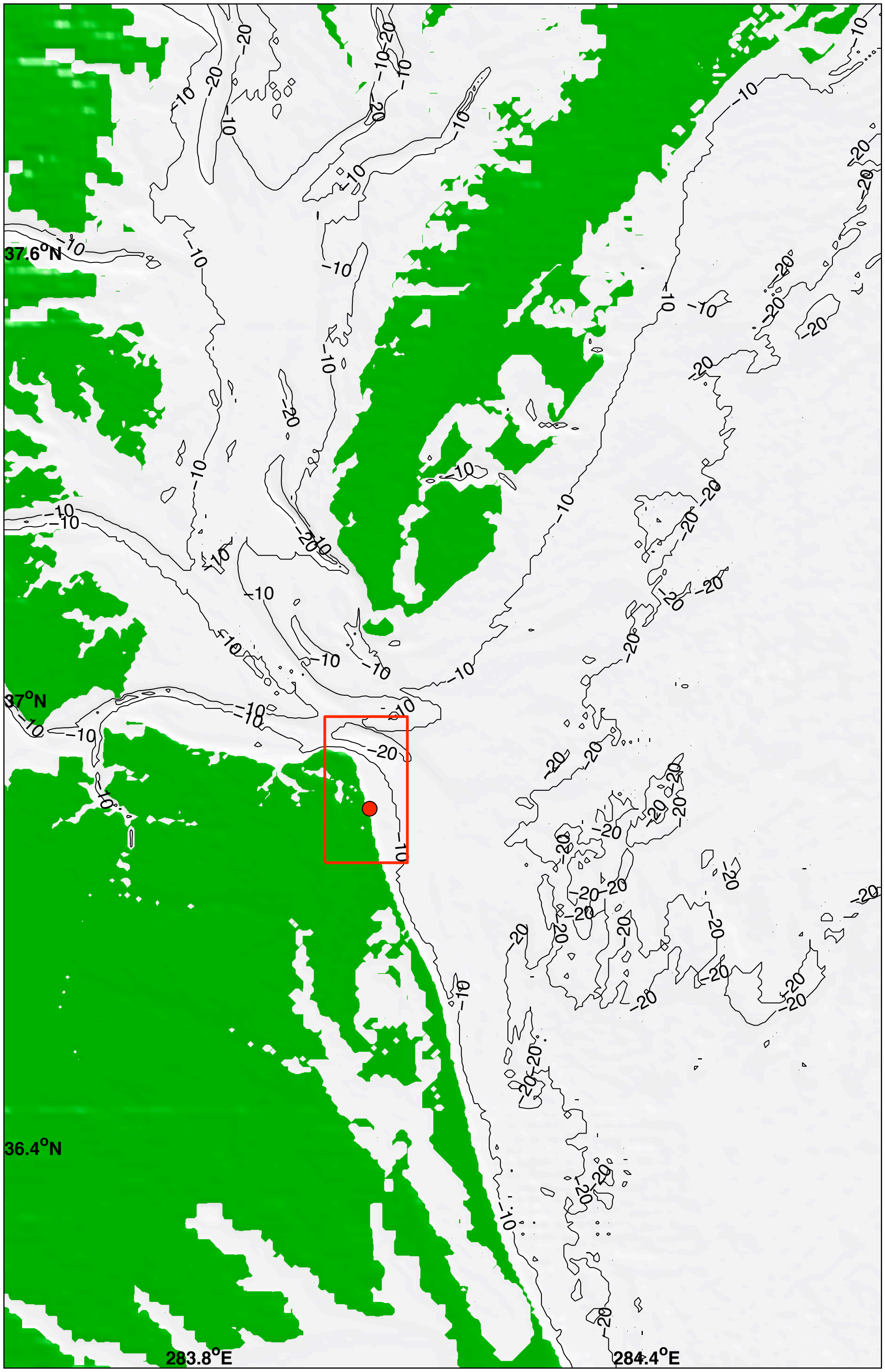

(b)

(c)

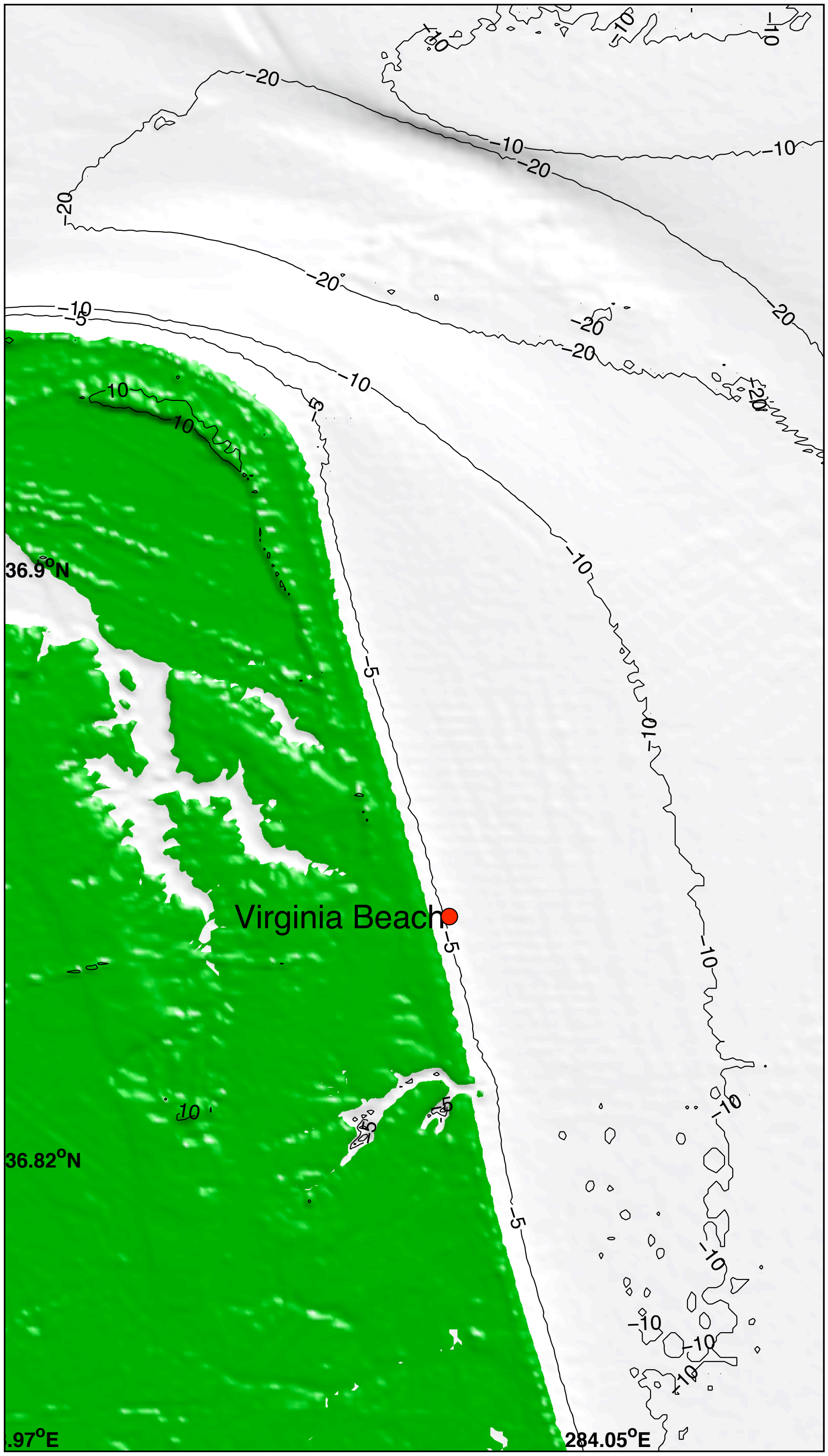

Figure 9 Grid setup for the Virginia Beach forecast model. Grid resolutions are (a) 60 ", (b) 18", and (c) 2". Red boxes, boundaries of the telescoping grids. Red dot, Virginia Beach warning point (284.0286°E, 36.8530°N; water depth= 6m).

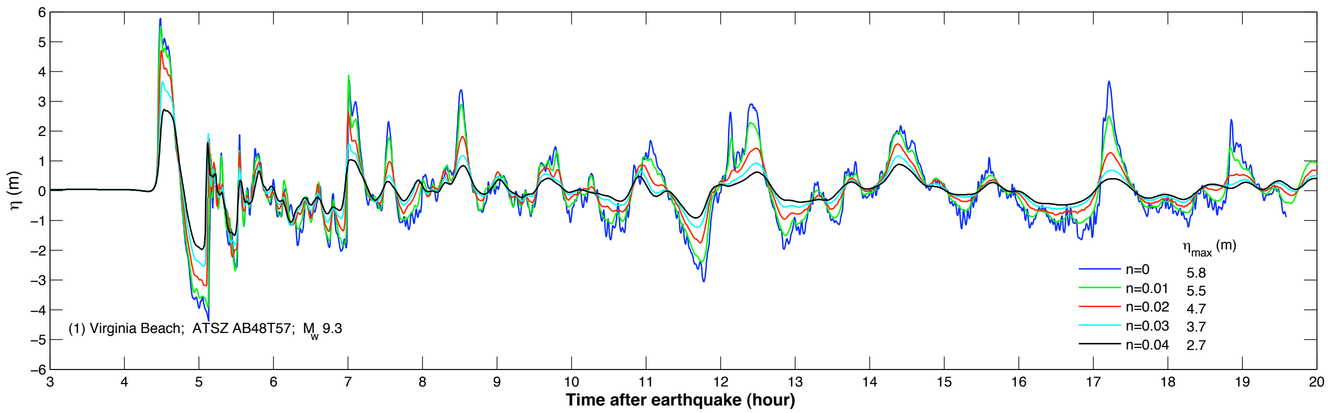

Figure 10 Sensitivity of η to friction coefficients. Results were computed by a set of testing grids (Fig. 11) for a magnitude 9.3 Caribbean tsunami.

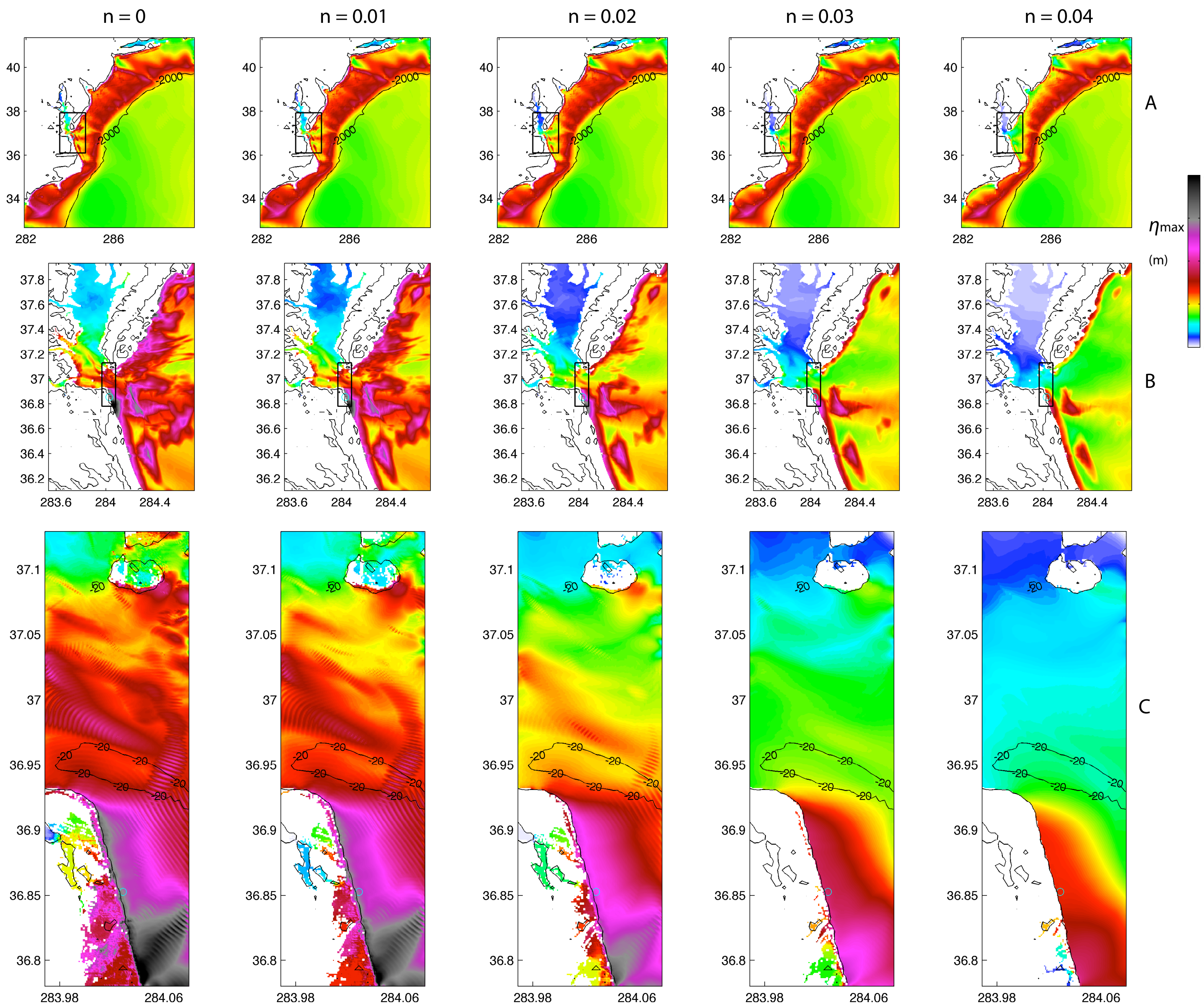

Figure 11 Sensitivity of η_{max} to friction coefficients. Results were computed by a set of testing grids for a magnitude-9.3 Caribbean tsunami.

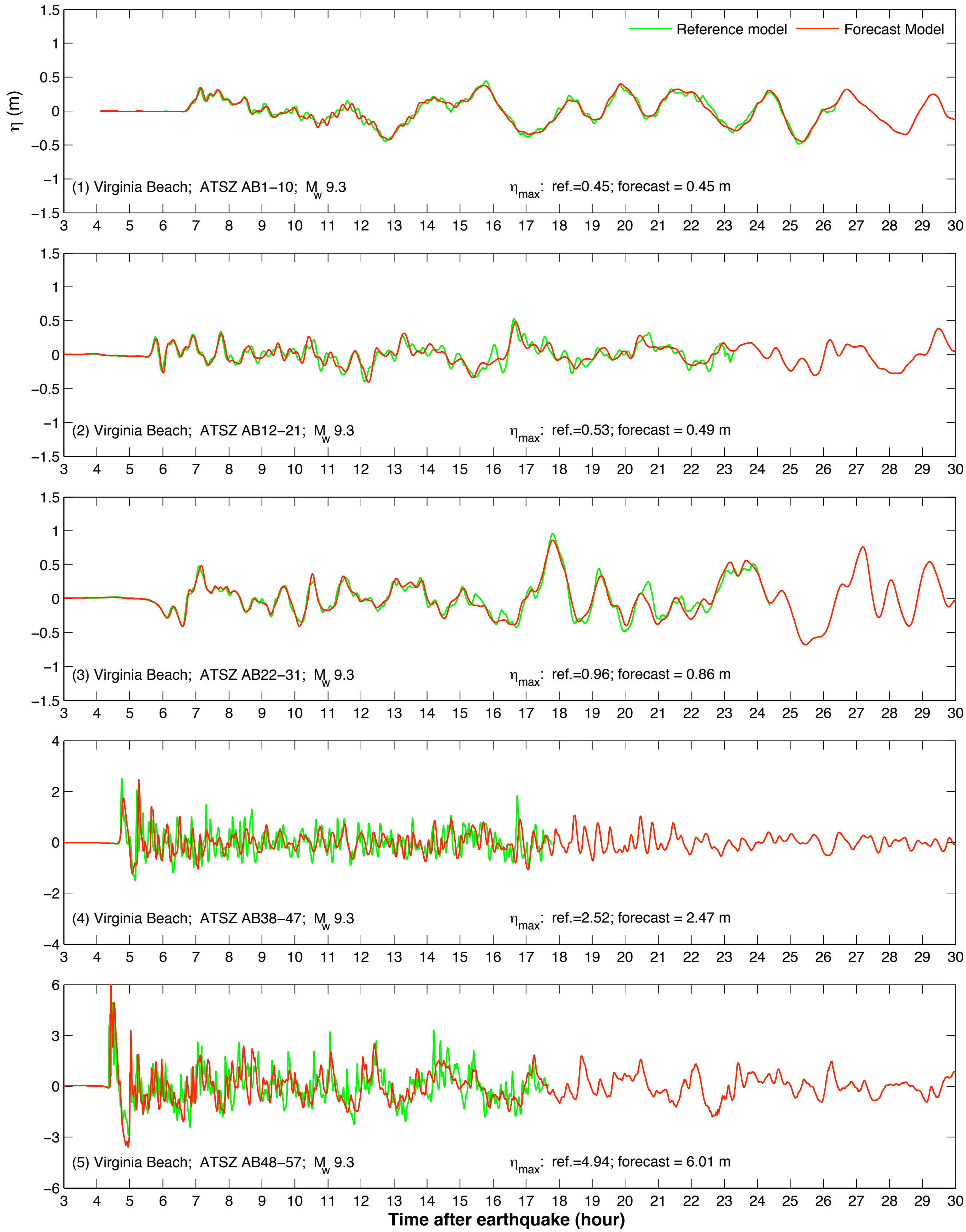
Reference model
Forecast Model
η (m)
(1) Virginia Beach; ATSZ AB1–10; Mw 9.3
ηmax: ref.=0.45; forecast = 0.45 m
(2) Virginia Beach; ATSZ AB12–21; Mw 9.3
ηmax: ref.=0.53; forecast = 0.49 m
(3) Virginia Beach; ATSZ AB22–31; Mw 9.3
ηmax: ref.=0.96; forecast = 0.86 m
(4) Virginia Beach; ATSZ AB38–47; Mw 9.3
ηmax: ref.=2.52; forecast = 2.47 m
(5) Virginia Beach; ATSZ AB48–57; Mw 9.3
ηmax: ref.=4.94; forecast = 6.01 m
Time after earthquake (hour)

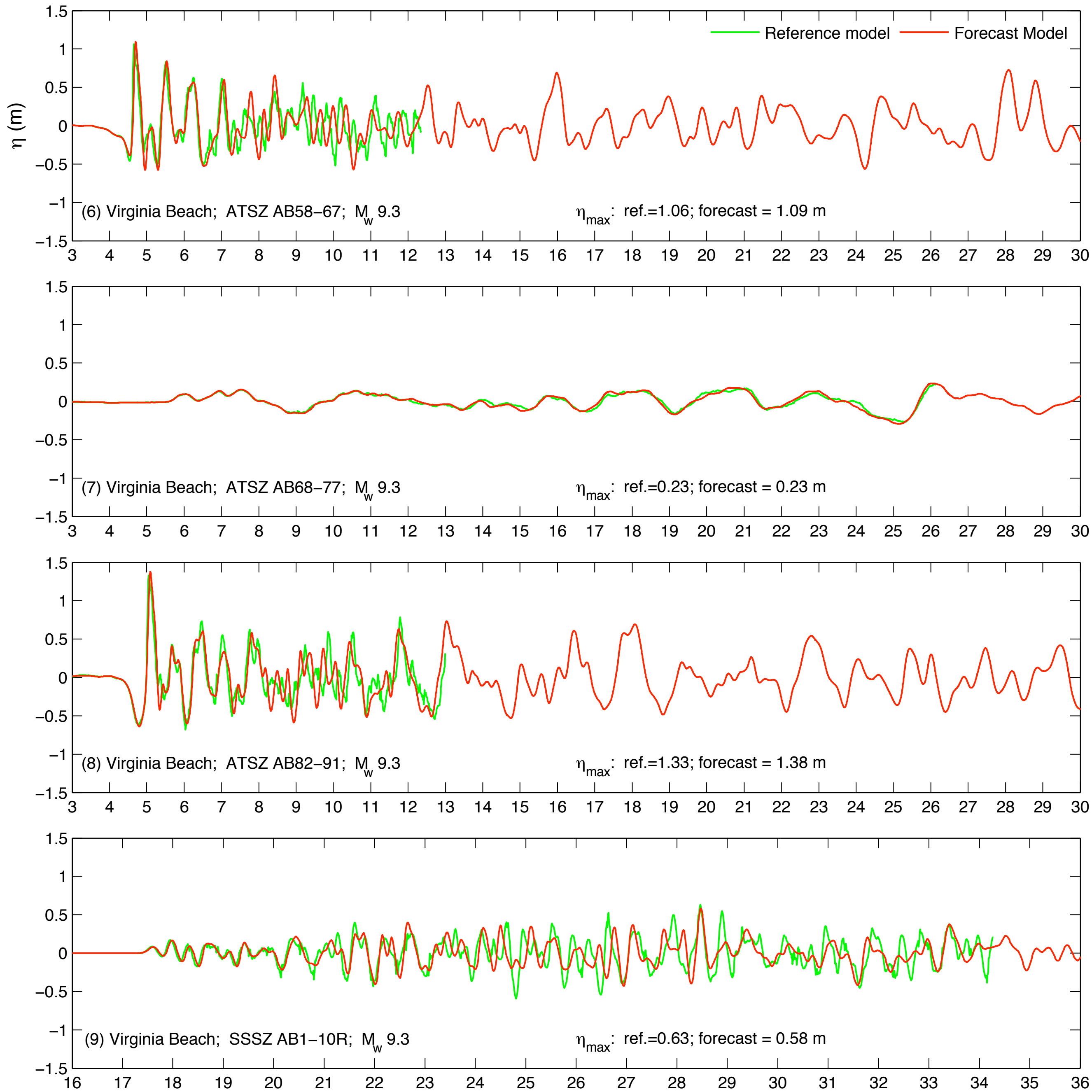

Figure 12 Modeled η time series by the Virginia Beach reference and forecast models for simulated magnitude-9.3 tsunamis.

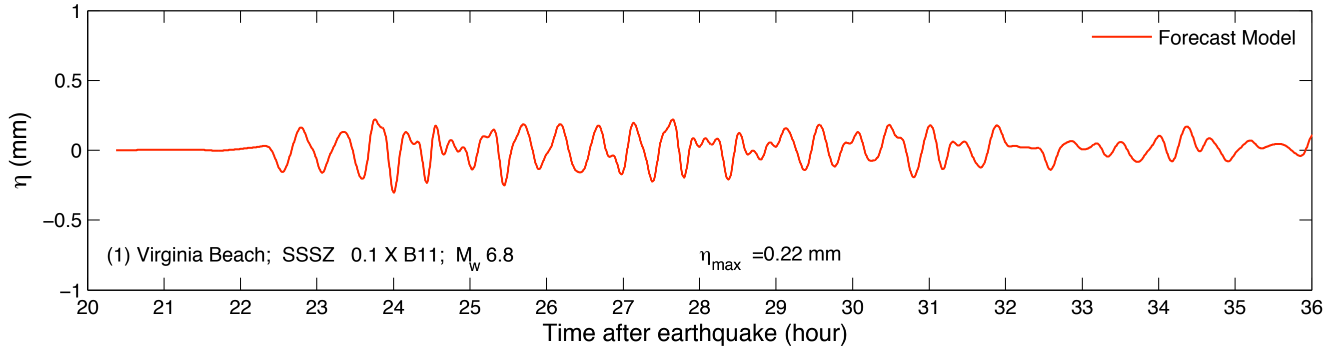

Figure 13 Modeled η time series computed by the Virginia Beach forecast model for a simulated micro tsunami. The tsunami was generated from a Magnitude 6.8 earthquake from South Sandwich Islands Subduction (0.1 × B11).

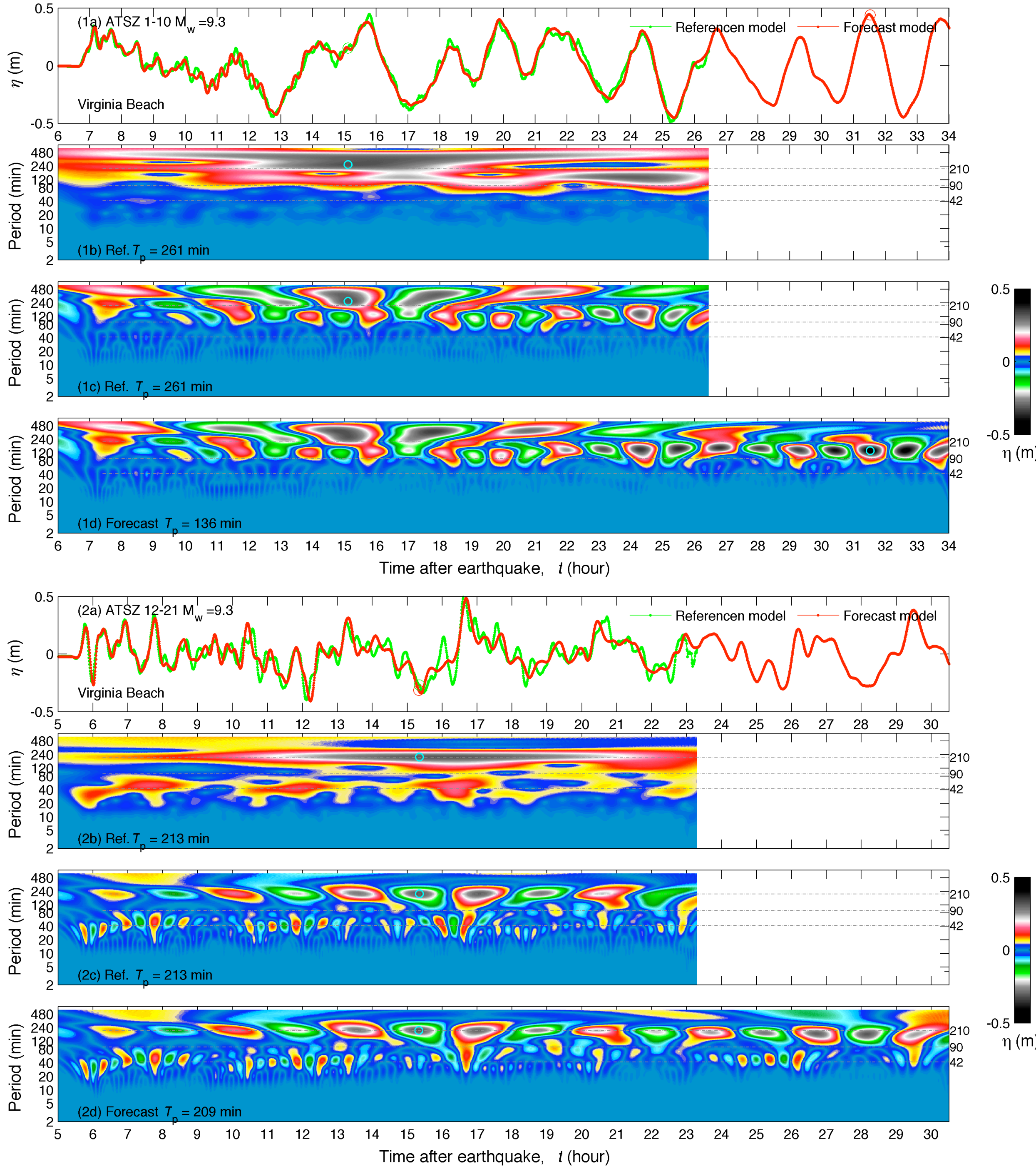
(1a) ATSZ 1-10 M_w =9.3
Referencen model
Forecast model
Virginia Beach
η (m)
(1b) Ref. T_p = 261 min
(1c) Ref. T_p = 261 min
(1d) Forecast T_p = 136 min
Period (min)
210
90
42
η (m)
Time after earthquake, t (hour)
(2a) ATSZ 12-21 M_w =9.3
Referencen model
Forecast model
Virginia Beach
(2b) Ref. T_p = 213 min
(2c) Ref. T_p = 213 min
(2d) Forecast T_p = 209 min
Time after earthquake, t (hour)

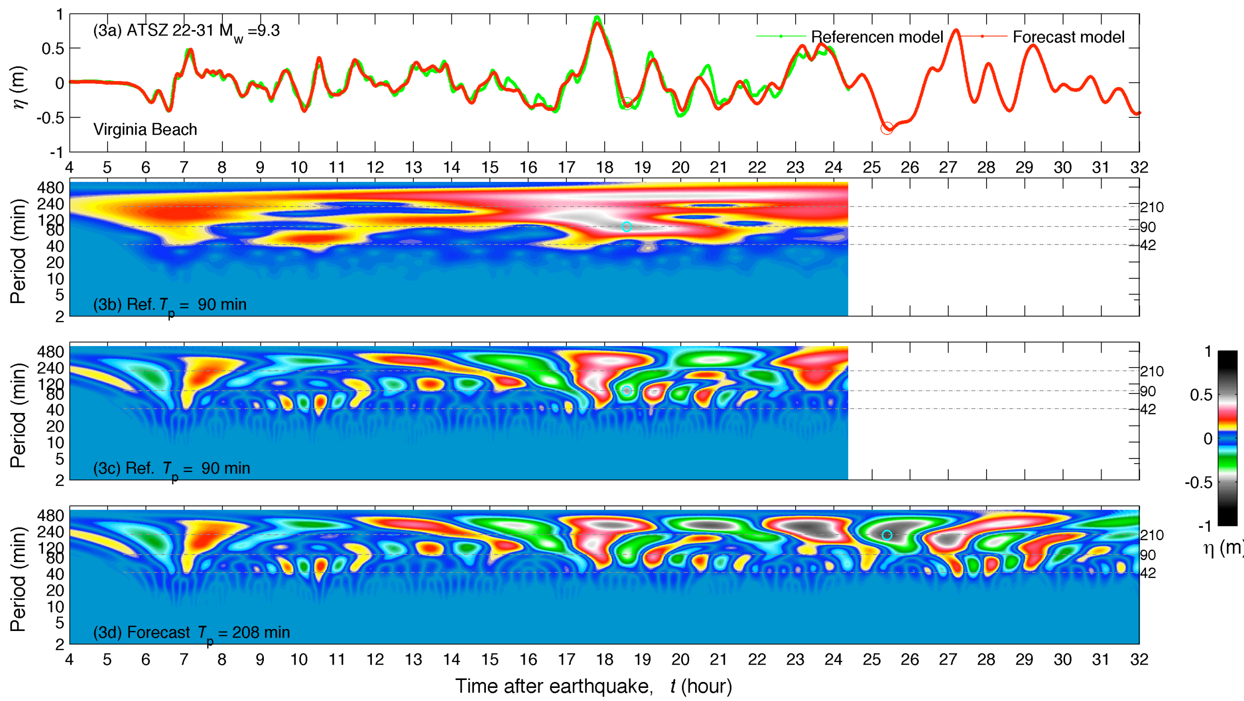
(3a) ATSZ 22-31 M_w =9.3
Referencen model
Forecast model
Virginia Beach
η (m)
Period (min)
(3b) Ref. T_p = 90 min
(3c) Ref. T_p = 90 min
(3d) Forecast T_p = 208 min
Time after earthquake, t (hour)
η (m)

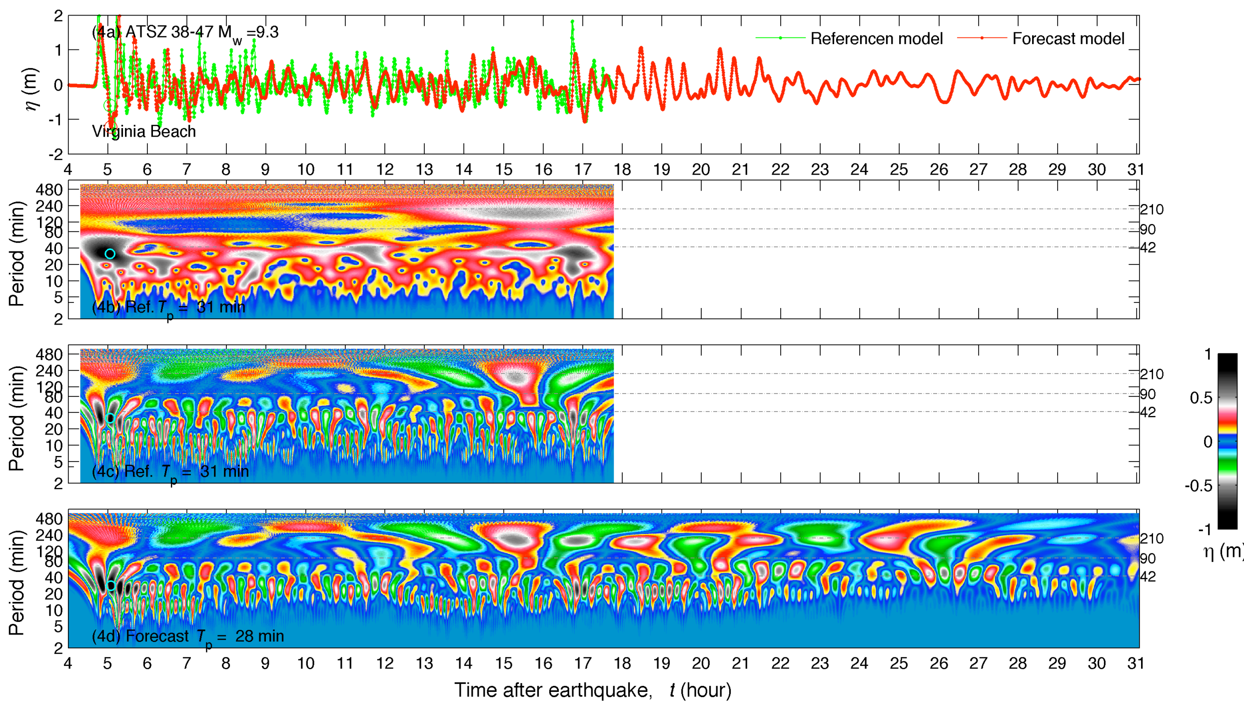
(4a) ATSZ 38-47 M_w =9.3
Referencen model
Forecast model
Virginia Beach
η (m)
Period (min)
(4b) Ref. T_p = 31 min
(4c) Ref. T_p = 31 min
(4d) Forecast T_p = 28 min
Time after earthquake, t (hour)
η (m)

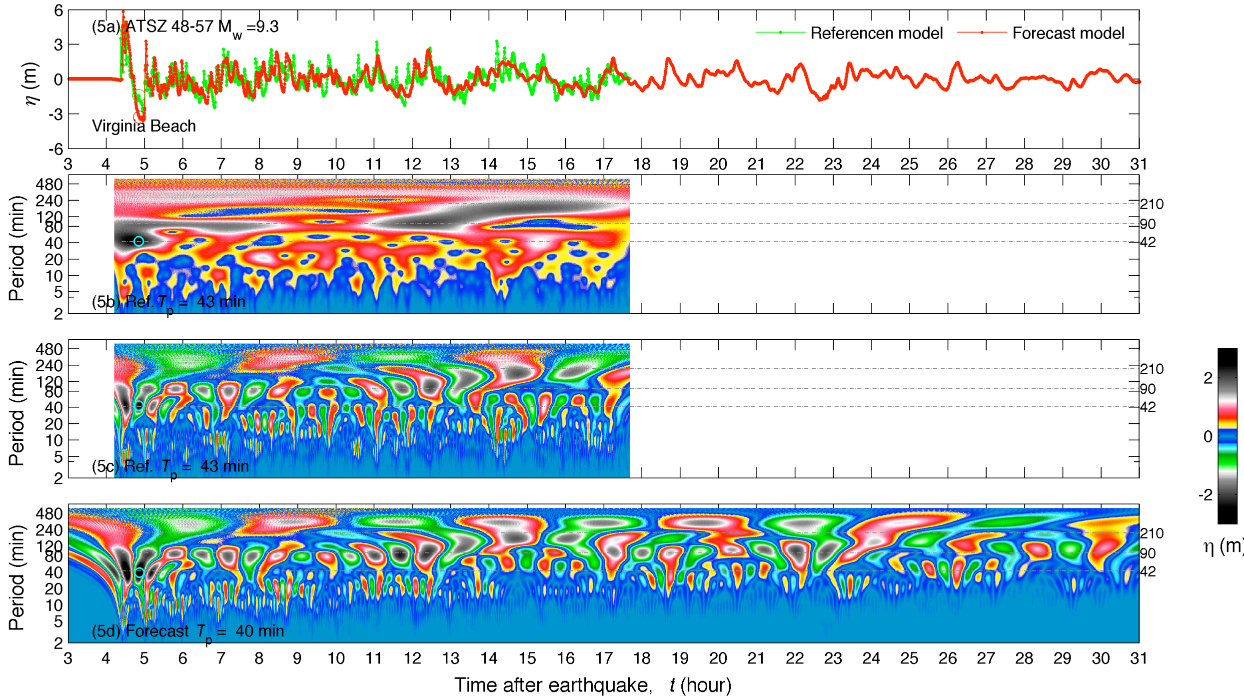
(5a) ATSZ 48-57 M_w =9.3
Referencen model
Forecast model
Virginia Beach
η (m)
(5b) Ref. T_p = 43 min
(5c) Ref. T_p = 43 min
(5d) Forecast T_p = 40 min
Period (min)
η (m)
Time after earthquake, t (hour)

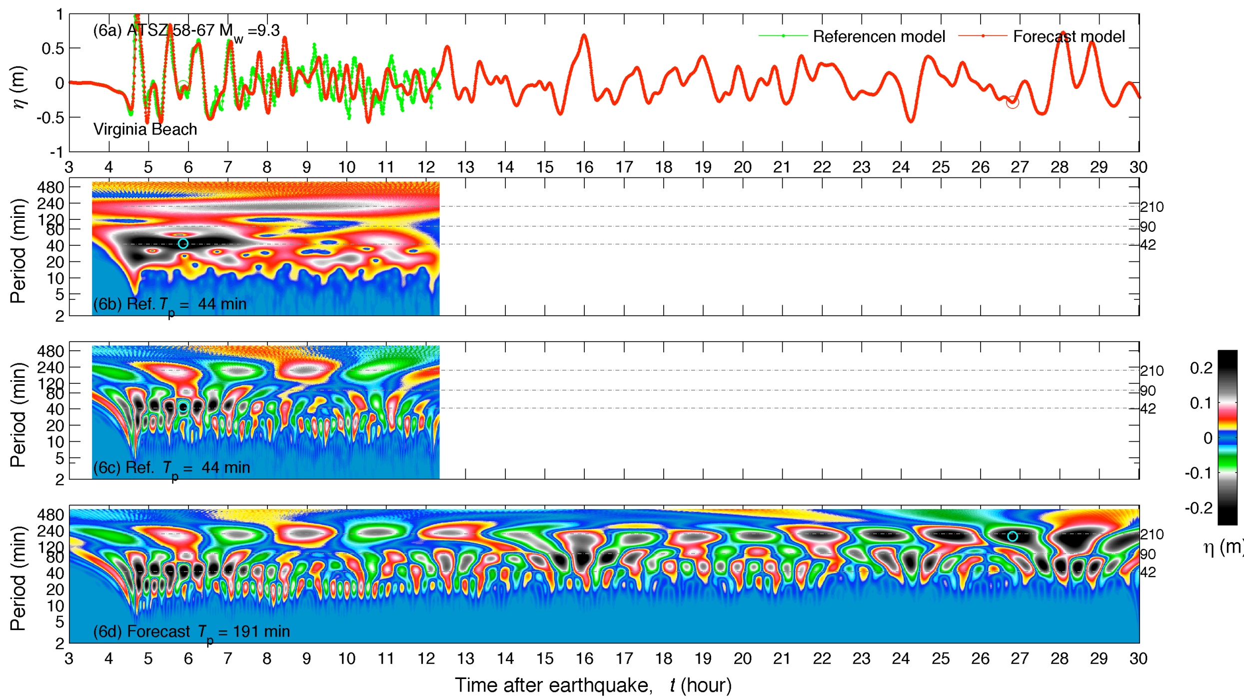
(6a) ATSZ 58-67 M_w =9.3
Referencen model
Forecast model
Virginia Beach
η (m)
(6b) Ref. T_p = 44 min
(6c) Ref. T_p = 44 min
(6d) Forecast T_p = 191 min
Period (min)
η (m)
Time after earthquake, t (hour)

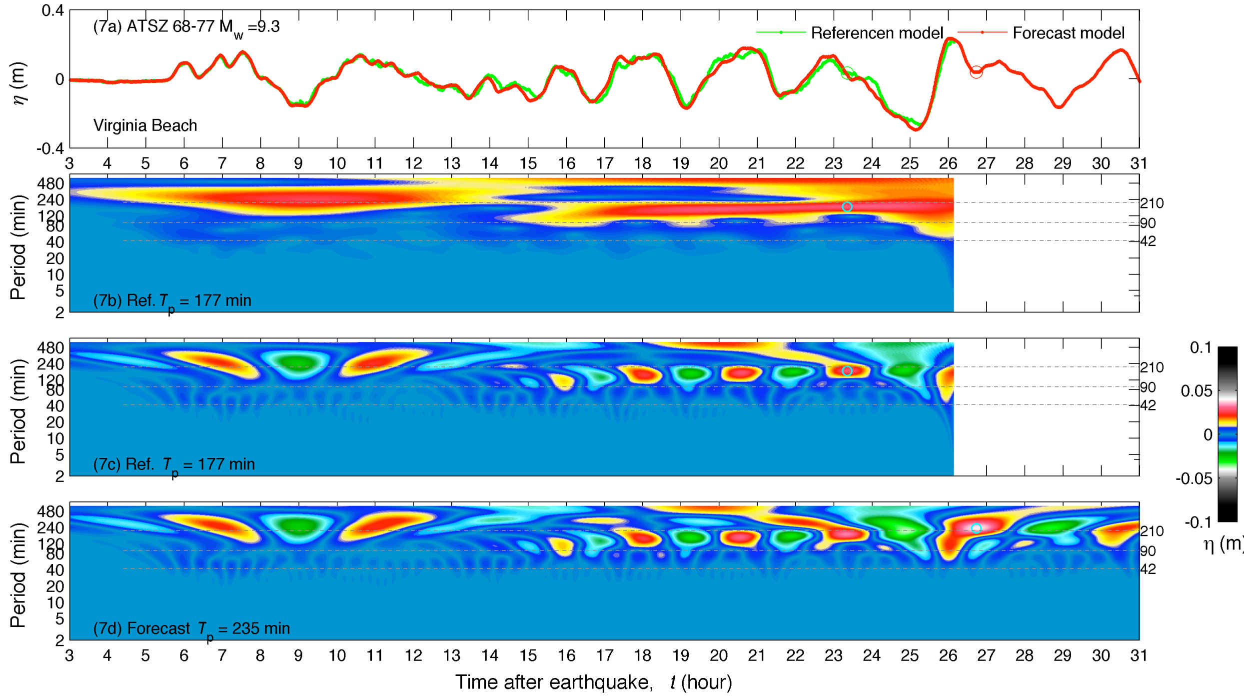
(7a) ATSZ 68-77 Mw =9.3
Referencen model
Forecast model
η (m)
Virginia Beach
Period (min)
(7b) Ref. Tp = 177 min
(7c) Ref. Tp = 177 min
(7d) Forecast Tp = 235 min
210
90
42
η (m)
Time after earthquake, t (hour)

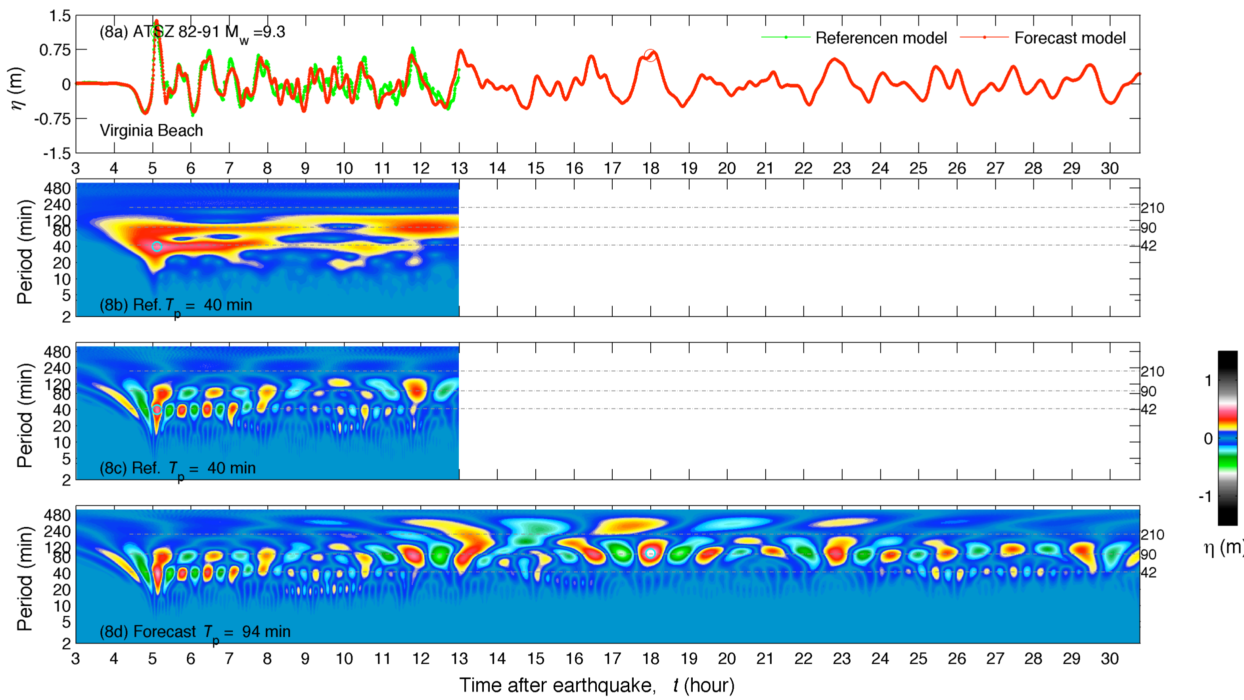
(8a) ATSZ 82-91 Mw =9.3
Referencen model
Forecast model
η (m)
Virginia Beach
Period (min)
(8b) Ref. Tp = 40 min
(8c) Ref. Tp = 40 min
(8d) Forecast Tp = 94 min
210
90
42
η (m)
Time after earthquake, t (hour)

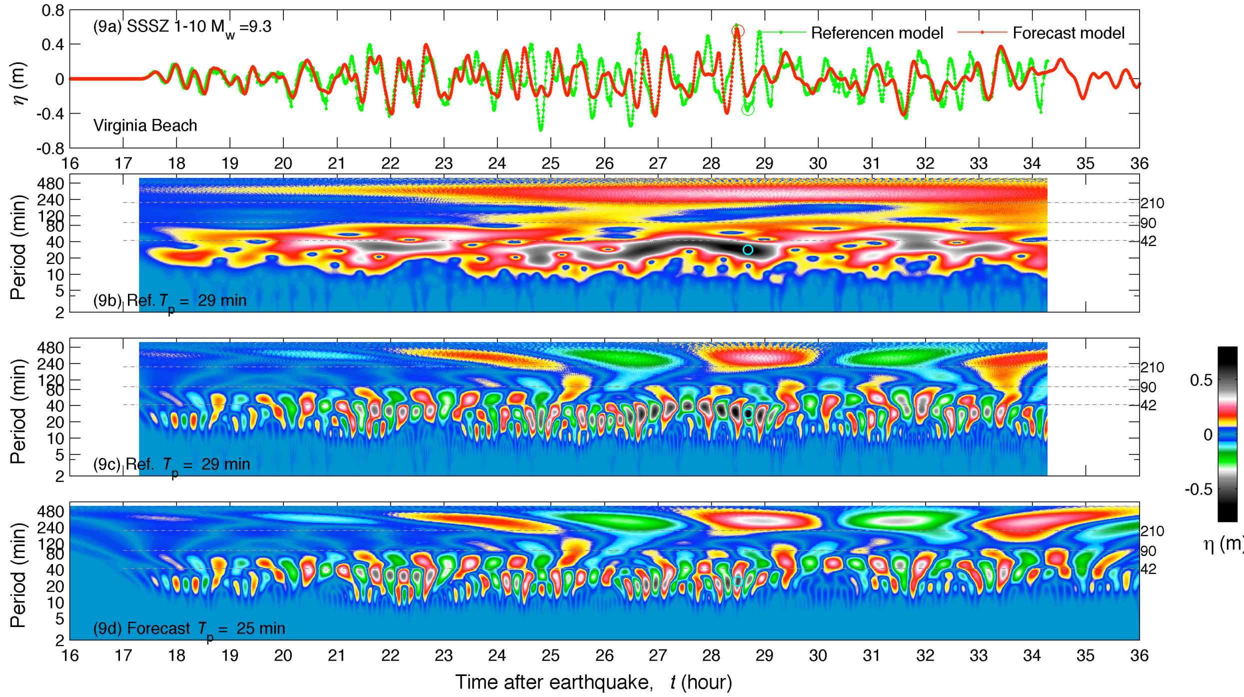

Figure 14 (a) Modeled η time series at Virginia Beach warning point for the nine simulated magnitude-9.3 tsunamis. (b) Wavelet–derived amplitude spectrogram for the reference model. (c and d) Real part of the spectrograms computed by the reference and forecast models.

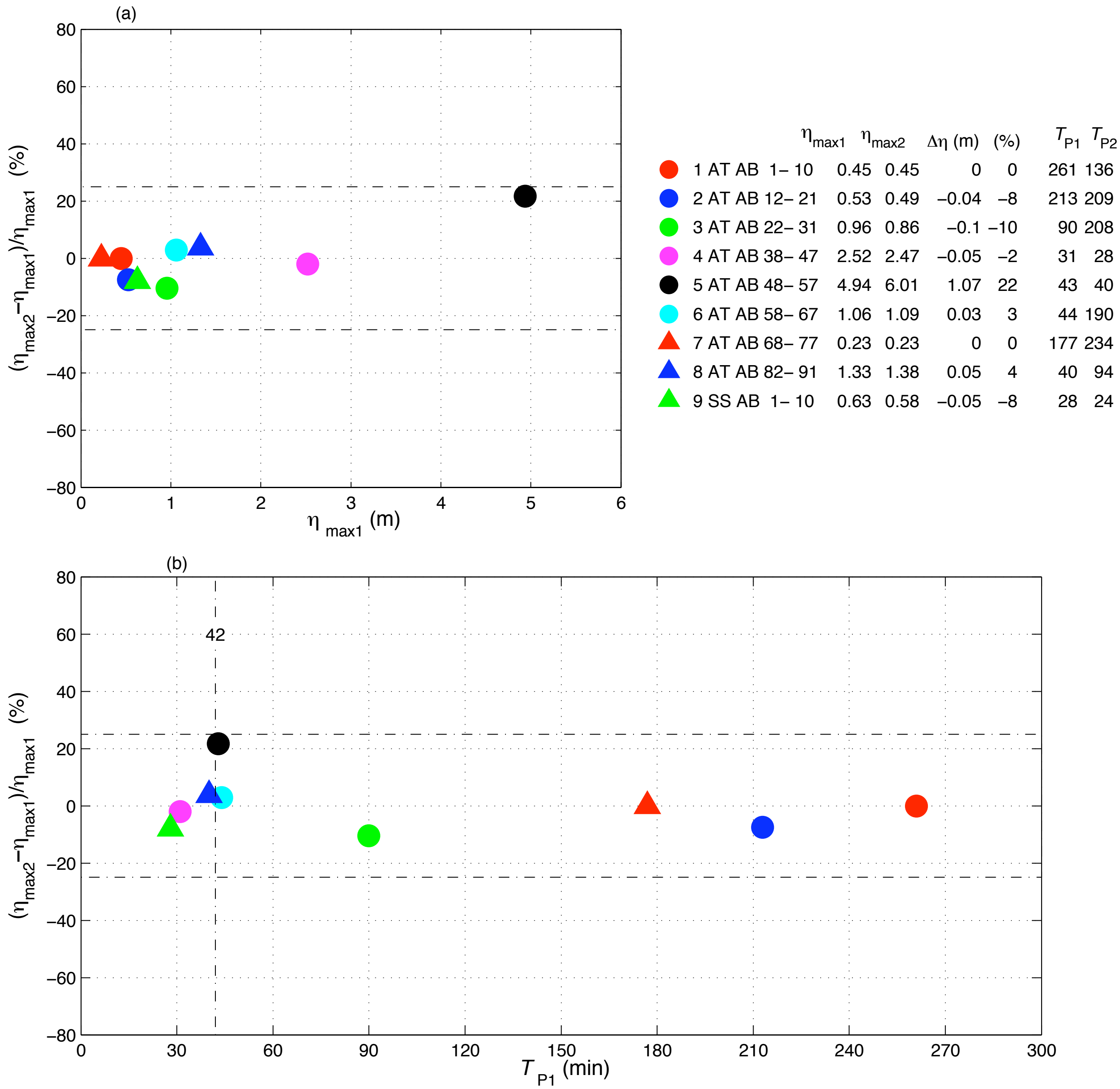

Figure 15 (a) Forecast uncertainty in the η_{max} at the Virginia Beach warning point. (b) Uncertainty v.s. peak period. η_{max1} and T_{p1}, maximum water elevation and peak period at the warning point from the reference model. η_{max2} and T_{p2}, maximum water surface elevation and peak period at the warning point computed by the forecast model.

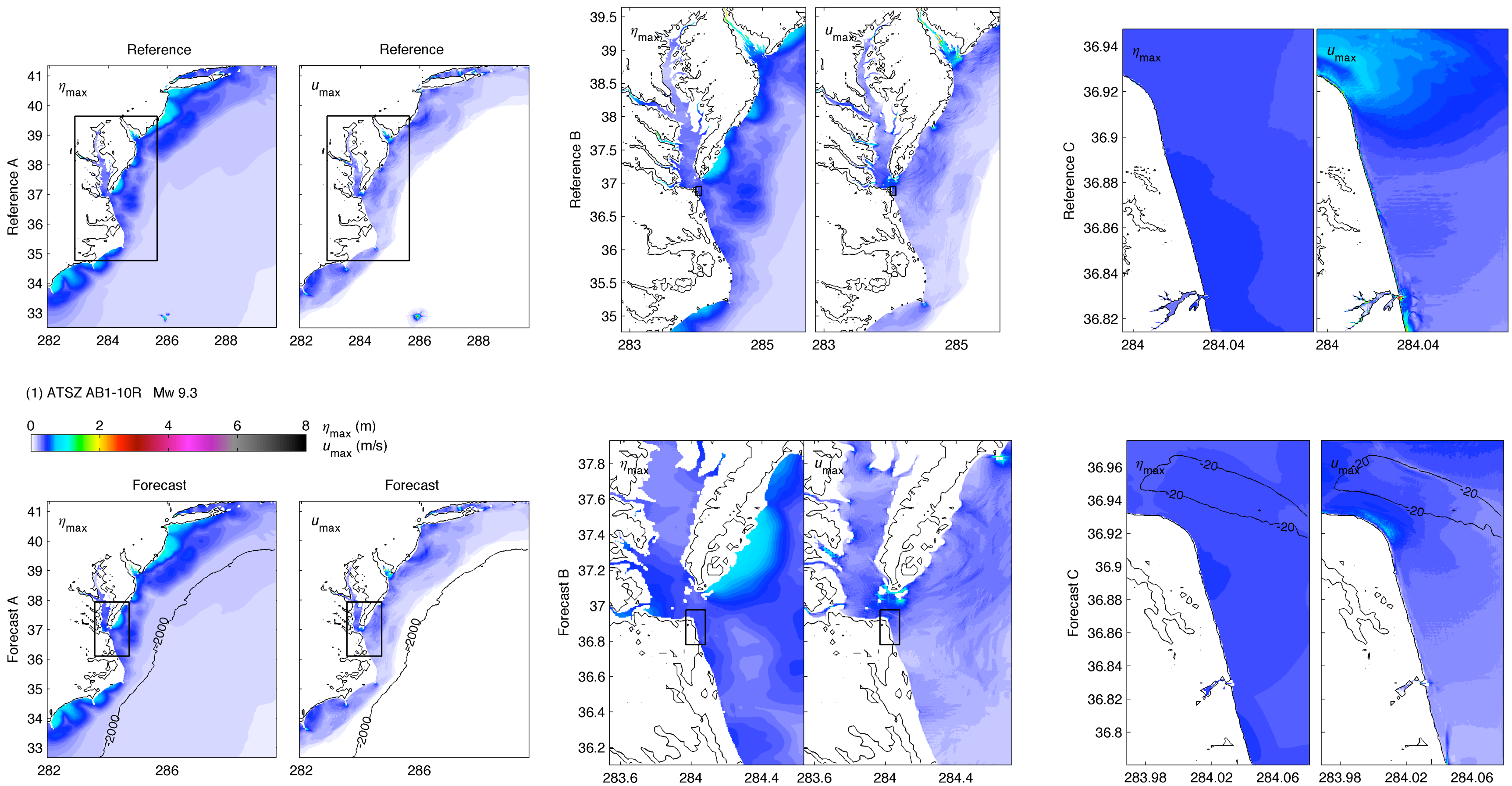

Reference
Reference
Reference A
Reference B
Reference C
Forecast
Forecast
Forecast A
Forecast B
Forecast C
(1) ATSZ AB1-10R Mw 9.3
η_{max} (m)
u_{max} (m/s)
2000
-20

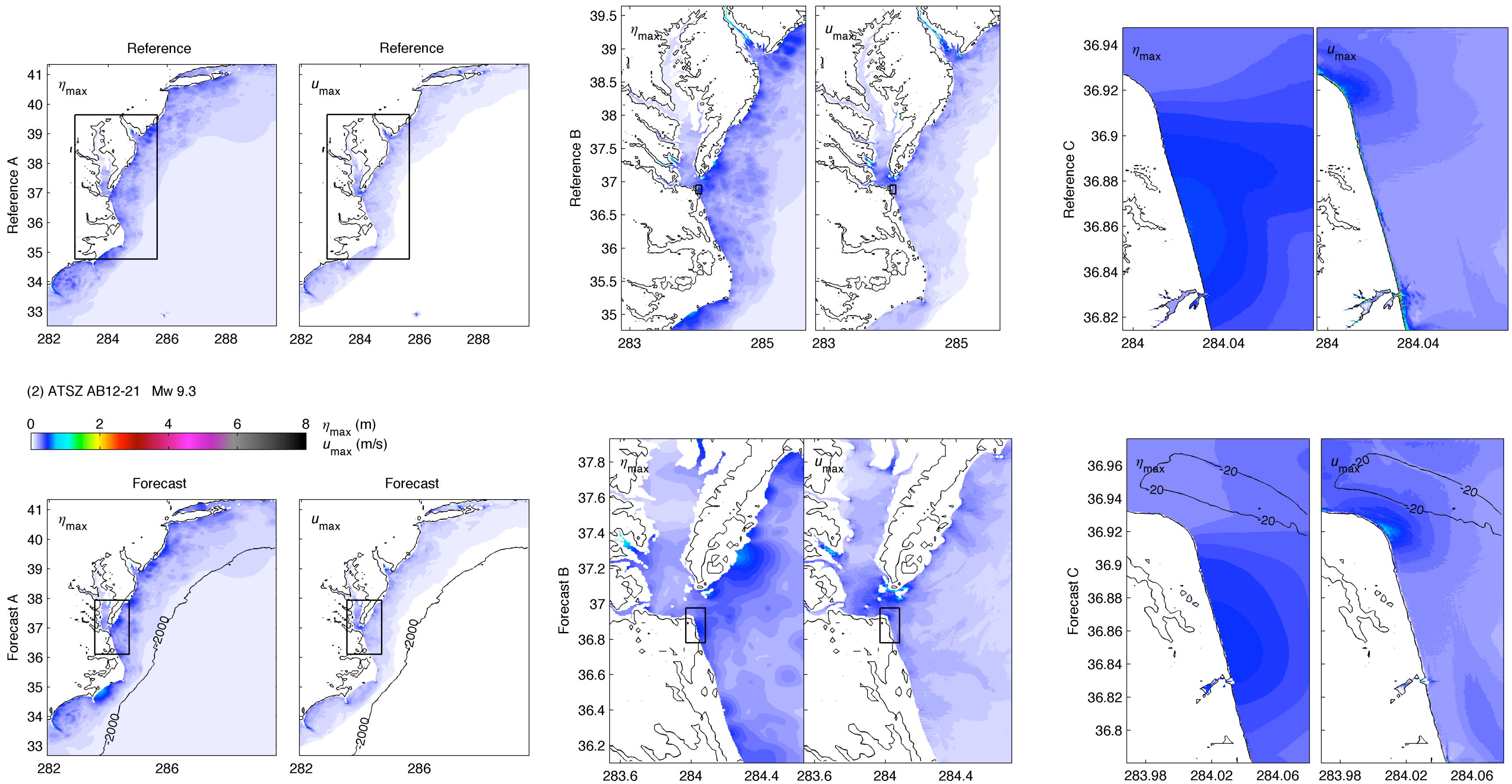
Reference
Reference
Reference A
Reference B
Reference C
η_{max}
u_{max}
(2) ATSZ AB12-21 Mw 9.3
0 2 4 6 8
η_{max} (m)
u_{max} (m/s)
Forecast
Forecast
Forecast A
Forecast B
Forecast C
2000
20

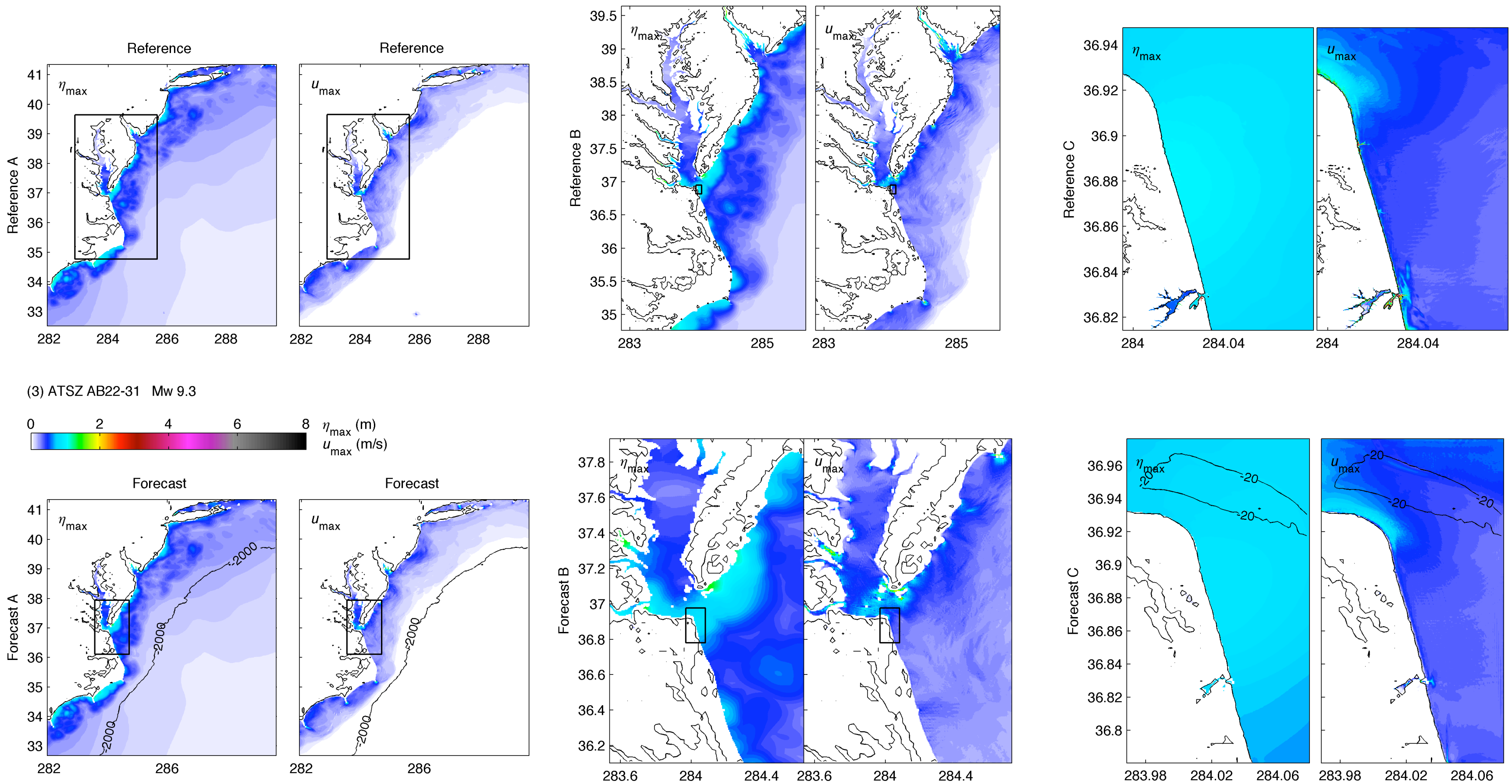

Reference
Reference
Reference A
Reference B
Reference C
(3) ATSZ AB22-31 Mw 9.3
η_{max} (m)
u_{max} (m/s)
Forecast
Forecast
Forecast A
Forecast B
Forecast C

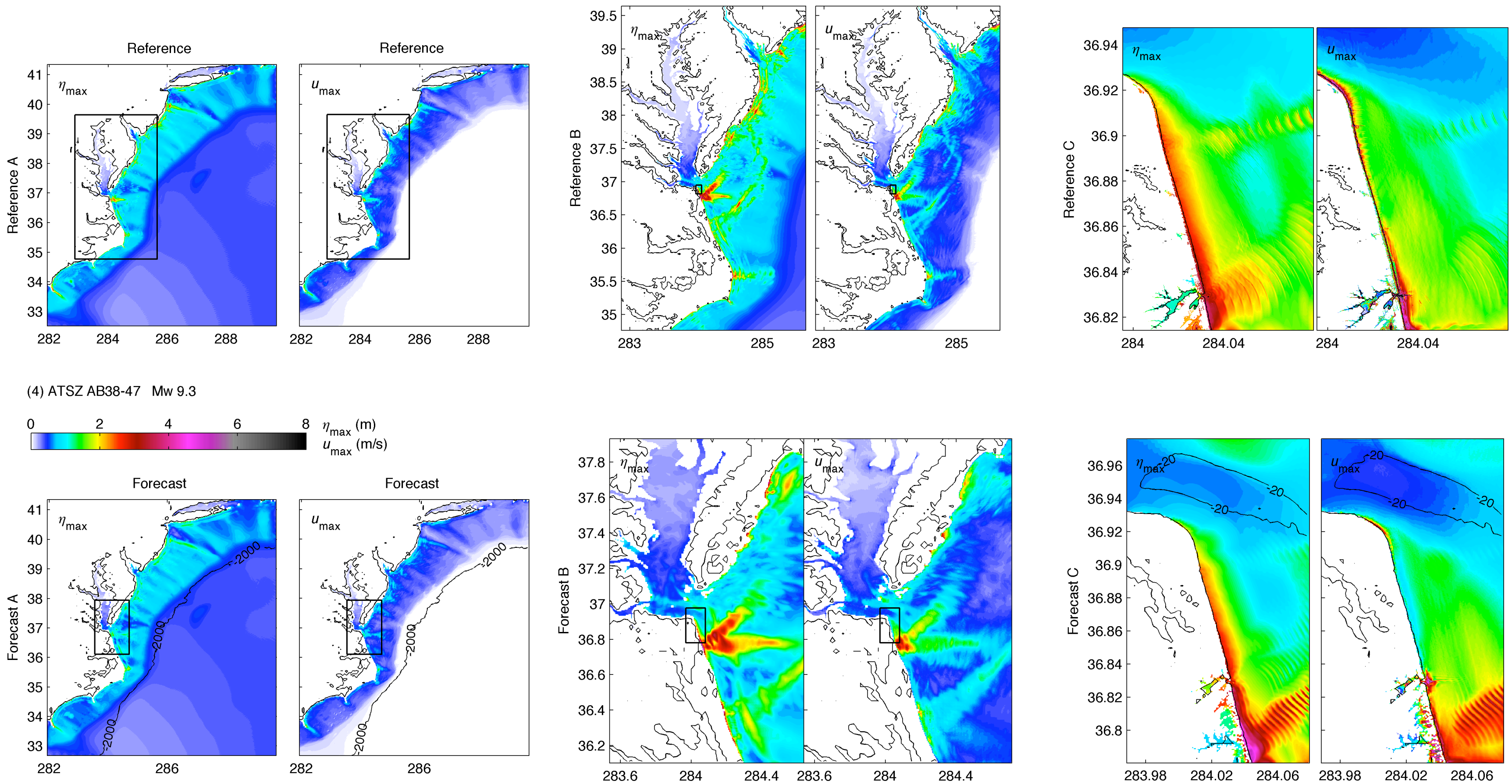
Reference
Reference
Reference A
Reference B
Reference C
(4) ATSZ AB38-47 Mw 9.3
η_{max} (m)
u_{max} (m/s)
0
2
4
6
8
Forecast
Forecast
Forecast A
Forecast B
Forecast C
η_{max}
u_{max}
-2000
-20

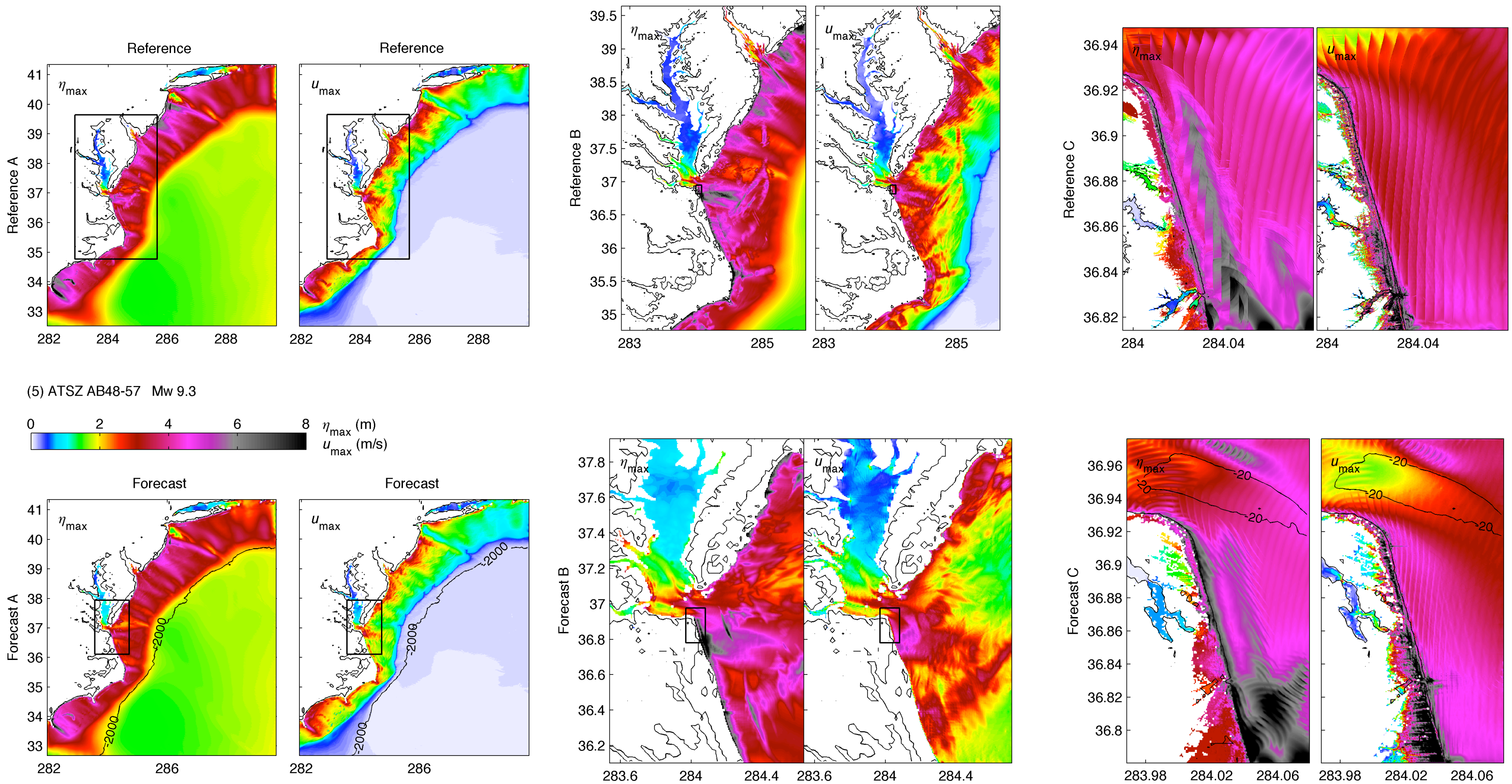

Reference
Reference
Reference A
Reference B
Reference C
η_{max}
u_{max}
(5) ATSZ AB48-57 Mw 9.3
0 2 4 6 8
η_{max} (m)
u_{max} (m/s)
Forecast
Forecast
Forecast A
Forecast B
Forecast C
2000
-20

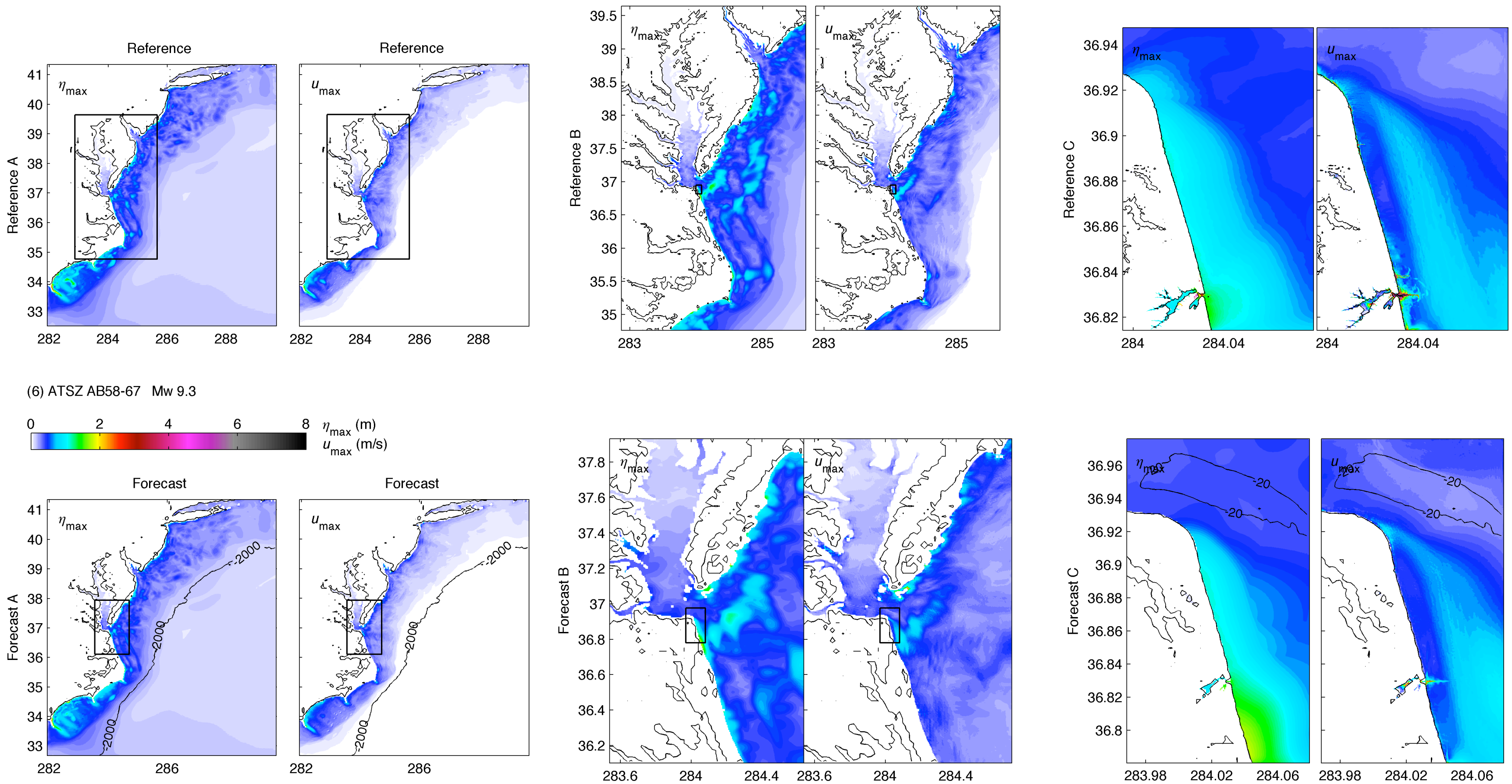

Reference
Reference
Reference A
Reference B
Reference C
(6) ATSZ AB58-67 Mw 9.3
0 2 4 6 8
ηmax (m)
umax (m/s)
Forecast
Forecast
Forecast A
Forecast B
Forecast C
ηmax
umax
2000
-20

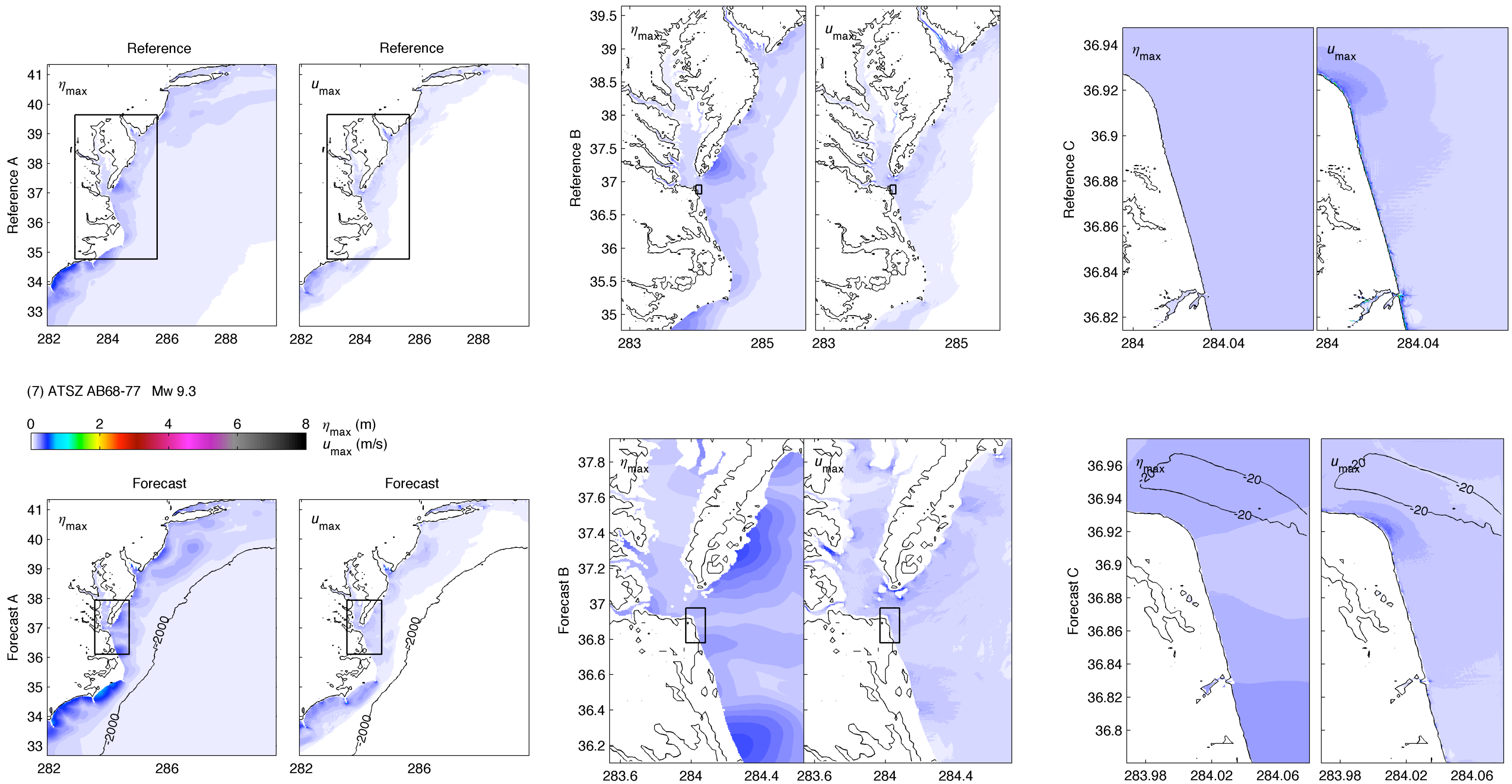
Reference
Reference
Reference A
Reference B
Reference C
η_{max}
u_{max}
(7) ATSZ AB68-77   Mw 9.3
0
2
4
6
8
η_{max} (m)
u_{max} (m/s)
Forecast
Forecast
Forecast A
Forecast B
Forecast C
2000
20

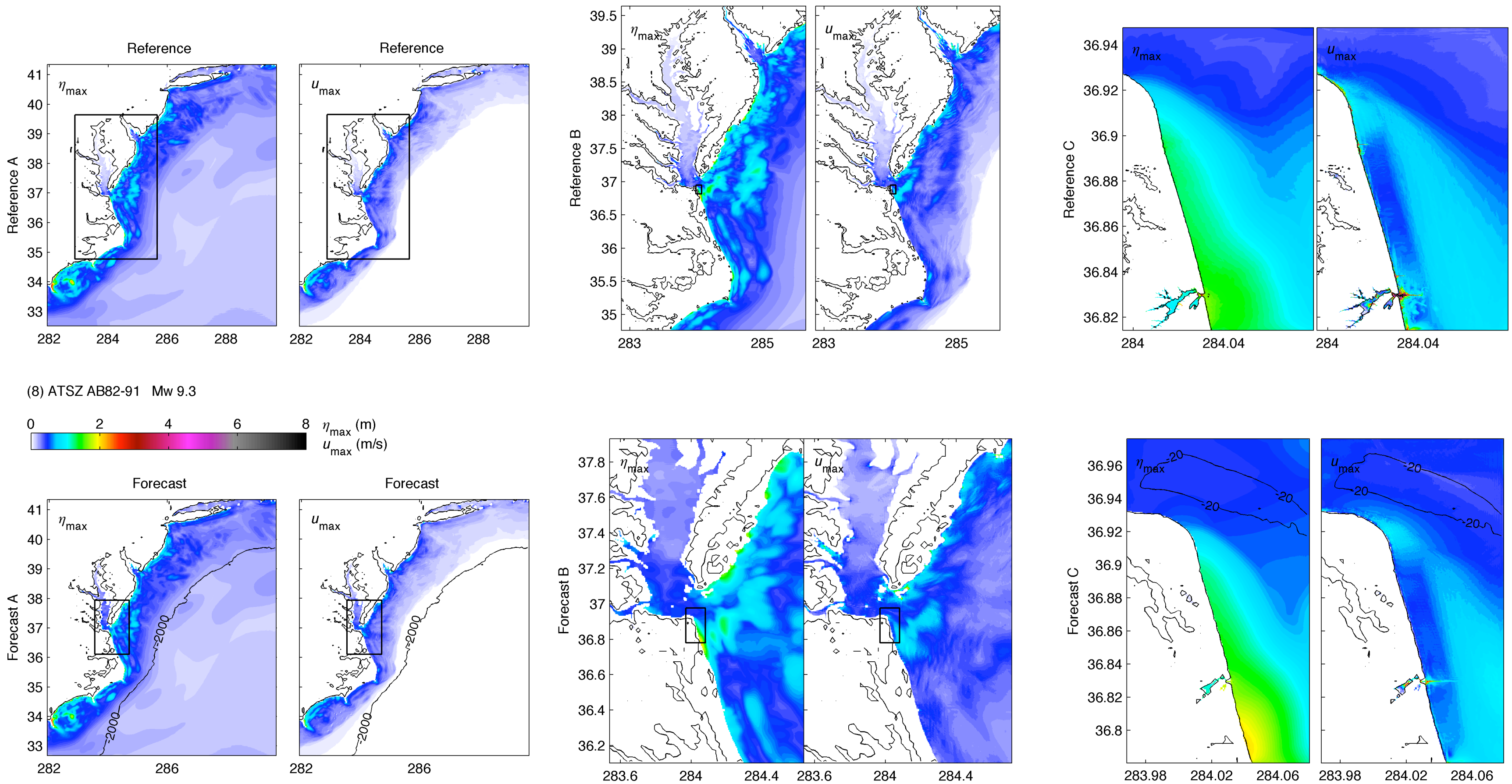
Reference
Reference
Reference A
Reference B
Reference C
ηmax
umax
(8) ATSZ AB82-91 Mw 9.3
0 2 4 6 8
ηmax (m)
umax (m/s)
Forecast
Forecast
Forecast A
Forecast B
Forecast C
2000
-20
282 284 286 288
283 285
284 284.04
283.6 284 284.4
283.98 284.02 284.06

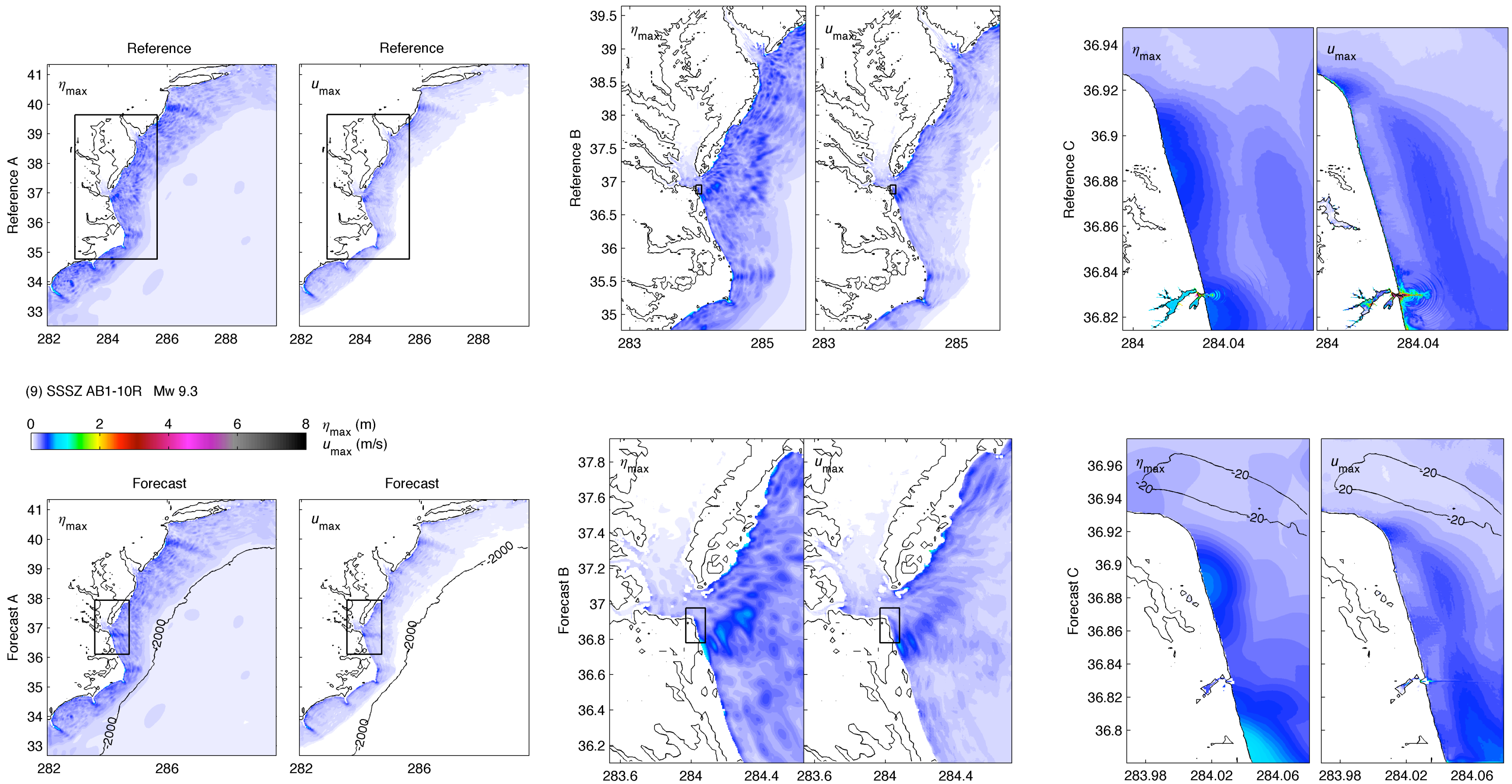

Figure 16 Maximum water elevation and current computed by the Virginia Beach reference and forecast models for the simulated magnitude-9.3 tsunamis.

Appendix B

Propagation Database: Atlantic Ocean Unit Sources

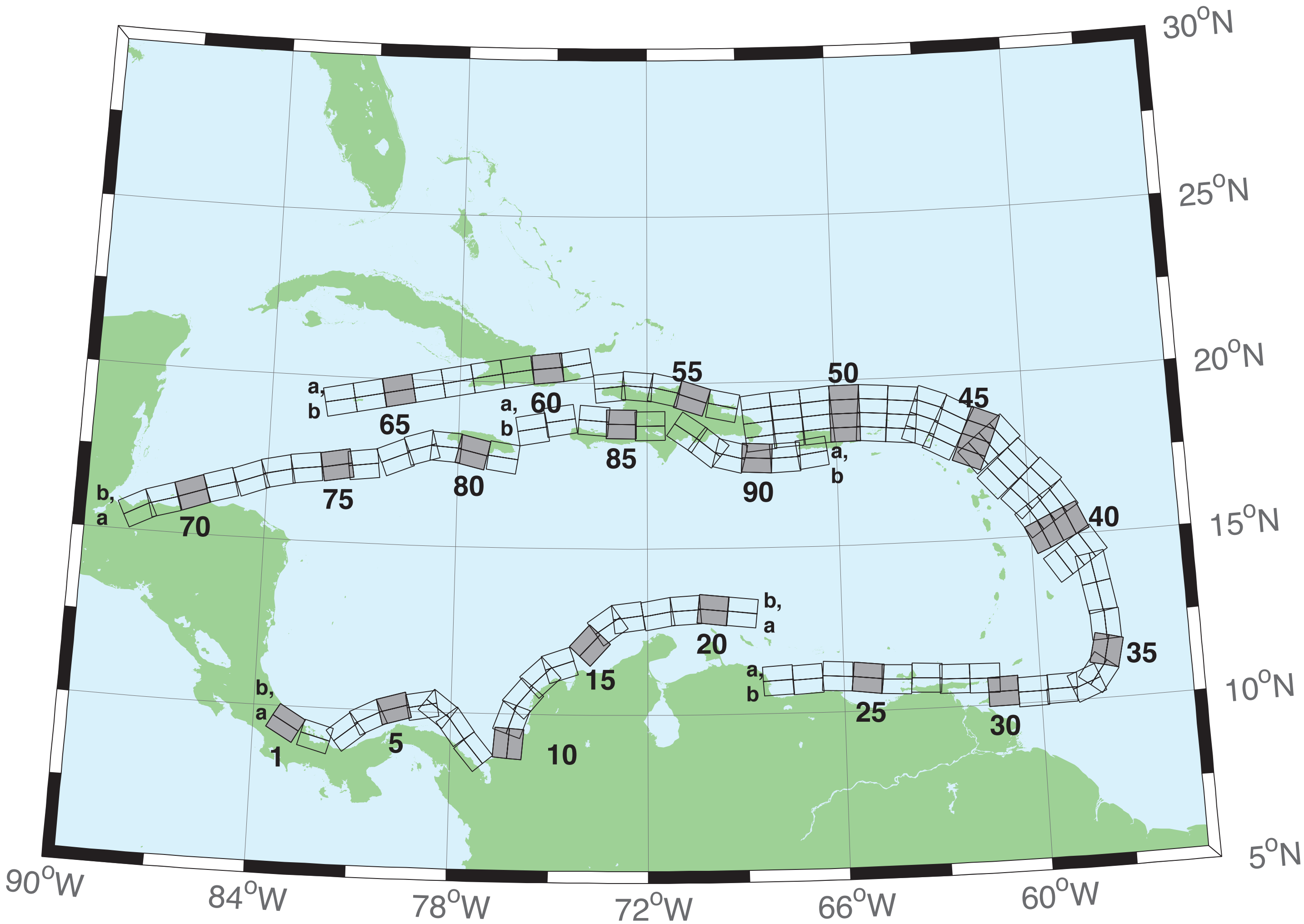

Figure B.1: Atlantic Source Zone unit sources.

Table B.1: Earthquake parameters for Atlantic Source Zone unit sources.

Segment	Description	Longitude(°E)	Latitude(°N)	Strike(°)	Dip(°)	Depth (km)
atsz–1a	Atlantic Source Zone	-83.2020	9.1449	120	27.5	28.09
atsz–1b	Atlantic Source Zone	-83.0000	9.4899	120	27.5	5
atsz–2a	Atlantic Source Zone	-82.1932	8.7408	105.1	27.5	28.09
atsz–2b	Atlantic Source Zone	-82.0880	9.1254	105.1	27.5	5
atsz–3a	Atlantic Source Zone	-80.9172	9.0103	51.31	30	30
atsz–3b	Atlantic Source Zone	-81.1636	9.3139	51.31	30	5
atsz–4a	Atlantic Source Zone	-80.3265	9.4308	63.49	30	30
atsz–4b	Atlantic Source Zone	-80.5027	9.7789	63.49	30	5
atsz–5a	Atlantic Source Zone	-79.6247	9.6961	74.44	30	30
atsz–5b	Atlantic Source Zone	-79.7307	10.0708	74.44	30	5
atsz–6a	Atlantic Source Zone	-78.8069	9.8083	79.71	30	30
atsz–6b	Atlantic Source Zone	-78.8775	10.1910	79.71	30	5
atsz–7a	Atlantic Source Zone	-78.6237	9.7963	127.2	30	30
atsz–7b	Atlantic Source Zone	-78.3845	10.1059	127.2	30	5
atsz–8a	Atlantic Source Zone	-78.1693	9.3544	143.8	30	30
atsz–8b	Atlantic Source Zone	-77.8511	9.5844	143.8	30	5
atsz–9a	Atlantic Source Zone	-77.5913	8.5989	139.9	30	30
atsz–9b	Atlantic Source Zone	-77.2900	8.8493	139.9	30	5
atsz–10a	Atlantic Source Zone	-75.8109	9.0881	4.67	17	19.62
atsz–10b	Atlantic Source Zone	-76.2445	9.1231	4.67	17	5
atsz–11a	Atlantic Source Zone	-75.7406	9.6929	19.67	17	19.62
atsz–11b	Atlantic Source Zone	-76.1511	9.8375	19.67	17	5
atsz–12a	Atlantic Source Zone	-75.4763	10.2042	40.4	17	19.62
atsz–12b	Atlantic Source Zone	-75.8089	10.4826	40.4	17	5
atsz–13a	Atlantic Source Zone	-74.9914	10.7914	47.17	17	19.62
atsz–13b	Atlantic Source Zone	-75.2890	11.1064	47.17	17	5
atsz–14a	Atlantic Source Zone	-74.5666	11.0708	71.68	17	19.62
atsz–14b	Atlantic Source Zone	-74.7043	11.4786	71.68	17	5
atsz–15a	Atlantic Source Zone	-73.4576	11.8012	42.69	17	19.62
atsz–15b	Atlantic Source Zone	-73.7805	12.0924	42.69	17	5
atsz–16a	Atlantic Source Zone	-72.9788	12.3365	54.75	17	19.62
atsz–16b	Atlantic Source Zone	-73.2329	12.6873	54.75	17	5
atsz–17a	Atlantic Source Zone	-72.5454	12.5061	81.96	17	19.62
atsz–17b	Atlantic Source Zone	-72.6071	12.9314	81.96	17	5
atsz–18a	Atlantic Source Zone	-71.6045	12.6174	79.63	17	19.62
atsz–18b	Atlantic Source Zone	-71.6839	13.0399	79.63	17	5
atsz–19a	Atlantic Source Zone	-70.7970	12.7078	86.32	17	19.62
atsz–19b	Atlantic Source Zone	-70.8253	13.1364	86.32	17	5
atsz–20a	Atlantic Source Zone	-70.0246	12.7185	95.94	17	19.62
atsz–20b	Atlantic Source Zone	-69.9789	13.1457	95.94	17	5
atsz–21a	Atlantic Source Zone	-69.1244	12.6320	95.94	17	19.62
atsz–21b	Atlantic Source Zone	-69.0788	13.0592	95.94	17	5
atsz–22a	Atlantic Source Zone	-68.0338	11.4286	266.9	15	17.94
atsz–22b	Atlantic Source Zone	-68.0102	10.9954	266.9	15	5
atsz–23a	Atlantic Source Zone	-67.1246	11.4487	266.9	15	17.94
atsz–23b	Atlantic Source Zone	-67.1010	11.0155	266.9	15	5
atsz–24a	Atlantic Source Zone	-66.1656	11.5055	273.3	15	17.94
atsz–24b	Atlantic Source Zone	-66.1911	11.0724	273.3	15	5
atsz–25a	Atlantic Source Zone	-65.2126	11.4246	276.4	15	17.94
atsz–25b	Atlantic Source Zone	-65.2616	10.9934	276.4	15	5
atsz–26a	Atlantic Source Zone	-64.3641	11.3516	272.9	15	17.94
atsz–26b	Atlantic Source Zone	-64.3862	10.9183	272.9	15	5
atsz–27a	Atlantic Source Zone	-63.4472	11.3516	272.9	15	17.94

Continued on next page

Table B.1 – continued from previous page

Segment	Description	Longitude(°E)	Latitude(°N)	Strike(°)	Dip(°)	Depth (km)
atsz–27b	Atlantic Source Zone	-63.4698	10.9183	272.9	15	5
atsz–28a	Atlantic Source Zone	-62.6104	11.2831	271.1	15	17.94
atsz–28b	Atlantic Source Zone	-62.6189	10.8493	271.1	15	5
atsz–29a	Atlantic Source Zone	-61.6826	11.2518	271.6	15	17.94
atsz–29b	Atlantic Source Zone	-61.6947	10.8181	271.6	15	5
atsz–30a	Atlantic Source Zone	-61.1569	10.8303	269	15	17.94
atsz–30b	Atlantic Source Zone	-61.1493	10.3965	269	15	5
atsz–31a	Atlantic Source Zone	-60.2529	10.7739	269	15	17.94
atsz–31b	Atlantic Source Zone	-60.2453	10.3401	269	15	5
atsz–32a	Atlantic Source Zone	-59.3510	10.8123	269	15	17.94
atsz–32b	Atlantic Source Zone	-59.3734	10.3785	269	15	5
atsz–33a	Atlantic Source Zone	-58.7592	10.8785	248.6	15	17.94
atsz–33b	Atlantic Source Zone	-58.5984	10.4745	248.6	15	5
atsz–34a	Atlantic Source Zone	-58.5699	11.0330	217.2	15	17.94
atsz–34b	Atlantic Source Zone	-58.2179	10.7710	217.2	15	5
atsz–35a	Atlantic Source Zone	-58.3549	11.5300	193.7	15	17.94
atsz–35b	Atlantic Source Zone	-57.9248	11.4274	193.7	15	5
atsz–36a	Atlantic Source Zone	-58.3432	12.1858	177.7	15	17.94
atsz–36b	Atlantic Source Zone	-57.8997	12.2036	177.7	15	5
atsz–37a	Atlantic Source Zone	-58.4490	12.9725	170.7	15	17.94
atsz–37b	Atlantic Source Zone	-58.0095	13.0424	170.7	15	5
atsz–38a	Atlantic Source Zone	-58.6079	13.8503	170.2	15	17.94
atsz–38b	Atlantic Source Zone	-58.1674	13.9240	170.2	15	5
atsz–39a	Atlantic Source Zone	-58.6667	14.3915	146.8	15	17.94
atsz–39b	Atlantic Source Zone	-58.2913	14.6287	146.8	15	5
atsz–39y	Atlantic Source Zone	-59.4168	13.9171	146.8	15	43.82
atsz–39z	Atlantic Source Zone	-59.0415	14.1543	146.8	15	30.88
atsz–40a	Atlantic Source Zone	-59.1899	15.2143	156.2	15	17.94
atsz–40b	Atlantic Source Zone	-58.7781	15.3892	156.2	15	5
atsz–40y	Atlantic Source Zone	-60.0131	14.8646	156.2	15	43.82
atsz–40z	Atlantic Source Zone	-59.6012	15.0395	156.2	15	30.88
atsz–41a	Atlantic Source Zone	-59.4723	15.7987	146.3	15	17.94
atsz–41b	Atlantic Source Zone	-59.0966	16.0392	146.3	15	5
atsz–41y	Atlantic Source Zone	-60.2229	15.3177	146.3	15	43.82
atsz–41z	Atlantic Source Zone	-59.8473	15.5582	146.3	15	30.88
atsz–42a	Atlantic Source Zone	-59.9029	16.4535	137	15	17.94
atsz–42b	Atlantic Source Zone	-59.5716	16.7494	137	15	5
atsz–42y	Atlantic Source Zone	-60.5645	15.8616	137	15	43.82
atsz–42z	Atlantic Source Zone	-60.2334	16.1575	137	15	30.88
atsz–43a	Atlantic Source Zone	-60.5996	17.0903	138.7	15	17.94
atsz–43b	Atlantic Source Zone	-60.2580	17.3766	138.7	15	5
atsz–43y	Atlantic Source Zone	-61.2818	16.5177	138.7	15	43.82
atsz–43z	Atlantic Source Zone	-60.9404	16.8040	138.7	15	30.88
atsz–44a	Atlantic Source Zone	-61.1559	17.8560	141.1	15	17.94
atsz–44b	Atlantic Source Zone	-60.8008	18.1286	141.1	15	5
atsz–44y	Atlantic Source Zone	-61.8651	17.3108	141.1	15	43.82
atsz–44z	Atlantic Source Zone	-61.5102	17.5834	141.1	15	30.88
atsz–45a	Atlantic Source Zone	-61.5491	18.0566	112.8	15	17.94
atsz–45b	Atlantic Source Zone	-61.3716	18.4564	112.8	15	5
atsz–45y	Atlantic Source Zone	-61.9037	17.2569	112.8	15	43.82
atsz–45z	Atlantic Source Zone	-61.7260	17.6567	112.8	15	30.88
atsz–46a	Atlantic Source Zone	-62.4217	18.4149	117.9	15	17.94
atsz–46b	Atlantic Source Zone	-62.2075	18.7985	117.9	15	5
atsz–46y	Atlantic Source Zone	-62.8493	17.6477	117.9	15	43.82
atsz–46z	Atlantic Source Zone	-62.6352	18.0313	117.9	15	30.88

Continued on next page

Table B.1 – continued from previous page

Segment	Description	Longitude(°E)	Latitude(°N)	Strike(°)	Dip(°)	Depth (km)
atsz–47a	Atlantic Source Zone	-63.1649	18.7844	110.5	20	22.1
atsz–47b	Atlantic Source Zone	-63.0087	19.1798	110.5	20	5
atsz–47y	Atlantic Source Zone	-63.4770	17.9936	110.5	20	56.3
atsz–47z	Atlantic Source Zone	-63.3205	18.3890	110.5	20	39.2
atsz–48a	Atlantic Source Zone	-63.8800	18.8870	95.37	20	22.1
atsz–48b	Atlantic Source Zone	-63.8382	19.3072	95.37	20	5
atsz–48y	Atlantic Source Zone	-63.9643	18.0465	95.37	20	56.3
atsz–48z	Atlantic Source Zone	-63.9216	18.4667	95.37	20	39.2
atsz–49a	Atlantic Source Zone	-64.8153	18.9650	94.34	20	22.1
atsz–49b	Atlantic Source Zone	-64.7814	19.3859	94.34	20	5
atsz–49y	Atlantic Source Zone	-64.8840	18.1233	94.34	20	56.3
atsz–49z	Atlantic Source Zone	-64.8492	18.5442	94.34	20	39.2
atsz–50a	Atlantic Source Zone	-65.6921	18.9848	89.59	20	22.1
atsz–50b	Atlantic Source Zone	-65.6953	19.4069	89.59	20	5
atsz–50y	Atlantic Source Zone	-65.6874	18.1407	89.59	20	56.3
atsz–50z	Atlantic Source Zone	-65.6887	18.5628	89.59	20	39.2
atsz–51a	Atlantic Source Zone	-66.5742	18.9484	84.98	20	22.1
atsz–51b	Atlantic Source Zone	-66.6133	19.3688	84.98	20	5
atsz–51y	Atlantic Source Zone	-66.4977	18.1076	84.98	20	56.3
atsz–51z	Atlantic Source Zone	-66.5353	18.5280	84.98	20	39.2
atsz–52a	Atlantic Source Zone	-67.5412	18.8738	85.87	20	22.1
atsz–52b	Atlantic Source Zone	-67.5734	19.2948	85.87	20	5
atsz–52y	Atlantic Source Zone	-67.4781	18.0319	85.87	20	56.3
atsz–52z	Atlantic Source Zone	-67.5090	18.4529	85.87	20	39.2
atsz–53a	Atlantic Source Zone	-68.4547	18.7853	83.64	20	22.1
atsz–53b	Atlantic Source Zone	-68.5042	19.2048	83.64	20	5
atsz–53y	Atlantic Source Zone	-68.3575	17.9463	83.64	20	56.3
atsz–53z	Atlantic Source Zone	-68.4055	18.3658	83.64	20	39.2
atsz–54a	Atlantic Source Zone	-69.6740	18.8841	101.5	20	22.1
atsz–54b	Atlantic Source Zone	-69.5846	19.2976	101.5	20	5
atsz–55a	Atlantic Source Zone	-70.7045	19.1376	108.2	20	22.1
atsz–55b	Atlantic Source Zone	-70.5647	19.5386	108.2	20	5
atsz–56a	Atlantic Source Zone	-71.5368	19.3853	102.6	20	22.1
atsz–56b	Atlantic Source Zone	-71.4386	19.7971	102.6	20	5
atsz–57a	Atlantic Source Zone	-72.3535	19.4838	94.2	20	22.1
atsz–57b	Atlantic Source Zone	-72.3206	19.9047	94.2	20	5
atsz–58a	Atlantic Source Zone	-73.1580	19.4498	84.34	20	22.1
atsz–58b	Atlantic Source Zone	-73.2022	19.8698	84.34	20	5
atsz–59a	Atlantic Source Zone	-74.3567	20.9620	259.7	20	22.1
atsz–59b	Atlantic Source Zone	-74.2764	20.5467	259.7	20	5
atsz–60a	Atlantic Source Zone	-75.2386	20.8622	264.2	15	17.94
atsz–60b	Atlantic Source Zone	-75.1917	20.4306	264.2	15	5
atsz–61a	Atlantic Source Zone	-76.2383	20.7425	260.7	15	17.94
atsz–61b	Atlantic Source Zone	-76.1635	20.3144	260.7	15	5
atsz–62a	Atlantic Source Zone	-77.2021	20.5910	259.9	15	17.94
atsz–62b	Atlantic Source Zone	-77.1214	20.1638	259.9	15	5
atsz–63a	Atlantic Source Zone	-78.1540	20.4189	259	15	17.94
atsz–63b	Atlantic Source Zone	-78.0661	19.9930	259	15	5
atsz–64a	Atlantic Source Zone	-79.0959	20.2498	259.2	15	17.94
atsz–64b	Atlantic Source Zone	-79.0098	19.8236	259.2	15	5
atsz–65a	Atlantic Source Zone	-80.0393	20.0773	258.9	15	17.94
atsz–65b	Atlantic Source Zone	-79.9502	19.6516	258.9	15	5
atsz–66a	Atlantic Source Zone	-80.9675	19.8993	258.6	15	17.94
atsz–66b	Atlantic Source Zone	-80.8766	19.4740	258.6	15	5
atsz–67a	Atlantic Source Zone	-81.9065	19.7214	258.5	15	17.94

Continued on next page

Table B.1 – continued from previous page

Segment	Description	Longitude(°E)	Latitude(°N)	Strike(°)	Dip(°)	Depth (km)
atsz–67b	Atlantic Source Zone	-81.8149	19.2962	258.5	15	5
atsz–68a	Atlantic Source Zone	-87.8003	15.2509	62.69	15	17.94
atsz–68b	Atlantic Source Zone	-88.0070	15.6364	62.69	15	5
atsz–69a	Atlantic Source Zone	-87.0824	15.5331	72.73	15	17.94
atsz–69b	Atlantic Source Zone	-87.2163	15.9474	72.73	15	5
atsz–70a	Atlantic Source Zone	-86.1622	15.8274	70.64	15	17.94
atsz–70b	Atlantic Source Zone	-86.3120	16.2367	70.64	15	5
atsz–71a	Atlantic Source Zone	-85.3117	16.1052	73.7	15	17.94
atsz–71b	Atlantic Source Zone	-85.4387	16.5216	73.7	15	5
atsz–72a	Atlantic Source Zone	-84.3470	16.3820	69.66	15	17.94
atsz–72b	Atlantic Source Zone	-84.5045	16.7888	69.66	15	5
atsz–73a	Atlantic Source Zone	-83.5657	16.6196	77.36	15	17.94
atsz–73b	Atlantic Source Zone	-83.6650	17.0429	77.36	15	5
atsz–74a	Atlantic Source Zone	-82.7104	16.7695	82.35	15	17.94
atsz–74b	Atlantic Source Zone	-82.7709	17.1995	82.35	15	5
atsz–75a	Atlantic Source Zone	-81.7297	16.9003	79.86	15	17.94
atsz–75b	Atlantic Source Zone	-81.8097	17.3274	79.86	15	5
atsz–76a	Atlantic Source Zone	-80.9196	16.9495	82.95	15	17.94
atsz–76b	Atlantic Source Zone	-80.9754	17.3801	82.95	15	5
atsz–77a	Atlantic Source Zone	-79.8086	17.2357	67.95	15	17.94
atsz–77b	Atlantic Source Zone	-79.9795	17.6378	67.95	15	5
atsz–78a	Atlantic Source Zone	-79.0245	17.5415	73.61	15	17.94
atsz–78b	Atlantic Source Zone	-79.1532	17.9577	73.61	15	5
atsz–79a	Atlantic Source Zone	-78.4122	17.5689	94.07	15	17.94
atsz–79b	Atlantic Source Zone	-78.3798	18.0017	94.07	15	5
atsz–80a	Atlantic Source Zone	-77.6403	17.4391	103.3	15	17.94
atsz–80b	Atlantic Source Zone	-77.5352	17.8613	103.3	15	5
atsz–81a	Atlantic Source Zone	-76.6376	17.2984	98.21	15	17.94
atsz–81b	Atlantic Source Zone	-76.5726	17.7278	98.21	15	5
atsz–82a	Atlantic Source Zone	-75.7299	19.0217	260.1	15	17.94
atsz–82b	Atlantic Source Zone	-75.6516	18.5942	260.1	15	5
atsz–83a	Atlantic Source Zone	-74.8351	19.2911	260.8	15	17.94
atsz–83b	Atlantic Source Zone	-74.7621	18.8628	260.8	15	5
atsz–84a	Atlantic Source Zone	-73.6639	19.2991	274.8	15	17.94
atsz–84b	Atlantic Source Zone	-73.7026	18.8668	274.8	15	5
atsz–85a	Atlantic Source Zone	-72.8198	19.2019	270.6	15	17.94
atsz–85b	Atlantic Source Zone	-72.8246	18.7681	270.6	15	5
atsz–86a	Atlantic Source Zone	-71.9143	19.1477	269.1	15	17.94
atsz–86b	Atlantic Source Zone	-71.9068	18.7139	269.1	15	5
atsz–87a	Atlantic Source Zone	-70.4738	18.8821	304.5	15	17.94
atsz–87b	Atlantic Source Zone	-70.7329	18.5245	304.5	15	5
atsz–88a	Atlantic Source Zone	-69.7710	18.3902	308.9	15	17.94
atsz–88b	Atlantic Source Zone	-70.0547	18.0504	308.4	15	5
atsz–89a	Atlantic Source Zone	-69.2635	18.2099	283.9	15	17.94
atsz–89b	Atlantic Source Zone	-69.3728	17.7887	283.9	15	5
atsz–90a	Atlantic Source Zone	-68.5059	18.1443	272.9	15	17.94
atsz–90b	Atlantic Source Zone	-68.5284	17.7110	272.9	15	5
atsz–91a	Atlantic Source Zone	-67.6428	18.1438	267.8	15	17.94
atsz–91b	Atlantic Source Zone	-67.6256	17.7103	267.8	15	5
atsz–92a	Atlantic Source Zone	-66.8261	18.2536	262	15	17.94
atsz–92b	Atlantic Source Zone	-66.7627	17.8240	262	15	5

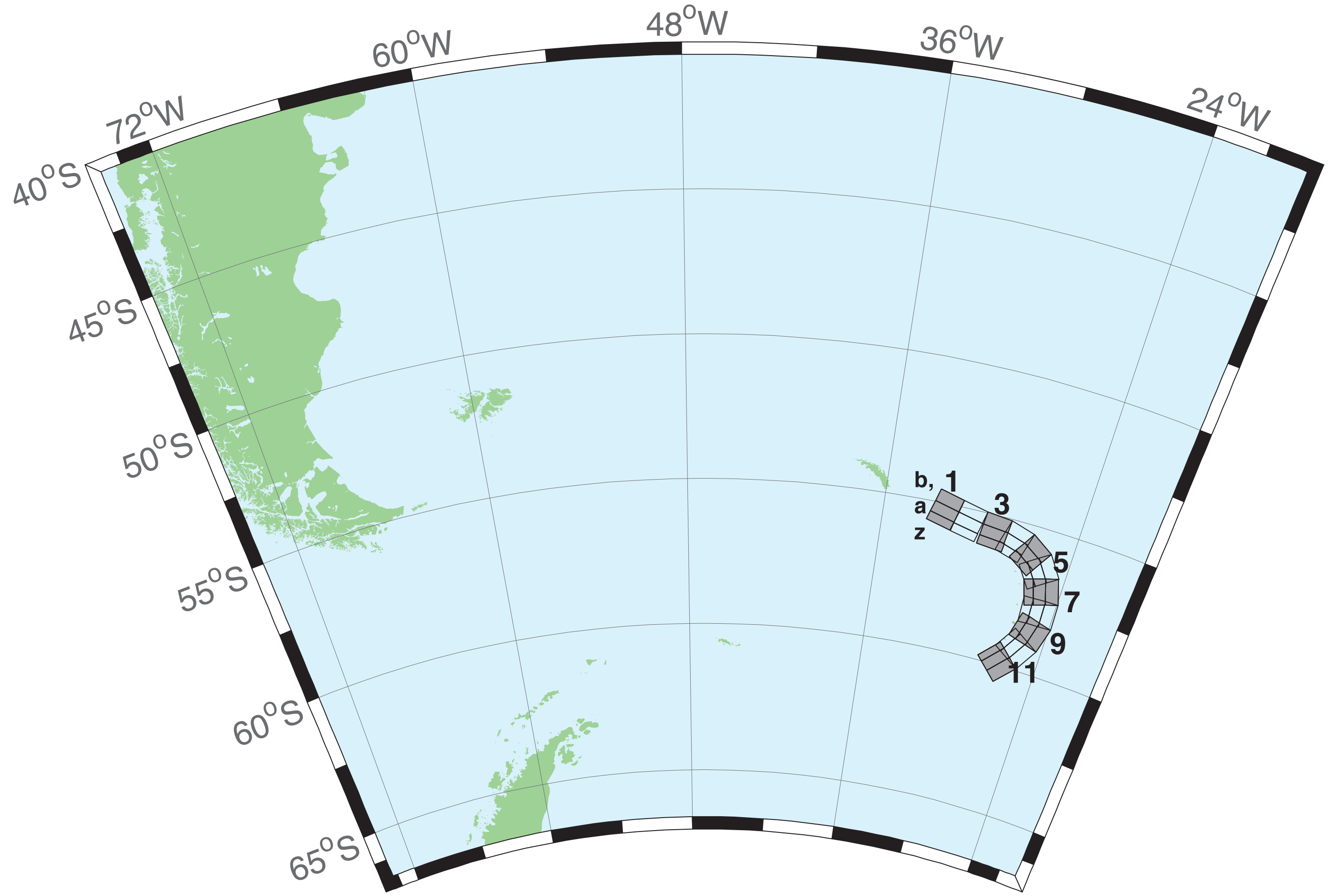

Figure B.2: South Sandwich Islands Subduction Zone.

Table B.2: Earthquake parameters for South Sandwich Islands Subduction Zone unit sources.

Segment	Description	Longitude(°E)	Latitude(°N)	Strike(°)	Dip(°)	Depth (km)
sssz–1a	South Sandwich Islands Subduction Zone	-32.3713	-55.4655	104.7	28.53	17.51
sssz–1b	South Sandwich Islands Subduction Zone	-32.1953	-55.0832	104.7	9.957	8.866
sssz–1z	South Sandwich Islands Subduction Zone	-32.5091	-55.7624	104.7	46.99	41.39
sssz–2a	South Sandwich Islands Subduction Zone	-30.8028	-55.6842	102.4	28.53	17.51
sssz–2b	South Sandwich Islands Subduction Zone	-30.6524	-55.2982	102.4	9.957	8.866
sssz–2z	South Sandwich Islands Subduction Zone	-30.9206	-55.9839	102.4	46.99	41.39
sssz–3a	South Sandwich Islands Subduction Zone	-29.0824	-55.8403	95.53	28.53	17.51
sssz–3b	South Sandwich Islands Subduction Zone	-29.0149	-55.4468	95.53	9.957	8.866
sssz–3z	South Sandwich Islands Subduction Zone	-29.1353	-56.1458	95.53	46.99	41.39
sssz–4a	South Sandwich Islands Subduction Zone	-27.8128	-55.9796	106.1	28.53	17.51
sssz–4b	South Sandwich Islands Subduction Zone	-27.6174	-55.5999	106.1	9.957	8.866
sssz–4z	South Sandwich Islands Subduction Zone	-27.9659	-56.2744	106.1	46.99	41.39
sssz–5a	South Sandwich Islands Subduction Zone	-26.7928	-56.2481	123.1	28.53	17.51
sssz–5b	South Sandwich Islands Subduction Zone	-26.4059	-55.9170	123.1	9.957	8.866
sssz–5z	South Sandwich Islands Subduction Zone	-27.0955	-56.5052	123.1	46.99	41.39
sssz–6a	South Sandwich Islands Subduction Zone	-26.1317	-56.6466	145.6	23.28	16.11
sssz–6b	South Sandwich Islands Subduction Zone	-25.5131	-56.4133	145.6	9.09	8.228
sssz–6z	South Sandwich Islands Subduction Zone	-26.5920	-56.8194	145.6	47.15	35.87
sssz–7a	South Sandwich Islands Subduction Zone	-25.6787	-57.2162	162.9	21.21	14.23
sssz–7b	South Sandwich Islands Subduction Zone	-24.9394	-57.0932	162.9	7.596	7.626
sssz–7z	South Sandwich Islands Subduction Zone	-26.2493	-57.3109	162.9	44.16	32.32
sssz–8a	South Sandwich Islands Subduction Zone	-25.5161	-57.8712	178.2	20.33	15.91
sssz–8b	South Sandwich Islands Subduction Zone	-24.7233	-57.8580	178.2	8.449	8.562
sssz–8z	South Sandwich Islands Subduction Zone	-26.1280	-57.8813	178.2	43.65	33.28
sssz–9a	South Sandwich Islands Subduction Zone	-25.6657	-58.5053	195.4	25.76	15.71
sssz–9b	South Sandwich Islands Subduction Zone	-24.9168	-58.6127	195.4	8.254	8.537
sssz–9z	South Sandwich Islands Subduction Zone	-26.1799	-58.4313	195.4	51.69	37.44
sssz–10a	South Sandwich Islands Subduction Zone	-26.1563	-59.1048	212.5	32.82	15.65
sssz–10b	South Sandwich Islands Subduction Zone	-25.5335	-59.3080	212.5	10.45	6.581
sssz–10z	South Sandwich Islands Subduction Zone	-26.5817	-58.9653	212.5	54.77	42.75
sssz–11a	South Sandwich Islands Subduction Zone	-27.0794	-59.6799	224.2	33.67	15.75
sssz–11b	South Sandwich Islands Subduction Zone	-26.5460	-59.9412	224.2	11.32	5.927
sssz–11z	South Sandwich Islands Subduction Zone	-27.4245	-59.5098	224.2	57.19	43.46

Appendix C SIFT Testing Report

Appendix C

SIFT Testing Report

Authors: Lindsey Wright, Liujuan Tang

1.0 PURPOSE

Forecast models are tested with synthetic tsunami events covering a range of tsunami source locations and magnitudes. Testing is also done with selected historical tsunami events when available.

The testing of a forecast model has three objectives. The first objective is to assure that the results obtained with the NOAA's tsunami forecast system software, which has been released to the Tsunami Warning Centers for operational use are consistent with those obtained by the researcher during the development of the forecast model. The second objective is to test the forecast model for consistency, accuracy, time efficiency, and quality of results over a range of possible tsunami locations and magnitudes. The third objective is to identify bugs and issues in need of resolution by the researcher who developed the Forecast Model or by the forecast system software development team before the next version release to NOAA's two Tsunami Warning Centers.

Local hardware and software applications, and tools familiar to the researcher(s), are used to run the Method of Splitting Tsunamis (MOST) model during the forecast model development. The test results presented in this report lend confidence that the model performs as developed and produces the same results when initiated within the forecast system application in an operational setting as those produced by the researcher during the forecast model development. The test results assure those who rely on the Virginia Beach tsunami forecast model that consistent results are produced irrespective of system.

2.0 TESTING PROCEDURE

The general procedure for forecast model testing is to run a set of synthetic tsunami scenarios and a selected set of historical tsunami events through the forecast system application and compare the results with those obtained by the researcher during the forecast model development and presented in the Tsunami Forecast Model Report. Specific steps taken to test the model include:

1. Identification of testing scenarios, including the standard set of synthetic events, appropriate historical events, and customized synthetic scenarios that may have been used by the researcher(s) in developing the forecast model.

2. Creation of new events to represent customized synthetic scenarios used by the researcher(s) in developing the forecast model, if any.

3. Submission of test model runs with the forecast system, and export of the results from A, B, and C grids, along with time series.

4. Recording applicable metadata, including the specific forecast system version used for testing.

5. Examination of forecast model results for instabilities in both time series and plot results.

6. Comparison of forecast model results obtained through the forecast system with those obtained during the forecast model development.

7. Summarization of results with specific mention of quality, consistency, and time efficiency.

8. Reporting of issues identified to modeler and forecast system software development team.

9. Retesting the forecast models in the forecast system when reported issues have been addressed or explained.

Synthetic model runs were tested on a DELL PowerEdge R510 computer equipped with two Xeon E5670 processors at 2.93 Ghz, each with 12 MBytes of cache and 32GB memory. The processors are hex core and support hyperthreading, resulting in the computer performing as a 24 processor core machine. Additionally, the testing computer supports 10 Gigabit Ethernet for fast network connections. This computer configuration is similar or the same as the configurations of the computers installed at the Tsunami Warning Centers so the compute times should only vary slightly.

Results

The Virginia Beach forecast model was tested with SIFT version 3.2. The same version of propagation database was used during the model development.

The Virginia Beach, Virginia forecast model was tested with three synthetic scenarios. Test results from the forecast system and comparisons with the results obtained during the forecast model development are shown numerically in Table C1 and graphically in Figures C1 to C3. The results show that the minimum and maximum amplitudes and time series obtained from the forecast system agree with those obtained during the forecast model development, and that the forecast model is stable and robust, with consistent and high quality results across geographically distributed tsunami sources. The model run time (wall clock time) was 24.75 minutes for 11.99 hours of simulation time, and 8.24 minutes for 4.0 hours. This run time is well within the 10 minute run time for 4 hours of simulation time.

A suite of three synthetic events was run on the Virginia Beach forecast model. The modeled scenarios were stable for all cases run. The largest modeled height was 601 centimeters (cm) from the Atlantic (ATSZ 48–57) source zone. The smallest signal of 40 cm was recorded at the South Sandwich (SSSZ 1–10) source zone. Maximum values for the SSSZ 1–10 differed slightly. This abnormality resulted from the development model being run for a longer window of time than the SIFT output and therefore an additional wave with a slightly higher amplitude was recorded at approximately 28 hours after the event. Visual comparisons between the development cases and the forecast system output were nearly identical in shape and amplitude for all cases. The Virginia Beach reference point used for the forecast model development is the same as what is deployed in the forecast system, so the results can be considered valid for the three cases studied.

Table C1. Table of maximum and minimum amplitudes (cm) at the Virginia Beach, Virginia warning point for synthetic and historical events tested using SIFT 3.2 and obtained during development.

Scenario Name	Source Zone	Tsunami Source	α [m]	SIFT Max (cm)	Development Max (cm)	SIFT Min (cm)	Development Min (cm)
Mega-tsunami Scenarios							
ATSZ 38-47	Atlantic	A38-A47, B38-B47	25	246.9	247	-122.8	-123
ATSZ 48-57	Atlantic	A48-A57, B48-B57	25	600.9	601	-356.9	-358
SSSZ 1-10	South Sandwich	A1-A10, B1-B10	25	39.9	58(40 for first 12 hours)	-40.6	-43

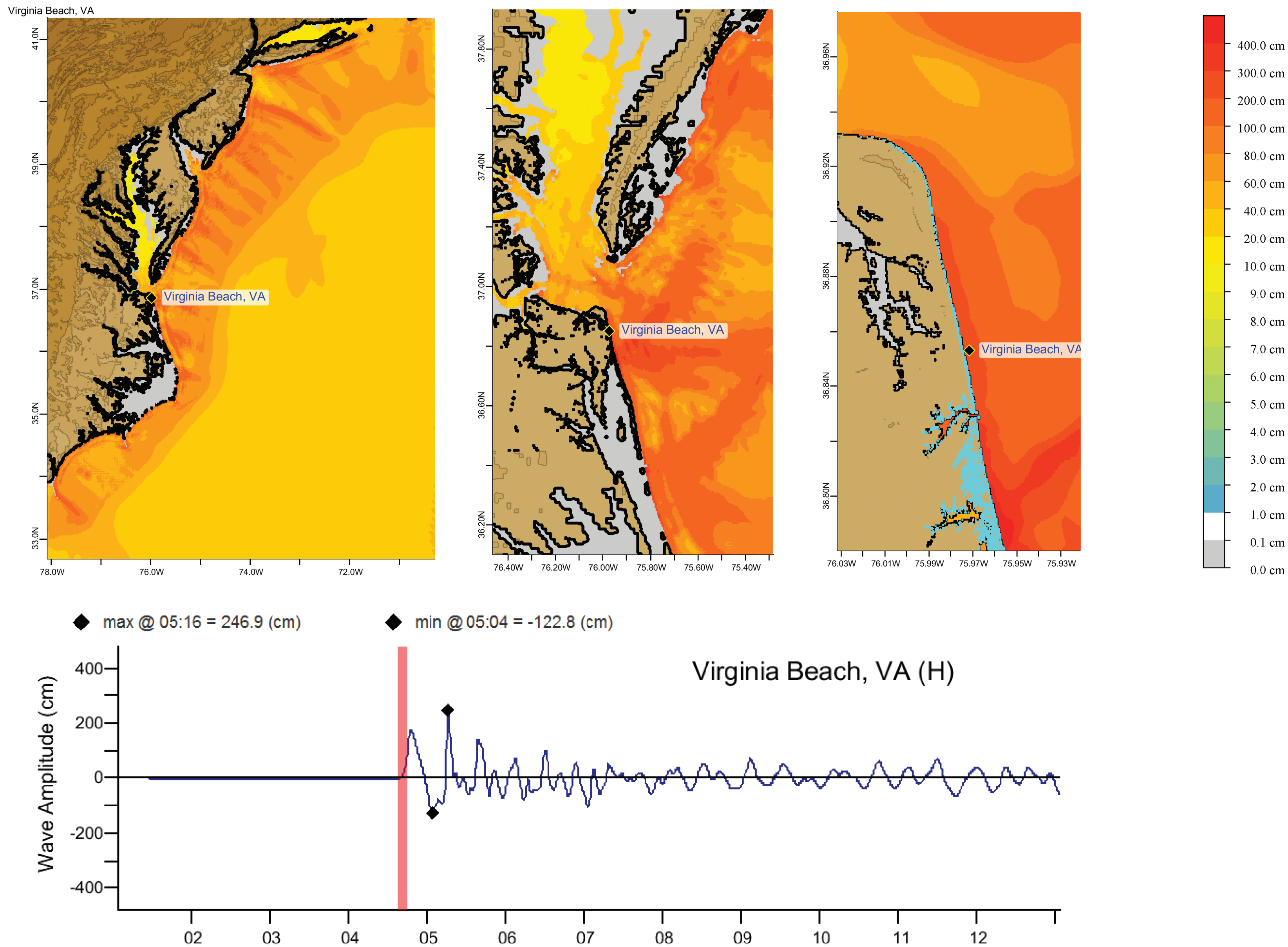

Figure C1 Response of the Virginia Beach forecast model to synthetic scenario ATSZ 38-47. (a, b, and c) Maximum sea surface elevation for A-, B- and C-grids. (d) Sea surface elevation time series at the C-grid warning point.

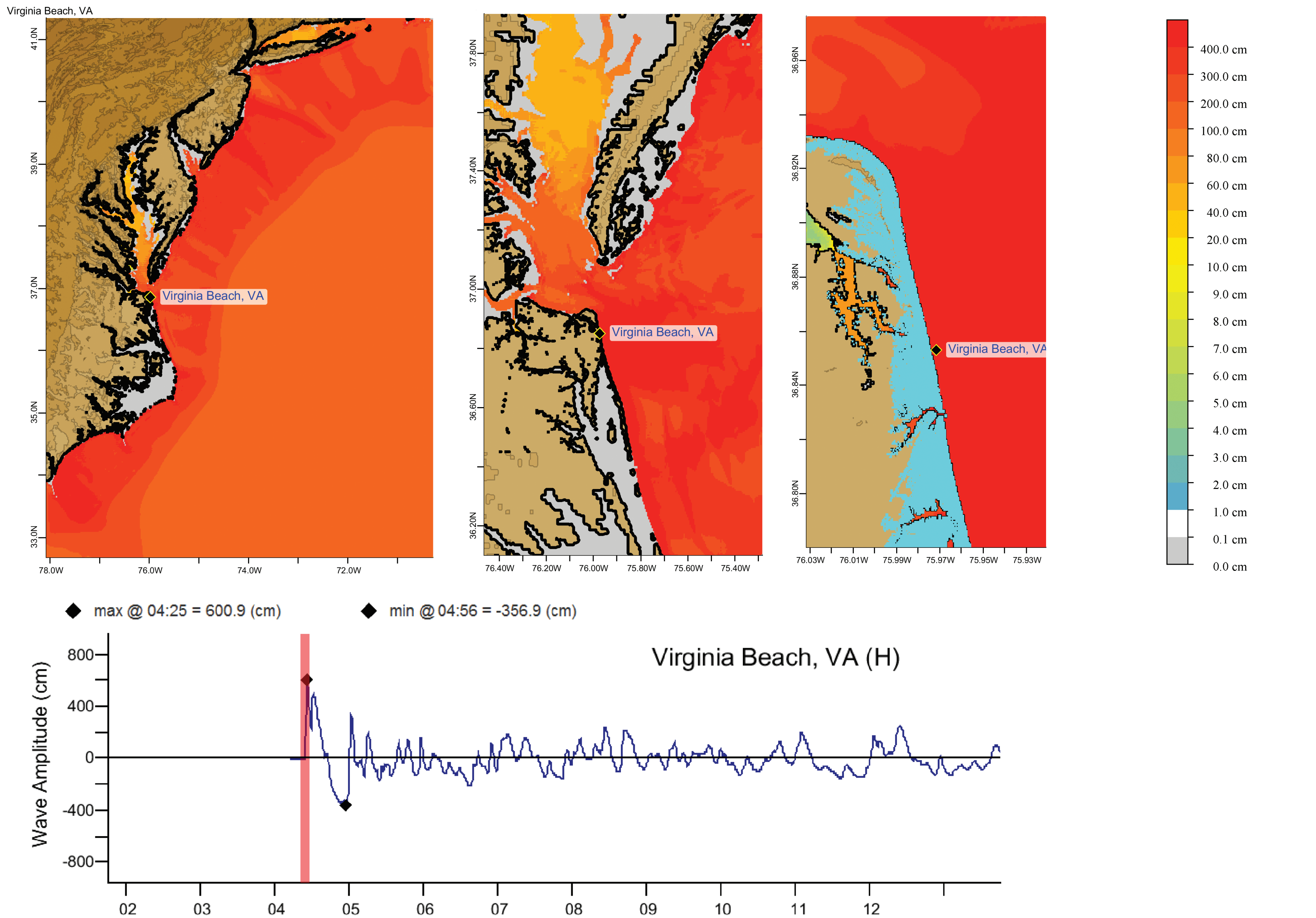

Figure C2 Response of the Virginia Beach forecast model to synthetic scenario ATSZ 48-57. (a, b, and c) Maximum sea surface elevation for A-, B- and C-grids. (d) Sea surface elevation time series at the C-grid warning point.

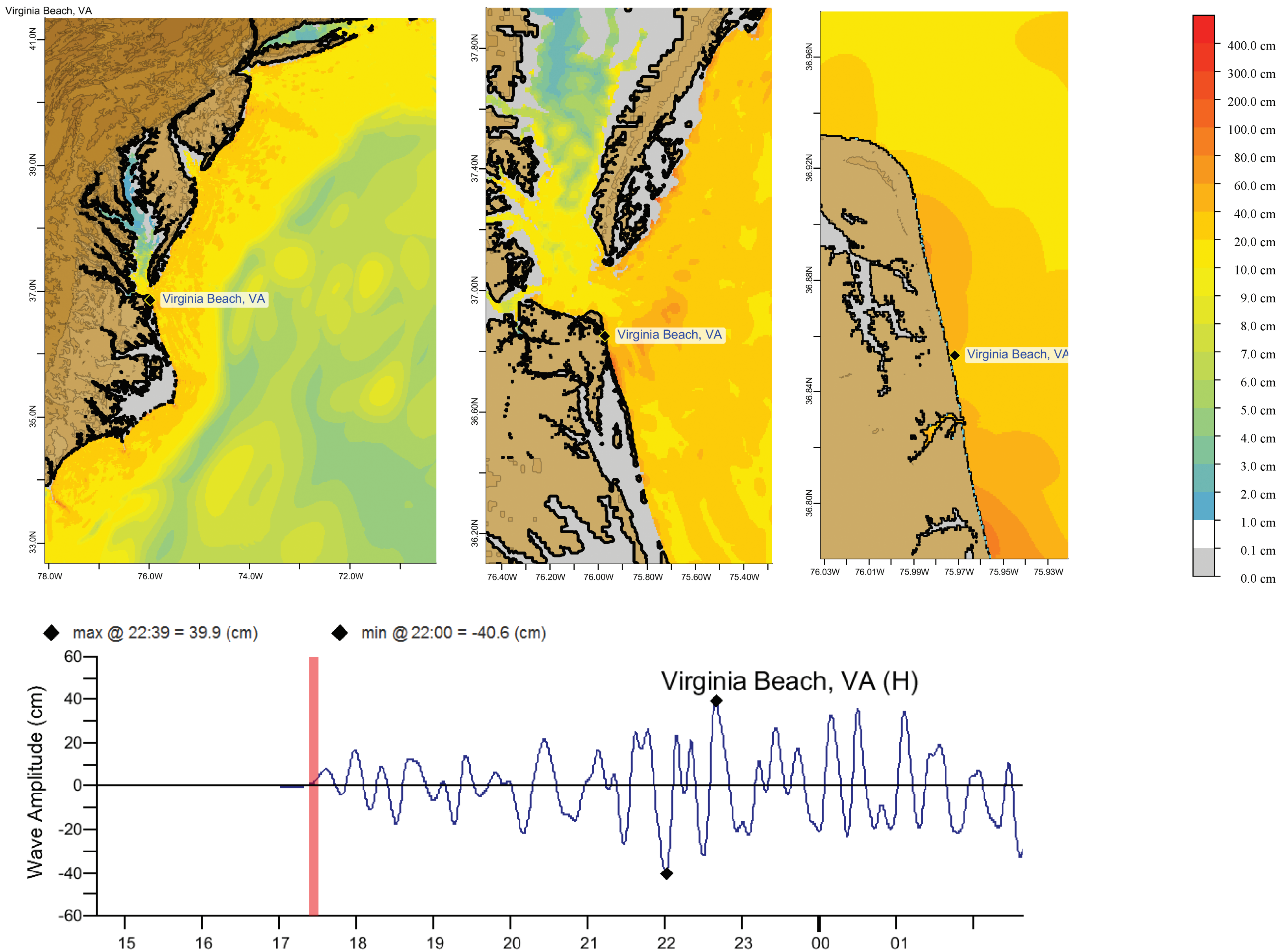

Figure C3 Response of the Virginia Beach forecast model to synthetic scenario SSSZ 1-10. (a, b, and c) Maximum sea surface elevation for A-, B- and C-grids. (d) Sea surface elevation time series at the C-grid warning point.